エンドミル加工における熱変形の統計的推定に関する研究

Doctoral Dissertation:

Research on statistical estimation of thermal deformation in End-milling

Mengmeng Yang

Muroran Institute of Technology

01.2023

Title:

Research on statistical estimation of thermal deformation in End-milling

Name: Mengmeng Yang

Supervisor: Professor Koji Teramoto

School: Muroran Institute of Technology

Date:27/01/2023

Outline of contents

Abstract

The thermal workpiece's deformation in end-milling process has significant effect on accuracy of machining. In-process direct measurement of workpiece deformation is difficult because of machining process disturbance. On the other hand, local temperatures of workpiece can be easily and accurately measured by common measuring methods. The objective of this research is to develop a method to monitor the workpiece's deformations. In order to estimate workpiece's thermal states in small-lot production, a sensor-configured thermal simulation has been proposed by combining local temperature measurements and thermal simulation. To accelerate the process time, an empirical modeling method to estimate workpiece's deformation from measured temperatures is introduced. It is indispensable to select appropriate measuring points for reliable estimation. In order to establish a relationship between thermal deformation and temperatures of measuring points in various machining situation, a statistic-based selection method is proposed by using the Multiple Linear Regression (MLR) method. By using FEM-based thermal simulation during end-milling process, predicted time-series of deformation at the machining point are regarded as output variable while time-series of temperature of measuring points are regarded as input variables. The number of measuring points are determined by evaluating Akaike's Information Criterion (AIC) and effective measuring points are selected by using p-value index. Proposed systematic construction method is evaluated by simulation-based case studies. A constructed temperature-based model for workpiece's deformation shows good agreement to the deformation calculated by the FEM simulation. The constructed model can represent workpiece's deformation with the minimum number of measuring points. After discussing the accuracy of proposed statistic model in various boundary conditions which correspond to various end-milling situation, two modified statistic model, such as modified coefficient statistic model (MCSM) and the adjusted statistic-

model (ASM), were proposed to achieve more suitable expression of the relationship between monitoring points temperature and thermal deformation at machining point of workpiece surface. The error analysis of two modified statistic model were respectively discussed. Consequently, MCSM and ASM are both more accuracy to describe the relationship between temperature of monitoring points and thermal deformation at machining point in various boundary condition. In addition, only when the ranges of the machining parameters are known in advance, MCSM is preferred to describe the relationship between temperature of monitoring points and thermal deformation at machining point rather than initially proposed statistic model.
Keywords: Statistic model, numerical simulation, MLR, error analysis, end-milling

Acknowledgements

For the 3 years' doctoral period, many thanks for everything to my advisor, Pro. Teramoto, for his guidance, encouragement and support during my doctoral studies at Muroran Institute of Technology. Thanks to the faculty and students of the Manufacturing Engineering Laboratory for their help and support not only for this research, but also for the kindly help to my daily life.
I appreciate the partial financial support from by KAKENHI Grant Number 19K04119 and the MuroranIT Scholarship for Privately Financed International Students. Especially, I would like to express my thanks to JST SPRING Grant Number JPMJSP2153.Most of my daily life was support by JST program from Dec. 2021, I can fully focus on my research after I obtained the support from JST. And also, I'm very appreciate for the recommendation from my advisor Pro. Teramoto, I could not obtain this support without his guidance in my research. Pro. Teramoto is a kindly professor also with open-mind, sometimes performs strict and he always tells me to keep positive when I was depressed or felt lost in the exploring of new researches.
Considering my future career plan, Pro. Teramoto also found an internship opportunity for me at Saitama University. It was really a precious memory for me to experience different atmosphere in the Department of Mechanical Engineering at Saitama Univ., which broaden my eyes to know what the laminated modeling, additional processing, numerical control machine especially the Additive Manufacturing are. I also had the opportunity to see the prosperity of Tokyo. Since the current research is focused on digital twining of statistical forecasting of thermal deformation in End-milling, it may be a brand-new field for me to research in which combined the empirical constructed model with the other fields.
In order to be an excellent researcher, I quitted the job in the company in China then came to Japan. For me, the life-changing moment was definitely when Teramoto sensei accepted me as a student to join his laboratory. I never imagined that I could live such a satisfying life with more options. In a brand-new field, I'm like a child learning to walk, fortunately, I met such a kind sensei and got the permission of graduation form supervisors. Wish them all the best and hope that my research results can be applied to the manufacturing engineering which could be the feedback I can give.
Finally, I should thank my family for the great support.

1 Introduction

The Digital Twinning is one of the fast-evolving digital technologies that support the digital transformation of the structural engineering to enable optimal decision support for improving the management, reliability, and sustainability of structures [1,2]. The Digital Twinning concept, originally conceived as a digital replica to a physical asset, was first coined in 2002 by Michael Grieves at the University of Michigan [3] although its first practical application to structures took place in 2012 in the aerospace sector [4,5].

End-milling is one of the most important machining process, which are satisfied with the requirement of high quality and agile production [6,7]. Comparing with near-net shape (NNS) methods such as additive manufacturing, the finish machining method of end milling process is certainly advantaged in manufacturing industry, especially in complex 3-dimentional parts or small-lot productions, which are almost low-cost, versatile, effective and accurate. Hence, end-milling is widely evaluated as promising machining method for finish machining of NNS parts in various industry, such as aerospace, automotive and military industry[8]. However, during the end-milling process, the size and shape of workpiece are correspondingly changed by temperature change, which has seriously effective on tool life and material removal rate. At last, the desired shape and dimensions of parts are hardly guaranteed. It is well-known that the main goal for manufacturing industries are high productive and low cost in addition to better surface finish and dimensional accuracy. As well as the quality of the machined part, the tool deflection, tool life, cutting force and vibration are directly influenced by temperature [9,10]. Therefore, the evaluation of thermal distribution is the key factor for guaranteeing the accuracy of parts, which are simultaneously benefit for conducting temperature monitoring to evaluate thermal deformation. In addition, the research result is also seriously benefit for conducting temperature monitoring of additive manufacturing and guaranteeing dimensional accuracy.

1.1 Research Background

Machining is the most widely used process in manufacturing industry since the 18th century, in which a desired shape and size of production is completely manufactured by a material removal process[11]. End-milling is an indispensable procedure in the process of small batch high precision parts, heat is bound to be generated in the process of end milling, which will cause the temperature change of the workpiece. The change of material structure caused by processing temperature is an unfavorable factor for the overall fatigue and mechanical properties of the structure. Moreover, the thermal residual stress caused by temperature gradient in the workpiece will produce thermal deformation after the release of clamping at the end of processing, which will affect the final surface morphology of the workpiece. With the rapid development of the industrial, the demand for high-performance machining parts is also growing rapidly. The research on the thermal deformation of end milling, especially the thermal deformation of workpiece end, has been urgent.

In industries with high quality requirements, an increasing number of difficult to process materials are being used, which have special properties such as superior strength, ultra-high hardness, and low thermal conductivity, resulting in considerably higher cutting temperatures during material removal. A large amount of heat is conducted to the workpiece in the process of processing, which will leave some residual stress on the surface of the workpiece after processing.

Because some parts have the characteristics of complex structure and weak rigidity, the springback deformation caused by heat residual stress after clamping release will cause a large error on the whole part, which has a great impact on the dimensional accuracy control and assembly accuracy requirements in production and application.

The development of manufacturing industry is included by advanced information and knowledge, modeling and simulation, advanced technology and equipment, system integration

and other key technologies [12]. Modeling and numerical simulation can drive and accelerate the development of related advanced manufacturing technology, which is regarded as an important method. According to the report of engineering technology in Committee of American Academy of Science, modeling and simulation technology can improve product quality by 5~15 times, increase material yield by 25%, reduce engineering cost by 13%~30%, reduce labor cost by 5%~20%, improve input equipment utilization rate by 30%~60%, shorten product design and trial production cycle by 30%~60% and so on[13].Simulation of machining process is an important part of digital manufacturing system [14]. It creates favorable conditions for the intelligence of the actual machining process through the effective prediction and optimization of various processing information in the machining system composed of machine tools, workpieces and tools, and also it is an important means to study and grasp the machining process. Numerical control machining simulation can be divided into geometric simulation and physical simulation according to whether physical factors are involved [15]. The cutting parameters, cutting force, and the other physical factors such as the machine tool, cutting tool and workpiece as a rigid body were not considered in geometric simulation, through the precise geometrical description, on the computer for processing cutting movement of the machine tool, cutting tool and workpiece in allowance removal process to obtain the dynamic display of the sense of reality, cut across to owe, collision test of machine tools and cutting tools, etc. Some advanced geometric simulation software, such as VERICUT [16], can also perform simple cutting load and speed (feed speed) optimization. Although process geometric simulation has many advantages, but the geometric simulation after all cannot fully reveal the real phenomenon and regularity of machining process, to guide the engineering application value by certain restrictions, so based on cutting force, cutting heat, factors such as machine tool dynamic characteristics has more value and significance of physics simulation, concern and attention. On the computer on the material removal rate, machine tools, cutting tools and

tooling system of power, heat and its dynamic change, to simulate the process of machining process can be observed visually physical properties, such as cutting trajectory, the chip formation process, stress field, temperature field, deformation and vibration movement form and characteristics of continuous or instantaneous parameters, such as, compensation for cutting parameter optimization, machining error prediction, improve Work efficiency and quality are of great significance and value [17].Currently, the research on geometric simulation is relatively comprehensive and in-depth, and many mature commercial processing simulation software has emerged, the typical one is UG of UGS Company in the United States. VERICUT developed by CGTech, Cimatron developed by Israel, MasterCAM developed by CNC Software, Virtual CNC developed by Predator, Camworks developed by Tesksoft, MPS developed by Huazhong University of Science and Technology and Tsinghua University, NCMPS developed by Harbin Institute of Technology, CAXA software developed by Haier Software Company of Beihang University, etc. However, due to objective reasons such as complex cutting mechanism and difficult modeling, there is no mature physical simulation system that can truly reflect the actual cutting process all over the world, and all research work is only in its infancy [18,19]. While the technology of digital had made considerable progress in recent decades. The concept of digital twin makes it possible to recognize the problems directly during machining processes, such as the deviations to the planning specifications or to derive targeted methods to the quality assurance and optimization of machining processes [20].

Currently, the investigation about end-milling was an involve extensive research lessons, such as temperature evaluation of tools energy consumption and heat flow, microstructure, stress state, surface roughness of workpiece [11]. During the completely end-milling process, the poor machinability and the consequent limitation on productive, tool life and workpiece integrity are mainly caused by high temperature in the machining system. However, the reports with regard to the evaluation of actual temperature distribution in the field of finish machining

of NNS parts are few [21]. In order to deal with an in-process visualization method of machining support the state recognition of human operators in machining, an accurate state estimation technique was proposed, which was associated with series of data in the machine simulation. By the new visualization method, the in-process evaluation of workpiece temperature and thermal deformation distribution were obviously established. Moreover, the coexistence of the real phenomenon and visualized information were very helpful for the operators to organize their own sensation and indicated information [22]. At last, the accurate machining states under the dispersion of phenomena was estimated by a Sensor-based Simulation (SBS) method. From the practical view, however it is very difficult to measure and evaluate the temperature and thermal deformation of workpiece during the end-milling process. Therefore, most of surface quality inspection was typically conducted as a post-process operation. In order to conduct temperature monitoring and to predict thermal deformation in finish machining of NNS part, a new method of selecting appropriate temperature measurement location was proposed, which is based on temperature variations of workpiece in machining process. The temperature variations are calculated by extending a conventional machining finite element method (FEM) simulation. In order to accurately estimate the temperature distribution in the end-milling process with limited number of measurement points, the effectiveness of measurable points (EoP) method had been proposed [23]. By combining the temperature history curve of FEM simulation and evaluation about sensitivity to process variation, appropriate measuring points could be determined. However, the number and location of measuring points were hardly decided by EoP method. Consequently, a new workpiece measuring framework was developed, which was focused on variety of workpieces, machining sequence, grasping workpiece and temperature state. Although the proposed simplification method was hard to apply various workpiece's shape, a statistic-based model simplification could generate simplified model.

1.2 Research Purpose

The objective of this research is to develop a systematic method to secure the machining accuracy in small-lot end-milling operation. To achieve the objective, we investigate a systematic procedure for model-based process monitoring for in-process estimation of thermal deformations from measured temperatures. In order to establish a relationship between the thermal deformation of workpiece and temperatures of measuring points in various machining situation, a systematic estimation procedure of workpiece deformation is proposed. The procedure can be an initial research about highly efficient digital twinning of machining process for small-lot production. For the pre-process evaluation of the machining process, a FEM based simulation for end-milling process, which can simultaneously calculated the time-series temperature and thermal deformation. Based on the predicted time-series information, it is possible to determine the complex relationship between the time-series temperature and time-series thermal deformation for various machining situation in advance. Consequently, in-process estimation of thermal deformation from measured temperature becomes promising.

- **Research Objective：**

In order to research on statistical forecasting of thermal deformation in End-milling, it is necessary to establish a more accurate method of screening thermally sensitive point and develop a digital twists monitor system by understanding the mechanism of frictional heat generation, thermal conduction and manufactural behavior in end milling process. According to the advanced research result, the initial EoP model was established, which was validated by combining FEM(Finite Element Method) simulation and end-milling machining experiment. The initial EoP model was based on the predicted thermal behavior of workpiece calculated by pre-process process simulation and estimated process variations. Magnitude of temperature change and sensitivity to the process variation are utilized to formulate the criterion. Effectiveness of the criterion is evaluated at limited cases. However, it is hard to determine a

sufficient number of measuring points. Hence, the research objective of program was proposed a new conservative measuring strategy such as utilizing maximum sensors and/or introducing preliminary evaluation. Then, the monitoring system of machining process would be developed by combining heat conduction simulator for workpiece machining, parameter identification system for heat conduction, digital twinning system developed.

1.3 Research construction

In this project, a systematic estimation method of workpiece's deformation is proposed. The relationship between the time-series of thermal deformations at machining points and temperatures in measuring points were analyzed by using Multiple Linear Regression (MLR) as a modeling tool, the data of which were completely conducted by FEM numerical simulation. In order to improve the effectiveness of temperature measuring points, the Akaike information criterion (AIC) and *p*-value were utilized to determine appropriate measuring points. After explaining proposed method, case studies for estimation of workpiece's thermal deformation were introduced. Estimation results with selected measuring points were compared with the results in different measuring points. The proposed estimation model to relate between thermal deformations and temperatures on selected points of workpiece could utilize to monitor the end-milling process. Finally, the application and error of proposed model in different case were discussed.

The research outline is shown as **Figure** 1.1.

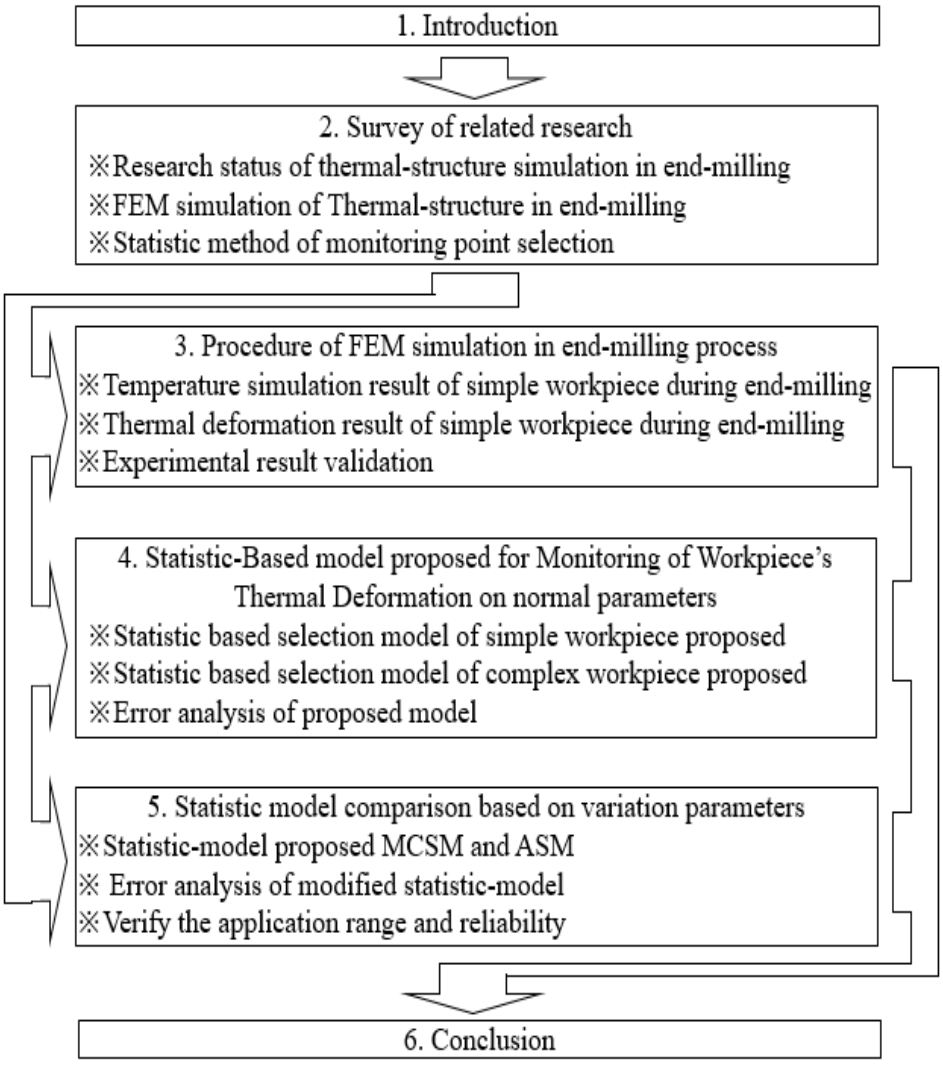

Figure 1.1 Research outline

In order to proposed a new conservative measuring strategy such as utilizing maximum sensors and/or introducing preliminary evaluation. The FEM simulation of workpiece's temperature and deformation are conducted. Based on various FEM simulation of workpiece's temperature series data, the new conservative measuring strategy is proposed. Then the parameter identification system is developed. In this step, the accurate parameters of heat source, heat conduct coefficient, specific heat and convective heat transfer coefficient are obtained. Finally, the statistical monitoring system of machining process would be developed by combining heat conduction simulator for workpiece machining, parameter identification system for heat conduction, digital twinning system developed.

The research work is mainly conducted as follow:

Step 1: Heat conduction simulator for workpiece machining

The ANSYS/APDL software is used in the heat conduction simulator for predicting the temperature distribution and evolution of workpiece during end-milling process. The material of workpiece is carbon steel S45C(JIS), of which the properties is consist of density, heat conduct coefficient and specific heat. The boundary conditions are initial temperature of workpiece, environment temperature, radius of end-milling tool, feed rate, interval distance between feed path and convective heat transfer coefficient, which is corresponding to the experiment condition. In order to analysis the effect factors of workpiece's temperature distribution and evolution, the response surface method is used in the heat conduction simulator. The initial parameters of heat source, heat conduct coefficient and convective heat transfer coefficient are 573 W, 58 W/(m×°C) and 550 W/(m^2×°C) respectively, which is change 50% as the up and down limitation. Hence, the total simulation groups is 13.

In this step, with the heat source, heat conduct coefficient and convective heat transfer coefficient changing, the evolution of maximum and minimum temperature of workpiece is detailed obtained, which is also the preparation for conservative measuring strategy of candidate points proposed.

Step 2: Parameter identification system for heat conduction problem

When the temperature series data of most sensitive measuring point in workpiece under different simulation parameters during end-milling machining process are extracted, the typical FEM simulation parameters is used for actual experiment conducting. Then the experimental temperature series data of the same measuring point is also extracted. By comparing and analyzing FEM simulation results and experimental results in the same temperature measuring points, the detail FEM simulation parameters of heat source, heat conduct coefficient and convective heat transfer coefficient in different end-milling machining segment are obtained.

Meanwhile, the temperature series data of other measuring points in actual experiment are also extracted to validate the FEM simulation result of corresponding measuring points. Hence, the accuracy of FEM simulation parameters are completely guarantee. Final, the parameter identification system is totally established.

In this step, it is necessary that temperature data at different time of measuring point in actual experiment is included by the range of different FEM simulation parameters result. The FEM simulation parameters are successfully identified. If not, the changing range of heat source, heat conduct coefficient and convective heat transfer coefficient have to be enlarged again. Hence, the accuracy of parameter identification system is suitability guarantee.

Step 3: A new conservative measuring strategy of candidate points proposed

The surface response method is used in the FEM simulation of workpiece's temperature evolution and distribution in end-milling machining process, which is benefit for saving calculation resource and covering all factors changing. Based on the EOP model, the sensitive temperature changing point under different FEM simulation parameters of heat source, heat conduct coefficient and convective heat transfer coefficient is selected from limited candidate points. However, the sensitive point is only limited in the candidate points. The number and location of candidate points are uncertain, which also leads an uncertain error of EoP model. In order to decrease the error of EoP, a new conservative measuring strategy such as utilizing maximum sensors and/or introducing preliminary evaluation is initially proposed to ensure the number and location of candidate points selected, which is the statistic-based measuring points selection model.

In this step, the most sensitive measuring point is accurately obtained by combining the statistic-based measuring points selection model and new conservative measuring strategy. Hence, the temperature series data of the most sensitive point during end-milling machining process is extracted, which is benefit and prepared for the parameter identification system

developed. The relationship between the time-series of thermal deformations at machining points and temperatures in measuring points were analyzed by using Multiple Linear Regression (MLR) as a modeling tool, the data of which were completely conducted by FEM numerical simulation. In order to improve the effectiveness of temperature measuring points, the Akaike information criterion (AIC) and *p*-value were utilized to determine appropriate measuring points.

Step 4: Temperature prediction error and new model application

In order to accurately and timely evaluate the temperature distribution of workpiece during end-milling process, the error model of measuring point's temperature between FEM simulation and experiment is established. With the error model, the parameters, such as heat source and convective heat transfer coefficient, are timely improved to closely actual experiment parameter. The FEM simulation is more accuracy to predict the temperature distribution of workpiece. As the temperature distribution of workpiece is accurately predicted, the deformation prediction of workpiece is also accurate in the end-milling process. According to combining the surface integrity requirement and the thermal deformation prediction, the parameters of end-milling machining process is timely optimal. Meanwhile, the FEM simulation parameters is modified again by comparing experiment temperature series data with FEM simulation results. The thermal deformation of workpiece under new end-milling machining process parameters is periodically predicted. Then the parameters of experimental end-milling machining process are periodically modified until the high surface integrity requirement is satisfied. Finally, the new model application would be discussed by combining numerical simulation result and experimental measuring point temperature monitoring result, which is the closed-loop system and used to conduct workpiece machining and guarantee better surface integrity in end-milling machining process.

In this step, the shorter period of parameters modification in experimental end-milling

machining process and parameters identification in FEM simulation are, the more surface integrity requirement satisfy. The error of the new model are also seriously important, which is systematically analysis in this program.

- **Research feature and innovation:**

(1)In order to improve the accuracy of EoP model, the statistic-based measuring points selection model is initially proposed, which is benefit for analysis the error between FEM simulation and experiment simulation.

(2)Comparing with the conventional FEM simulation research, the parameters of FEM simulation are variable value, which is real-time corresponding to the experiment result of measuring point during the end-milling process.

(3)The application of statistic-based measuring points selection model is discussed. The multiple model is proposed by basing the statistic-based measuring points selection model. Hence, the FEM simulation is closely to visualize the actual temperature distribution of workpiece.

1.4 The value of interdisciplinary research

Combining information technology into conventional research discipline has been investigated as researches of Cyber-Physical System. The basic method of this research is applying statistic modelling to production field. To achieve appropriate results, it is not an application problem but a practical implementation based on the deep understanding of actual process. Through the implementation, an ideal procedure of the modelling can be polished and the applicability of the procedure will enhanced. This bi-directional interaction leads higher technological phase. In this research, simple application of standard statistic methods are not suitable because of lack of preliminary information. Therefore, a process simulation technology and process knowledge of end-milling process should be integrated to enhance the modeling

procedure. Moreover, this research can be accelerated when the advanced modelling method like Deep Learning is involved to this research. End-milling is one of the most important machining process, which is satisfied with the requirement of high quality and agile production. However, during the end-milling process, the friction heat between tool and workpiece is very larger, which is sharply increased the temperature of workpiece to lead thermal expansion generation. The error generation process of the end-milling is complex and affected by many peripheral conditions. Therefore, it is hardly to guarantee the dimension precision of workpiece, especially for location of heat source. In order to improve the dimension precision of workpiece during end-milling process, a quasi-empirical modeling method is proposed to real-time forecast the temperature and thermal expand of workpiece, which is possible by the rapid development of computer technology. Finite element method (FEM) is generally used in process simulation of end-milling. However, real-time calculation of FEM analysis is time consuming, especially for complex workpiece, which reduces the efficiency of process simulation in end-milling. Therefore, the Multiple Linear Regression (MLR) and Akaike Information Criterion (AIC) of statistic method are adopted to propose a quasi-empirical model to evaluate the complex relationship between the time-series temperature and time-series thermal deformation for various machining situation in advance. In addition, the time-series temperature is easy and convenient to measure by the temperature sensor during the end-milling process. Hence, in-process estimation of thermal deformation from measured temperature becomes promising by utilizing a quasi-empirical model, which is benefit for increasing the efficiency of guaranteeing dimension precision of workpiece during end-milling.

1.5 The social value of research result

As one of Japanese competitive industries in world, machining industry including end-milling operation generates large production value every years. Billions of workpieces are

produced by end-milling machining. Meanwhile, so many workpieces are disqualified by low dimension precision, which is partly effected by thermal expand. Therefore, if process monitoring with the quasi-empirical model is equipped in end-milling machine, the dimension precision of workpiece would be certainly guaranteed to improve the qualification rate of production. As the dimension precision of workpiece is guaranteed, the application range of end-milling would be extended. The more complex workpiece would be produced by end-milling to further increase production value, which is also benefit for enhancing Japanese competitive end-milling industry. In addition, the cost of production would be obviously reduced, which is benefit for Japanese company to obtain more profit.

2 Survey of related research

2.1 Thermal analysis models in machining

So far, although the researchers from all over the world in order to better forecast and measure the cutting temperature and work for a large number of theories and experiments, but they mainly devoted to grinding, turning and other simple processing temperature field researches, there are little progress in milling progress, and milling machining mentioned is little achievements. The moving heat source method was proposed by Jaeger[24] in 1942, and most of analytical modeling work followed this idea, but the heat source model, heat distribution ratio and boundary condition of different models should be modified according to the specific cutting conditions. The current mainstream cutting temperature measurement methods include thermocouple method, optical/thermal radiation method, thermophysical effect method, etc. [25,26]. However, the existing technical methods are limited by the detection range and accuracy, so it is difficult to accurately measure the temperature field in the cutting deformation zone in the three-dimensional complex machining process.

The moving heat source method was firstly introduced into the research of grinding heat conduction by Outwater [27], he believed that the grinding heat came from the shear surface, and the sliding heat source theory could be applied to analyze the workpiece heat conduction under the influence of the shear plane heat source. The criterion for the existence of grinding wheel continuous heat source was analyzed [28], an explanation of the grinding heat was mainly generated on the abrasive wear plane was given. The grinding heat converted to the workpiece, grinding wheel, chip and coolant were quantitatively analyzed and the boundary of thermal damage to the workpiece was predicted[29,30]. An oblique plane thermal analysis method was used to estimate the grinding temperature of deep grinding processes [31]. The influence of different grinding processes on temperature and heat distribution ratio under Minimum quantity lubrication (MQL) was investigated [32,33].

A lot of systematic and extensive temperature field modeling for right-angle

cutting were researched [34-37]. Komanduri[38-40] summarized this previous work and predicted the temperature distributions of chips, tools and workpieces using improved Jaeger and Hahn models and the mirror heat source method. The variation factor of workpiece and tool material heat characteristic varied according to the temperature. The factors of the thermal characteristics of workpiece and tool material with the temperature into consideration in cutting temperature modeling, which could determine the material thermal characteristic parameters under different temperatures combining moving heat source and iterative method[41]. Karpat[42] further applied Komanduri's method to modeling the temperature field of a negative fore-angle chamfering tool, besides the heat sources in the first and second deformation zones were considered, a dead zone heat source was added near the chamfering zone in the model, and the predicted temperature distributions on the workpiece, chip and tool were compared and verified with the finite element simulation results.

The moving heat source method is suitable for the condition that the cutting heat source moves uniformly in a straight line, although this method can be reasonably revealed in cutting heat transfer law of two-dimensional cutting processes, such as grinding, right-angel cutting and so on, but there are in the process of milling cutter complex geometry, intermittent non-right angle cutting, variation of cutting thickness according to cutting time which were different from the two-dimensional cutting, moving heat source in response to these challenges seem to be powerless[43,44]. During milling, the heat source on the tool and the heat conductor remain relatively static, while the heat source in the workpiece moves on the surface of the heat conductor as the milling cutter rotates, so it is more difficult to establish the workpiece temperature model under the influence of the rotating heat source than the tool temperature field modeling. Based on the above reasons, the current achievements in terms of milling temperature field analytical modeling is not great, a little about the document of milling temperature field and more focus on the temperature distribution of cutting tools and its influence on the cutting tool service life and wear, the research reports about the temperature field of orthogonal milling workpiece end and its effect on the machined

surface quality are more difficult to find [45].

The heat source is separated into moving line heat sources during the solution, since the rotation angle and instantaneous cut thickness corresponding to each line heat source are different, the heat flux density on each line heat source is also different. Richardson established the relationship between the heat flux density of each line heat source and the average heat flux density of the arc surface heat source [46]. The average heat flux density of the arc surface heat source was calibrated by experiments, and the temperature field of the workpiece can be obtained by integrating the temperature rise function of each discrete line heat source within the tangent antenna.

A good arrangement and review of the existing cutting temperature monitoring methods was conducted, among which the most important thermocouple method and optical/thermal radiation method occupy the majority of the application share in this field [47]. Since the thermocouple technology was applied to the turning temperature measurement test by Gottwein[48] in Germany and Shore[49] in the United States almost at the same time in 1920s, this traditional and practical method has been widely used by researchers engaged in cutting research for nearly a century.

Thermocouple method can be divided into natural thermocouple method [50,51] artificial thermocouple method [52] and semi-artificial thermocouple method [53] according to different measurement methods. A method of measuring grinding temperature by metal film/workpiece thermocouple is proposed [54]. Li[55] measured tool temperature in hard turning by embedding a thin-film thermocouple array into a PCBN tool. Light/heat radiation method is based on the cutting heating radiation of infrared or color spectrum to indirectly determine the size of the cutting temperature, according to the different testing principles can be divided into infrared thermal imager (CCD) method [56,57] and optical fiber one-two-color thermometer [58] and other factions. Thermophysical effect law is a method to indirectly infer the cutting temperature based on some physical properties of materials easily affected by temperature, including metallographic structure method, microhardness method, coloring method and so on.

2.2 Temperature monitoring research of Thermal-structure in machining

Thermal variation is important physical phenomena in cutting process. Cutting heat and cutting temperature caused by cutting heat, not only directly affect the tool wear and service life, cause the workpiece temperature rise, also directly affect the machining precision of workpiece (deformation) and the surface quality of the parts has been processed (work hardening, workpiece burn), etc., therefore, the study of the production of thermal and its variation, which is an important aspect of the metal cutting process. According to different modeling methods, the cutting temperature model can be divided into analytical model and numerical model.

For the analytical calculation of cutting temperature, Jaeger[59] first gives the analytical results of the approximate steady-state temperature distribution caused by a band heat source moving at a constant speed on the surface of a semi-infinite body as its action time approaches infinity, which is a classic example of the heat source method. This moving heat source model is of great significance to the theoretical calculation of cutting temperature and has become the theoretical basis of many analytical models of cutting temperature. The heat source on the shear surface moves at the cutting speed along the cutting direction of the semi-infinite body, and all the mechanical energy is converted to the shear energy on the shear surface, and the average temperature in the cutter-chip contact zone is predicted[60,61]. The shear surface heat source moves at a shear speed over a semi-infinite body, calculate the heat flux by assuming that all the mechanical energy is converted into heat energy. The heat conduction problem during chip formation is equivalent to the sliding contact heat conduction problem described by Jaeger moving heat source model [62]. The shear surface heat source is treated as plane heat source in the above models, so the predicted shear surface temperature is sometimes too high. A distributed heat source model to deal with the friction heat source on the front tool surface was used, so that the predicted temperature tends to be reasonable [45]. The model established by Wright [63] is similar to Boothroyd's model, but more complex assumptions are used to deal with the friction heat source on the rake surface. He treats the rake surface contact as partially plastic (viscous friction) and

partially elastic (sliding friction) contact. Venuvinod and Lau [64] used a modeling method similar to Loewen-Shaw's model to establish a slanting moving heat source model on the shear plane of a semi-infinite body, and adopted more general assumptions to make the model's adaptive surface wider. This model is the only analytical model which can be directly applied to 3d bevel cutting process. The tool temperature was calculated by assuming that the shear surface was a heat source with infinite roughly moving heat and uniform heat, and calculates the average temperature of tool front surface by simplifying the shear surface to an inclined moving surface heat source with the same speed and cutting speed. An analysis different from Jaeger's that the intensity distribution of the friction heat source on the knife-chip friction surface was proposed, which is not uniform in most cases and has a great influence on the friction temperature. He derived the formula for calculating the temperature distribution of the knife-chip friction surface and the formula for the average temperature distribution. Domestic and foreign researchers have done a lot of research work on the analytical calculation of cutting temperature field, but the theoretical analytical calculation of iron cutting temperature field is very little. Because theoretical analytical calculations need to simplify many conditions, in most cases, obviously unreasonable assumptions will be adopted; otherwise, the solution will not be obtained [65-69]. With the development of computer software and hardware technology, numerical calculation method has been widely used in the research of cutting temperature field [70-72]. Similar to the finite element prediction model of cutting force, the cutting temperature field is mainly simulated from the Angle of orthogonal cutting mechanism, and the numerical methods adopted include boundary element method [73,74], finite difference method [68,75,76] and finite element method [77-81]. Finite element method was used in Hamid and Wifi [82] et al researches to analyze thermal-mechanical coupling of discontinuous cutting process. In the three-dimensional finite element model, the shear and friction heat sources are regarded as uniformly distributed plane heat sources. The shear surface temperature and friction heat were calculated according to the capacity of loss in the cutting process, and then the mean temperature of the shear surface was calculated by

the formula of mean temperature in the steady cutting process.

The numerical models of continuous cutting and iron cutting was established based on the finite difference method , which can be used to predict the temperature field of the tool and chip in the cutting process. In order to determine the transient temperature change of iron cutting, the cutting thickness is discretized with time, and each discrete cutting interval can be regarded as the steady cutter-chip temperature field [83]. The simulation results of continuous and discontinuous cutting agree well with the experimental temperature. The temperature model of waveform cutting edge blade based on Jaeger theory and plane blade temperature model was established by Li Zhenjia et al. [84] which could predict the tool iron cutting temperature. The theoretical predicted value was consistent with the experimental results. In addition, some researches were researching in the cutting temperature field based on the finite element model of a given heat source. 3d finite element method was applied to simulate the temperature distribution of the contact surface between the workpiece and the tool and the temperature distribution inside the workpiece in the process of high-speed milling aluminum alloy thin-walled parts [85]. In the simulation, the discontinuous cutting in high speed milling is simplified to continuous cutting, and the heat flux density is averaged over time to keep the total heat flowing into the workpiece in unit time unchanged. The model was assumed that the heat source in the iron cutting area is static, the action of the heat source in the iron cutting area was not considered before the time, and the discontinuous cutting characteristics of the iron cutting process would not be reflected. Therefore, the result of calculation is relatively rough. A finite element model was established for predicting the temperature field of workpiece iron cutting by considering the characteristics of discontinuous cutting in iron cutting. In the model, the heat source in the process of cutting workpiece from cutter tooth to cutter tooth was regarded as surface heat source. The surface heat source acts on the iron cutting surface, and the heat source intensity was equal to the superposition of all line heat source intensity generated by cutter tooth in the process of cutting workpiece once. The finite element model based on the given heat source was to load the known heat source as the

known boundary condition, to calculate the temperature field distribution. The advantage of this model was that it can directly reflect the heat conduction process of the cutting temperature field, but the disadvantage was that this method usually needs more assumptions to simplify the boundary conditions, and too many assumptions will reduce the truth of the simulation.

2.3 FEM simulation of Thermal-structure in machining

2.3.1 Heat conductive classic theory

In the process of metal cutting, the heat conduction problem is characterized by the heat source has a certain shape and size, and it is dynamic and has a certain heat output, but the boundary conditions are mostly unknown. Therefore, heat source method is more suitable than traditional analytical method or numerical method for heat conduction in machining process. The heat source method is the solution of the solid differential equation of heat conduction. For those whose thermal conductivity is infinite and where the heat source is concentrated in a very small volume, the heat source method yields the simplest solution. Therefore, heat source method was conducted in this topic.

① Differential equation of thermal conductivity

First, the differential equation of heat conduction is established. Fourier proved by experiments [86], in solid heat conduction, heat flux is proportional to temperature gradient:

$$q \propto \frac{dT}{dx} \tag{2-1}$$

Where q is heat flow density in the equation,

$$q=\frac{Q}{A} \tag{2-2}$$

In above equation: Q -- heat flux;

A-- Cross sectional area of heat flow

By incorporating the proportionality constant, Equation (2-1) can be written as:

$$q=-\lambda\frac{dT}{dx} \tag{2-3}$$

Fourier's heat conduction law could be obtained by substituting equation (2-2)

$$Q = -\lambda A \frac{dT}{dx} \tag{2-4}$$

The above formula applies to one-dimensional heat conduction, and is extended to multidimensional heat conduction.

$$Q = -\lambda A \partial T / \partial n \tag{2-5}$$

The physical meaning of constant proportionality is the heat flux density generated in an object per unit temperature gradient, known as the thermal conductivity of the material (thermal conductivity).

The differential equation of solid heat conduction could be obtained by the principle of heat flux balance. The solid thermal conductivity model is shown in **Fig.** 2.1. Take any piece of solid with volume *V* and corresponding interface *S*, and take micro element *dS* on the closed surface *S*. Then the temperature gradient in the normal direction *n* is:

$$\frac{\partial T}{\partial n} = \frac{\partial T}{\partial x}\cos\alpha + \frac{\partial T}{\partial y}\cos\beta + \frac{\partial T}{\partial z}\cos\gamma \tag{2-6}$$

In the formula, $\frac{\partial T}{\partial x}$, $\frac{\partial T}{\partial y}$, $\frac{\partial T}{\partial z}$ are the temperature gradients in x, y and z directions; α, β, γ are the included angles between the normal line n and the x, y and z coordinate axes respectively.

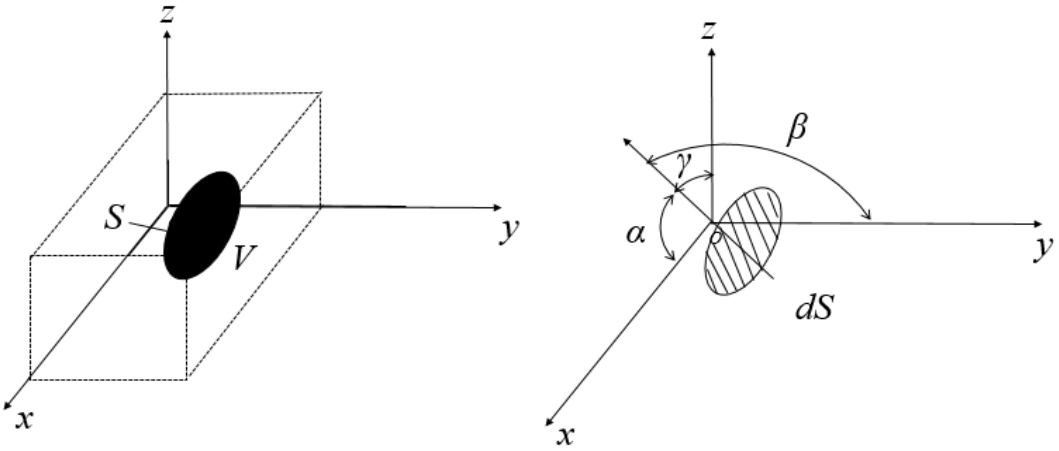

Figure 2.1 Solid thermal conductivity analysis diagram

According to Fourier's law, the heat outflow through dS in unit time can be determined as:

$$-\lambda\left[\frac{\partial T}{\partial x}cos\,\alpha+\frac{\partial T}{\partial y}cos\,\beta+\frac{\partial T}{\partial z}cos\,\gamma\right]dS$$

The sign of the above formula changed and double integral, the heat inflow of the whole interface S could be obtained:

$$\iint_S \lambda\left[\frac{\partial T}{\partial x}cos\,\alpha+\frac{\partial T}{\partial y}cos\,\beta+\frac{\partial T}{\partial z}cos\,\gamma\right]dS$$

The divergence theorem could be applied to transform the above equation into triple integral:

$$\iint_S \lambda\left[\frac{\partial T}{\partial x}cos\,\alpha+\frac{\partial T}{\partial y}cos\,\beta+\frac{\partial T}{\partial z}cos\,\gamma\right]dS=\iiint_V \lambda\left[\frac{\partial}{\partial x}\left(\frac{\partial T}{\partial x}\right)+\frac{\partial}{\partial y}\left(\frac{\partial T}{\partial y}\right)+\frac{\partial}{\partial z}\left(\frac{\partial T}{\partial z}\right)\right]dV$$

The left side of the equals sign represents the heat inflow through the interface S in unit time; The right-hand side is the heat absorbed per unit time by volume V. So this equation is consistent with the conservation of heat.

In addition, according to the concept of heat conduction, the total heat in volume V is:

$$\iiint_V cpT(x,y,z,\tau)dV$$

The growth rate for time τ is:

$$\frac{\partial}{\partial x}\iiint_V cpT(x,y,z,\tau)dV=\iiint_V cp\frac{\partial T}{\partial \tau}dV$$

The right side of equations (a) and (b) are different expressions of the same physical quantity, so it can be obtained:

$$\iiint_V\left[cp\frac{\partial T}{\partial \tau}-\lambda\left(\frac{\partial^2 T}{\partial x^2}+\frac{\partial^2 T}{\partial y^2}+\frac{\partial^2 T}{\partial z^2}\right)\right]dV=0$$

Since V is arbitrarily taken in the conducting product, the integrand function is identical

$$cp\frac{\partial T}{\partial \tau}=\lambda\left(\frac{\partial^2 T}{\partial x^2}+\frac{\partial^2 T}{\partial y^2}+\frac{\partial^2 T}{\partial z^2}\right)$$

Or

$$\frac{\partial T}{\partial \tau}=a\left(\frac{\partial^2 T}{\partial x^2}+\frac{\partial^2 T}{\partial y^2}+\frac{\partial^2 T}{\partial z^2}\right) \tag{2-7}$$

Where T is temperature, τ is time, λ is thermal conductivity, c is specific heat capacity, ρ is density, and a is thermal diffusivity ($a=\lambda/c\rho$).

In equations (2-6) and (2-7) are three-dimensional unsteady thermal conductivity differential equations.

② Temperature field of instantaneous point heat source

The basis of heat source temperature field addition is the temperature at any moment after the heat source emits a certain amount of heat in infinite medium. The temperature field of point heat source is shown in **Fig.** 2.2. There is a transient point heat source at coordinate origin O, and its calorific value is Q_O, the temperature rise of any point M(x,y,z,τ) (R is the distance from the origin O) at any time is T.

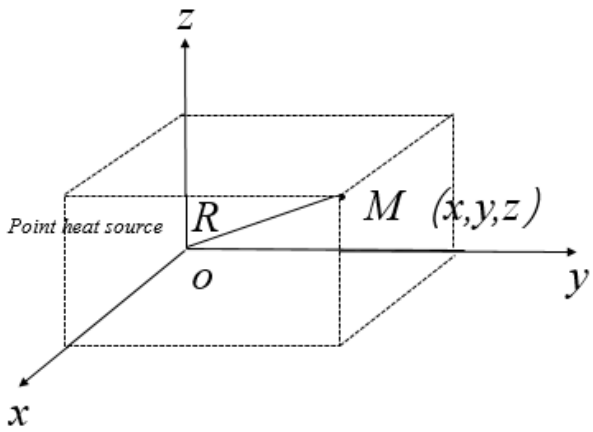

Figure 2.2 Temperature field of point heat source

According by formula (2-7),

$$\frac{\partial Q_O}{\partial \tau}=a\left(\frac{\partial^2 T}{\partial x^2}+\frac{\partial^2 T}{\partial y^2}+\frac{\partial^2 T}{\partial z^2}\right)$$

In the formula above, τ is time (s)

Fourier transform of the above equation was taken, then:

$$\frac{\partial F}{\partial \tau}=-a(\alpha^2+\beta^2+\gamma^2)F$$

In the formula above, α, β, γ represent the three components of the vector when the position of point M is represented by a vector, the magnitude of the vector

was assumed to be K, $K^2=\alpha^2+\beta^2+\gamma^2$

The formula above could be transferred into below

$$\frac{dF}{F}=-\alpha K^2 dt$$

Integrated both sides: $InF=-\alpha K^2 t+c$

$$F(K,t)=Aexp(-\alpha K^2 t)$$

The inverse Fourier transform of the above equation can be obtained:

$$T(R,t)=\frac{A}{(4\pi\alpha t)^{3/2}}exp\left(\frac{-R^2}{4\alpha t}\right)$$

According to the conservation of energy:

$$\frac{Q_O}{c\rho}=\int_0^{\infty}4\pi R^2\frac{A}{(4\pi\alpha t)^{3/2}}exp\left(\frac{-R^2}{4\alpha t}\right)dR$$

After integrating the above equation:

$$A=\frac{Q_O}{c\rho}$$

Therefore, the temperature rise generated by the instantaneous point heat source in the infinite conductor is:

$$T=\frac{Q_O}{c\rho(4\pi\alpha t)^{3/2}}exp\left(\frac{-R^2}{4\alpha t}\right) \quad (2\text{-}8)$$

Or

$$T=\frac{Q_O}{c\rho(4\pi\alpha t)^{3/2}}exp\left(-\frac{x^2+y^2+z^2}{4\alpha t}\right) \quad (2\text{-}9)$$

③ Temperature field of instantaneous finite-length heat source

The instantaneous finite-length heat source model was shown in **Fig.** 2.3, there is a linear heat source of length L in the infinite thermal conductivity medium, which produces instantaneous heat. The linear heat source recombines with the Z-axis, and the calorific value is Q.

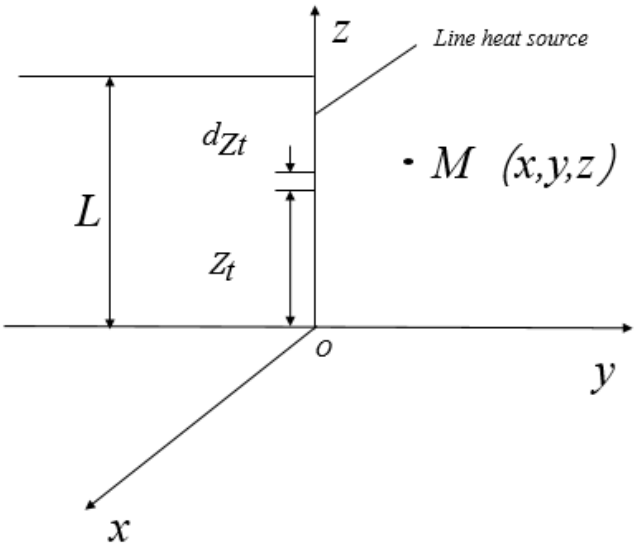

Figure 2.3 Temperature field of instantaneous finite-length heat source

If any micro segment dz_i of line heat source is taken,, then dz_i, segment heat source can be regarded as point heat source, and its calorific value is $Q_i dz_i$, and the temperature rise generated by it at any point *M(x, y,z)* :

$$dT=\frac{Q_i dz_i}{c\rho(4\pi\alpha t)^{3/2}} e^{\frac{x^2+y^2+(z-z_i)^2}{4\alpha t}} \tag{2-10}$$

Then, the total temperature rise generated by the whole heat source on point *M* is:

$$T=\frac{Q_i}{c\rho(4\pi\alpha t)^{3/2}} e^{-\frac{x^2+y^2}{4\alpha t}} \int_0^L e^{-\frac{(z-z_i)^2}{4\alpha t}} dz_i \tag{2-11}$$

It was assumed that, $\frac{z-z_i}{\sqrt{4\alpha t}}=u$, $z-z_i=u\sqrt{4\alpha t}$, then $-dz_i=\sqrt{4\alpha t}du$, when $z_i=0$, $u=\frac{z}{\sqrt{4\alpha t}}$, when $z_i=L$, $u=\frac{z-L}{\sqrt{4\alpha t}}$, the formula we can obtain shown as below,

$$\int_0^L e^{-\frac{(z-z_i)^2}{4\alpha t}} dz_i=\sqrt{4\alpha t}\int_{\frac{z-L}{\sqrt{4\alpha t}}}^{\frac{z}{\sqrt{4\alpha t}}} e^{-U^2} du=\frac{\sqrt{4\pi\alpha t}}{2}\left[erf\left(\frac{z}{\sqrt{4\alpha t}}\right)-erf\left(\frac{z-L}{\sqrt{4\alpha t}}\right)\right]$$

The $erf\left(\frac{z}{\sqrt{4\alpha t}}\right)$ in formula above is error function, its basic form$\frac{2}{\sqrt{\pi}}\int_0^p e^{-U^2} du=erf(p)$, different *p*-value error function can be obtained by looking up the table. Therefore, the temperature field of the finite long line heat source is:

$$T=\frac{Q_i}{2c\rho(4\pi\alpha t)} e^{-\frac{x^2+y^2}{4\alpha t}}\left[erf\left(\frac{z}{\sqrt{4\alpha t}}\right)-erf\left(\frac{z-L}{\sqrt{4\alpha t}}\right)\right] \tag{2-13}$$

④ Temperature field of heat source with finite motion duration

Now the temperature field of the heat source with finite duration of motion was established. Established the model of the heat source with finite length of motion as

shown in **Fig.** 2.4. It was assumed that a heat source with finite length of moving line L in z direction moves forward to x axis at velocity V, and the heat flux per unit time is q_i. The temperature rise at any point *M(x,y,z)* of the workpiece after time t is required. The whole time process T is decomposed into numerous tiny time intervals $d_{\tau i}$, and a tiny time interval $d_{\tau i}$ at time τ_i is taken for analysis. At the time interval $d_{\tau i}$, the heat generated by the instant moving line heat source $q_i d_{\tau i}$, acts on the beginning moment t, the time from this moment to the observation moment is τ $(\tau = t - \tau_i)$, and the distance from the instant point *M(x,y,z)* to the heat source is $x - v\tau_i$. According to Formula (2-13)

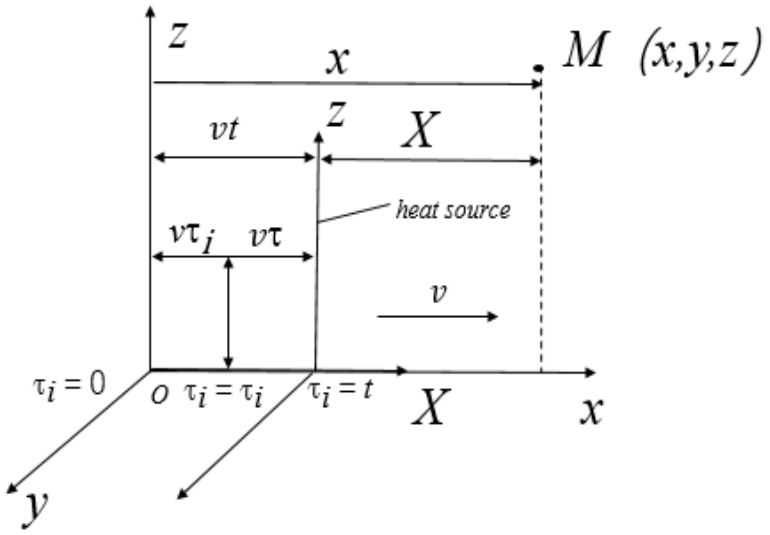

Figure 2.4 Heat source schematic diagram of moving finite length line

$$dT=\frac{q_i d_{\tau i}}{2c\rho(4\pi\alpha t)} e^{-\frac{(x-v\tau_i)^2+y^2}{4\alpha t}} \left[erf\left(\frac{z}{\sqrt{4\alpha t}}\right) - erf\left(\frac{z-L}{\sqrt{4\alpha t}}\right)\right] \tag{2-14}$$

Because of $\tau_i = t - \tau$, above formula could be transferred into

$$dT=\frac{q_i d_{\tau i}}{2c\rho(4\pi\alpha t)} e^{-\frac{(x-vt+v\tau)^2+y^2}{4\alpha t}} \left[erf\left(\frac{z}{\sqrt{4\alpha t}}\right) - erf\left(\frac{z-L}{\sqrt{4\alpha t}}\right)\right] \tag{2-15}$$

Then the temperature rise caused by the heat source to the point *M(x,y,z)* in the whole movement process is:

$$T=\frac{q_i}{8c\rho\pi\alpha} \int_0^L \frac{e^{-\frac{(x-vt+v\tau)^2+y^2}{4\alpha t}}}{\tau} \left[erf\left(\frac{z}{\sqrt{4\alpha t}}\right) - erf\left(\frac{z-L}{\sqrt{4\alpha t}}\right)\right] d_{\tau i} \tag{2-16}$$

Because of $d\tau = -d_{\tau i}$, when τi=0, τ_i=t, τ=0, substituted into the above formula:

$$T=\frac{q_i}{8c\rho\pi\alpha}\int_0^L \frac{e^{-\frac{(x-vt+v\tau)^2+y^2}{4\alpha t}}}{\tau}\left[erf\left(\frac{z}{\sqrt{4\alpha t}}\right)-erf\left(\frac{z-L}{\sqrt{4\alpha t}}\right)\right]d_\tau \quad (2\text{-}17)$$

In the above formula, $x-vt$ is the x-direction position of point *M(x,y,z)* at the observation time τ_i=t, namely the moving coordinate of x direction, which is represented by *X*, so $x-vt+v\tau=Xv$ can be substituted into the above formula:

$$T=\frac{q_i}{8c\rho\pi\alpha}\int_0^L \frac{e^{-\frac{(x+v\tau)^2+y^2}{4\alpha t}}}{\tau}\left[erf\left(\frac{z}{\sqrt{4\alpha t}}\right)-erf\left(\frac{z-L}{\sqrt{4\alpha t}}\right)\right]d_\tau \quad (2\text{-}18)$$

2.3.2 Basic theory of Thermal-structure in FEM simulation

Then the mathematical model of high speed cutting temperature is established by using the basic theory of heat source method.

① Temperature field generated by shear plane

In 1951, Hahn[87] established a model of moving in an infinite medium with the shear plane as the heat source, as shown in **Fig.** 2.5. According to the mechanism of chip formation during metal cutting, Hahn regarded the shear plane as a moving oblique band heat source, which moves at velocity in the workpiece.

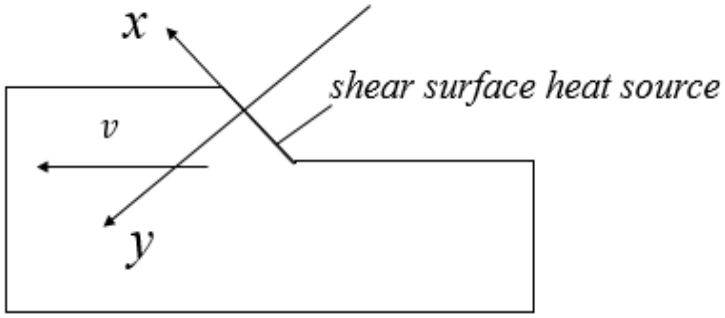

Figure 2.5 Schematic diagram of heat source on shear plane

The model established by Hahn is a heat transfer model moving in an infinite product.

In fact, there is still air above the object, and the thermal conductivity of air is much smaller than that of metal, so it can be regarded as an adiabatic boundary, so the object can be regarded as a semi-infinite object. In order to apply the heat transfer model

of moving in an infinite object established by Hahn to a semi-infinite object, it can be assumed that in addition to a real heat source Q_m, a heat source Q_m, which is exactly the same as Q_i, is placed at the symmetry of the boundary plane, and Q_i is called the mirror heat source of Q_m. If we still think of it as infinite, then the heat flux from Q_m going through the upper plane must be the same as the heat flux from the mirror reservoir. So there's no heat coming out of the upper plane, and that satisfies the adiabatic boundary. The improved model is shown in **Figure** 2.6.

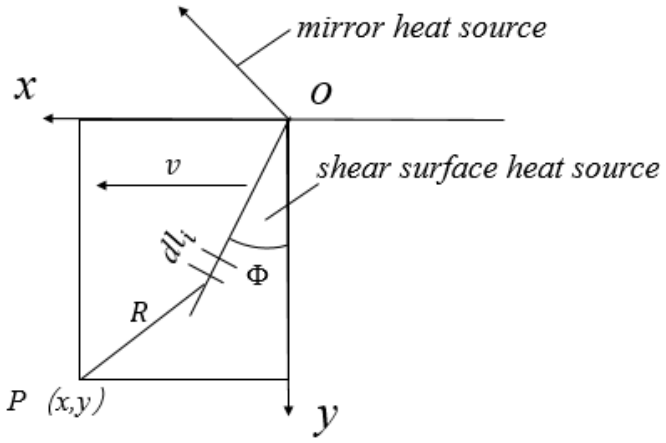

Figure 2.6 Improved shear heat source model

Based on the previous mathematical model of cutting temperature field, the shear heat source is regarded as composed of finite long line heat source with continuous motion, and a new model is established as three-dimensional heat conduction model.

In summary, the mirror heat source of the shear heat source is set up in **Fig**. 2.6. The shear heat source is *l* in width and *L* in length. The heat flux per unit time is q_{pl}. The width direction of the shear heat source is divided into several elements of length dl_i.

The distance from the micro original point *O* is l_i. Each element can be regarded as a linear moving heat source of finite length. *P (x, y, z)* relative shear point heat source infinitesimal, the coordinates of $x_i = \mathrm{x} - l_i \sin\emptyset$, $y_i = \mathrm{y} - l_i \cos\emptyset$, According to Equation (2-18), the temperature rise of any point *P(x, y,z)* generated by the element dl_i of the shear heat source is:

$$dT_{pl}=\frac{q_{pldl_i}}{8c\rho\pi\alpha}\int_0^l \frac{e^{-\frac{(x-l_i\sin\varnothing+v\tau)^2+(y-l_i\cos\varnothing)^2}{4\alpha t}}}{\tau}\left[erf\left(\frac{z}{\sqrt{4\alpha t}}\right)-erf\left(\frac{z-L}{\sqrt{4\alpha t}}\right)\right]d_\tau \tag{2-19}$$

Then the temperature rise of the shear heat source on *P(x,y,z)* is:

$$T_{pl}=\frac{q_{pl}}{8c\rho\pi\alpha}\int_{l_i=0}^l\int_0^l \frac{e^{-\frac{(x-l_i\sin\varnothing+v\tau)^2+(y-l_i\cos\varnothing)^2}{4\alpha t}}}{\tau}\left[erf\left(\frac{z}{\sqrt{4\alpha t}}\right)-erf\left(\frac{z-L}{\sqrt{4\alpha t}}\right)\right]d_\tau dl_i \tag{2-20}$$

Similarly, the temperature generated by the mirror heat source at point *P(x,y,z)* is:

$$T_{p2}=\frac{q_{pl}}{8c\rho\pi\alpha}\int_{l_i=0}^l\int_0^l \frac{e^{-\frac{(x-l_i\sin\varnothing+v\tau)^2+(y+l_i\cos\varnothing)^2}{4\alpha t}}}{\tau}\left[erf\left(\frac{z}{\sqrt{4\alpha t}}\right)-erf\left(\frac{z-L}{\sqrt{4\alpha t}}\right)\right]d_\tau dl_i \tag{2-21}$$

So, the temperature generated at *P(x,y,z)* is: $T_p=T_{p1}+T_{p2}$

② Temperature field generated by cutter/chip friction surface

The temperature field generated by the friction heat source on the tool/chip contact surface can be solved by the method of shear heat source. The difference is that the temperature field of the tool and chip should be calculated separately. Below respectively chip and tool temperature field distribution.

A) The friction generates a temperature field against the chip

The heat source on the friction surface is a moving band heat source relative to the chip, and the built model is shown in **Fig**. 2.7.

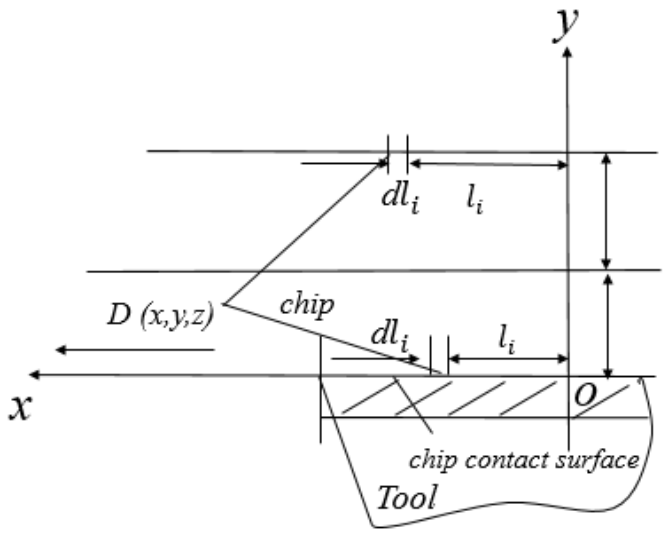

Figure 2.7 Temperature field of chip produced by friction heat source

The heat source with width of *l* friction surface (relative chip) is divided into

several differential units with length of dl_i, each of which is a heat source with linear motion of finite length (length L), and the heat source density is q_{dl}. According to Formula (2-18), the temperature of any chip point $D(x,y,z)$ generated by the heat source micro element on the friction surface is:

$$dT_{d1}=\frac{q_{dldl_i}}{8c\rho\pi\alpha}\int_0^l \frac{e^{-\frac{(x-l_i+v\tau)^2+(y)^2}{4a\tau}}}{\tau}\left[erf\left(\frac{z}{\sqrt{4a\tau}}\right)-erf\left(\frac{z-L}{\sqrt{4a\tau}}\right)\right]d_\tau$$

Thus, the temperature generated by the heat source on $D(x,y,z)$ of the friction surface can be obtained:

$$T_{d1}=\frac{q_{dl}}{8c\rho\pi\alpha}\int_{l_i=0}^l\int_0^l \frac{e^{-\frac{(x-l_i+v\tau)^2+(y)^2}{4a\tau}}}{\tau}\left[erf\left(\frac{z}{\sqrt{4a\tau}}\right)-erf\left(\frac{z-L}{\sqrt{4a\tau}}\right)\right]d_\tau dl_i \quad (2\text{-}22)$$

For the same reason, the temperature generated by the mirror heat source in $D(x,y,z)$ is:

$$T_{d2}=\frac{q_{dl}}{8c\rho\pi\alpha}\int_{l_i=0}^l\int_0^l \frac{e^{-\frac{(x-l_i+v\tau)^2+(y)^2}{4a\tau}}}{\tau}\left[erf\left(\frac{z}{\sqrt{4a\tau}}\right)-erf\left(\frac{z-L}{\sqrt{4a\tau}}\right)\right]d_\tau dl_i \quad (2\text{-}23)$$

Thus, the temperature generated by the heat source on $D(x,y,z)$, $T_d=T_{d1}+T_{d2}$

B) Friction generates a temperature field against the tool

The tool/chip friction heat source is a fixed rectangular heat source [89] for the tool, and the model is shown in **Fig**. 2.8.

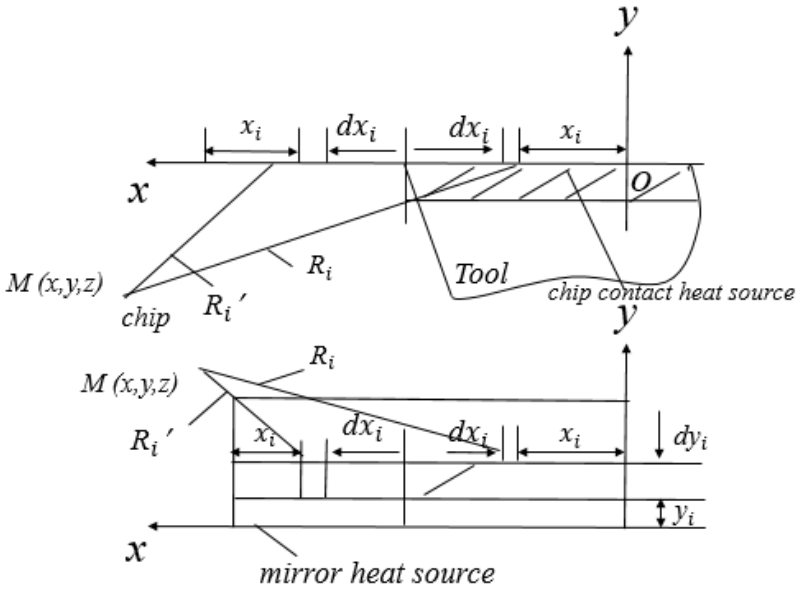

Figure 2.8 The frictional heat source produces a temperature field on the tool

Supposed the rectangular heat source is L in length and l in width, divide the

rectangular heat source into several differentials of d_{xi} and d_{zi} in width, then the heat flux per unit time of differentials is:

$$q_{dl}=\frac{q_0 d_{xi} d_{zi}}{Ll}$$

q_0 is the heat flow density of rectangular heat source; q_{dl} is the heat flux per unit time. The temperature generated by the micro element is:

$$T=\frac{q_{dl}}{2\pi\lambda R}$$

Then the temperature generated by the rectangular heat source element and mirror heat source element at any point *M(x, y,z)* is:

$$dT_M=\frac{q_{dl}}{2\pi\lambda}\left(\frac{1}{R_i}+\frac{1}{R_i}\right)d_{xi}d_{zi}$$

$$R_i=\sqrt{(\mathrm{x}-x_i)^2+y^2+(\mathrm{z}-z_i)^2}$$

$$R_i=\sqrt{(\mathrm{x}-2\mathrm{l}+\mathrm{x_i})^2+\mathrm{y}^2+(\mathrm{z}-\mathrm{z_i})^2}$$

The temperature at any point *M(x,y,z)* of the cutter is:

$$T_M=\frac{q_{dl}}{2\pi\lambda}\int_{z_i=0}^{L} d_{zi}\int_{x_i=0}^{L}\left(\frac{1}{R_i}+\frac{1}{R_i}\right)d_{xi} \qquad (2\text{-}24)$$

③ Temperature field under the combined action of shear heat source and knife/chip friction heat source

In practice, the cutting process is the result of the interaction of the two heat sources. The established model is shown in Fig. 2.9.

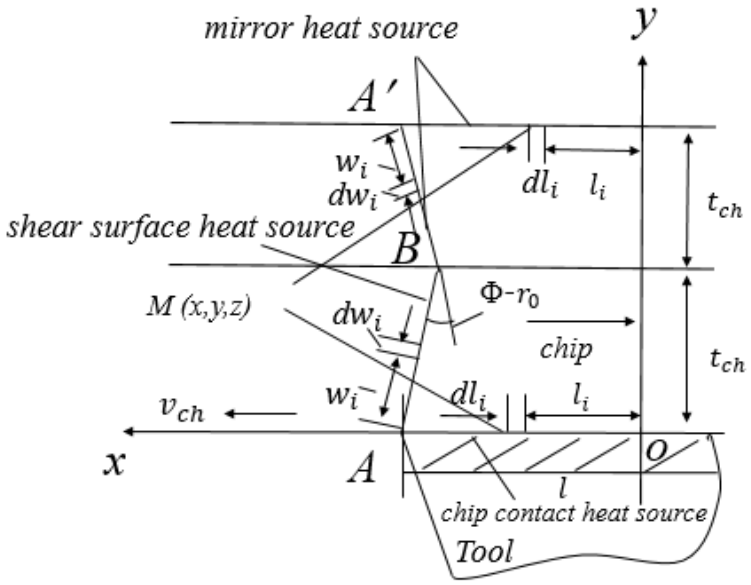

Figure 2.9 Temperature field under the combined action of shear heat source and friction heat source

As shown in **Fig**. 2.9, the shear heat source zone can be regarded as composed of many micro-segments with *A* distance of w and d_{wi} width along the direction of the heat source width. In the chip region, the shear heat source generates the temperature at any point *M(x,y,z)* in the chip:

$$dT_{M1}=\frac{q_{dl}d_{wi}}{8c\rho\pi\alpha}\int_0^l \frac{e^{-\frac{(x-x_i+v\tau)^2+(y-y_i)^2}{4\alpha t}}}{\tau}\left[erf\left(\frac{z}{\sqrt{4\alpha t}}\right)-erf\left(\frac{z-L}{\sqrt{4\alpha t}}\right)\right]d_\tau$$

The shear heat source generates temperature for *M(x,y,z)* :

$$T_{M1}=\frac{q_{pl}}{8c\rho\pi\alpha}\int_{wi=0}^{l_{ch}/\cos(\phi-r_0)}\int_0^l \frac{e^{-\frac{(x-x_i+v\tau)^2+(y-y_i)^2}{4\alpha t}}}{\tau}\left[erf\left(\frac{z}{\sqrt{4\alpha t}}\right)-erf\left(\frac{z-L}{\sqrt{4\alpha t}}\right)\right]d_\tau d_{wi} \quad (2\text{-}25)$$

Similarly, the mirror heat source of the shear heat source generates temperature on *M(x,y,z)* :

$$T_{M2}=\frac{q_{pl}}{8c\rho\pi\alpha}\int_{wi=0}^{l_{ch}/\cos(\phi-r_0)}\int_0^l \frac{e^{-\frac{(x-x_i+v\tau)^2+(2t_{ch}-y-y_i)^2}{4\alpha t}}}{\tau}\left[erf\left(\frac{z}{\sqrt{4\alpha t}}\right)-erf\left(\frac{z-L}{\sqrt{4\alpha t}}\right)\right]d_\tau d_{wi} \quad (2\text{-}26)$$

In above two formula, $x_i=l-w_i\sin(\phi-r_0)$, $y_i=w_i\cos(\phi-r_0)$, $w_i=0-t_{ch}/\cos(\phi-r_0)$, q_{pl} is the thermal intensity of the heat source in the shear plane.

Then the shear heat source and its mirror heat source generate temperature

$T_M=T_{M1}+T_{M2}$ on *M(x, y,z)*. Combined equations (2-22) and (2-23) generate the temperature by the friction heat source on *M(x,y,z)* :

$$T_{d1}=\frac{q_{pl}}{8c\rho\pi\alpha}\int_{l_i=0}^{l}\int_0^l \frac{e^{-\frac{(x-l_i+v\tau)^2+y^2}{4a\tau}}}{\tau}\left[erf\left(\frac{z}{\sqrt{4a\tau}}\right)-erf\left(\frac{z-L}{\sqrt{4a\tau}}\right)\right]d_\tau dl_i$$

And the mirror image of the frictional heat source at point *M(x,y,z)* :

$$T_{d2}=\frac{q_{pl}}{8c\rho\pi\alpha}\int_{l_i=0}^{l}\int_0^l \frac{e^{-\frac{(x-l_i+v\tau)^2+(2t_{ch}-y)^2}{4a\tau}}}{\tau}\left[erf\left(\frac{z}{\sqrt{4a\tau}}\right)-erf\left(\frac{z-L}{\sqrt{4a\tau}}\right)\right]d_\tau dl_i$$

q_{dl} is the thermal intensity of the friction heat source.

The temperature generated when the shear heat source and friction heat source sit together at any point *M(x,y,z)* in the chip:

$$T_M=T_{M1}+T_{M2}+T_{d1}+T_{d2}$$

The temperature rise analysis method for any place in the tool is similar to the above method. Since equations (2-25) and (2-26) are used to calculate the moving heat source, they cannot be used to calculate the distribution of the shear surface heat source on the tool. The shear surface heat source relative to the tool can be regarded as a fixed rectangular heat source simplified to the tool/chip contact surface, which can be calculated by equation (2-24). Equations (2-25) and (2-26) can be used to calculate the average temperature rise of the heat source on the shear surface at the chip edge (that is, the chip edge of the cutter contact surface). Due to the continuity of the heat flow, the temperature rise distribution of the chip edge on the cutter/chip contact surface should be the same as the temperature rise of the tool edge. By using equations (2-25) and (2-26) to get the average temperature rise, the heat flux density q_{pls} per unit time of the simplified heat source can be obtained. Using the same method of function analysis, we can obtain the related coefficients and exponents. Temperature generated at any point *M(x,y,z)* in the tool area:

$$T_M=\frac{q_{dl}}{2\pi\lambda}\int_{z_i=0}^{L} d_{zi}\int_{x_i=0}^{L}\left(\frac{1}{R_i}+\frac{1}{R_i}\right)d_{xi}+\frac{q_{dls}}{2\pi\lambda}\int_{z_i=0}^{L} d_{zi}\int_{x_i=0}^{L}\left(\frac{1}{R_i}+\frac{1}{R_i}\right)d_{xi} \quad (2\text{-}27)$$

$$R_i=\sqrt{(x-x_i)^2+y^2+(z-z_i)^2}$$

$$R_i=\sqrt{(x-2l+x_i)^2+y^2+(z-z_i)^2}$$

④ Mathematical Model of High Speed Milling Temperature

Next, a new mathematical model of the instantaneous temperature field of high-speed iron cutting is established.

End-milling coordinate system is shown in **Fig.** 2.10. The local coordinate system of the end-mill single-tooth cutter is *(x,y,z)*, while the overall coordinate system is *(X,Y,Z)*. Its local coordinate system *(x,y,z)* is the same as the coordinate system of the upper section (2.1.7) , to the local coordinate system *(X,Y,Z)*, the temperature rise of point *M* can be calculated according to the equations (2-22), (2-23), (2-25), (2-26) in Section 2.1.7.

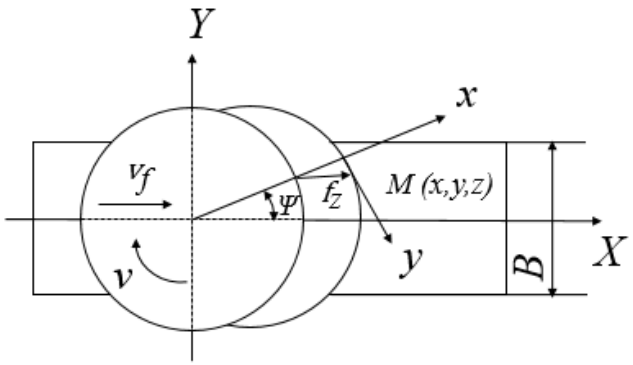

Figure 2.10 End-milling coordinate system

The coordinates of *M(X,Y,Z)* are transformed into the local coordinate system *(x, y, z)* as follows:

$$\begin{bmatrix} x \\ y \\ z \\ 1 \end{bmatrix} = \begin{bmatrix} \cos\varphi & \sin\varphi & 0 & -R \\ \sin\varphi & -\cos\varphi & 0 & 0 \\ 0 & 0 & 1 & 0 \\ 0 & 0 & 0 & 1 \end{bmatrix} = \begin{bmatrix} X \\ Y \\ Z \\ 1 \end{bmatrix}$$

φ is instantaneous position Angle, blade for end milling cutter radius R. *(x,y,z)* is the coordinates of point *M* in the local coordinate system, and *(X,Y,Z)* is the coordinates of point *M* in the global coordinate system. Using the above formula, the temperature rise of point *M* caused by single tooth cutting can be calculated. To obtain the joint action of multiple teeth on point *M*, the temperature rise of the cutting teeth on point *M* can be calculated separately and then superposed. The temperature field model of multi-tooth instantaneous cutting can be constructed by using the method of multi-tooth instantaneous cutting force model in end milling.

2.3.3 Stress-strain field theory of thermal elastic-plastic deformation in milling

Micro milling process, milling depth is small, the main interactions between the cutter and workpiece is squeeze, rub and plastic deformation, etc., due to the plastic deformation is more complex, there is no correspondence relationship between stresses and strains, but generally speaking, in a particular milling status, if there is a stress variation, the value must be a corresponding changed strain value, therefore, the theoretical model of residual stress on workpiece surface can only be established from the relationship between stress and strain increment. The formation of residual stress on the workpiece surface is caused by the elastic-plastic deformation of the material surface under mechanical load and thermal stress, in this article, the theoretical model of residual stress on workpiece surface is established in this paper based on the basic theory of thermo-elastic-plastic, and the influence of milling force and milling cutting heat on residual stress on workpiece surface is considered simultaneously.

According to the stress-strain increment relationship of material thermoelastic-plastic, the total strain increment of milling workpiece in elastic-plastic state includes elastic strain increment, plastic strain increment and temperature strain increment [88,89]

In elastic region, the total strain increment $d\{\varepsilon\} = d\{\varepsilon\}_e + d\{\varepsilon\}_T$ (2.27)

$\{\varepsilon\}_e$ and $\{\varepsilon\}_T$ is elastic strain increment and temperature strain increment respectively.

$$\{\varepsilon\}_e = [D]^{-1}\{\sigma\} \tag{2.28}$$

$$\{\varepsilon\}_T = [\alpha]dT \tag{2.39}$$

$$d\{\varepsilon\}_e = \frac{[D]^{-1}}{dT}\{\sigma\}dt + [D]^{-1}d\{\sigma\} \tag{2.30}$$

The equation (2.30) is substituted into (2.27), the new equation can be obtained shown as below

$$d\{\sigma\} = [D]\left(d\{\varepsilon\} - \left(\{\alpha\} + \frac{d[D]^{-1}}{dT}\{\sigma\}dT\right)\right) \tag{2.31}$$

It was set that $d\{\varepsilon\}_T = \left(\{\alpha\} + \frac{d[D]^{-1}}{dT}\{\alpha\}dT\right)$

Then it can be known that $d\{\sigma\} = [D](d\{\varepsilon\} - d\{\varepsilon\}_T)$, $[D]$ is elastic matrix of material.

In plastic region, the incremental stress-strain relationship of the material is as follows:

$$d\{\sigma\} = [D]_{ep}(d\{\varepsilon\} - d\{\varepsilon\}_T + d\{\sigma\}_T) \quad (2.32)$$

In equation (2.32), $[D]_{ep}$ is elastoplastic matrix of material; Since the thermo-elastic-plastic stress-strain of materials is nonlinear without one-to-one correspondence, the incremental stress-strain relationship needs to be linearized.

Elastic region, $\Delta\sigma = [D](\Delta\{\varepsilon\} - \Delta\{\varepsilon\}_T)$ (2.33)

Plastic region, $\Delta\sigma = [D]_{ep}(\Delta\{\varepsilon\} - \Delta\{\varepsilon\}_T + \Delta\{\sigma\}_T)$ (2.34)

$\Delta\{\varepsilon\}_T, \Delta\{\sigma\}_T$ are the parameters related to the temperature and stress, which can be regarded as initial stress and strain converted into equivalent nodal load.

Elastic region, $\Delta(R)_e = \iint_e [B]^T [D]\Delta\{\varepsilon\}_T dv$ (2.35)

Plastic region, $\Delta(R)_{ep} = \iint_e [B]\left([D]_{ep}\Delta\{\varepsilon\}_T - \Delta\{\sigma\}_T\right)dv$ (2.36)

In equation (2.35), (2.36), $[B]$ is geometric matrix

Finally we can obtain the equilibrium equation, $[K]\Delta\{u\} = \Delta\{R\}$ (2.37)

In equation (2.37), $[K]$ is overall stiffness matrix, the node displacement increment $\Delta\{u\}$ is calculated theoretically, and then according to the relationship between the displacement increment and the strain increment, the element strain increment $\Delta\{\varepsilon\}$ is calculated, finally, the stress increment $\Delta\{\sigma\}$ can be calculated from formula (2.33) or (2.34).

2.3.4 FEM simulation of workpiece's thermal-structure in End-milling

Thermodynamic coupling is the interaction and influence between cutting heat and cutting force generated in the contact zone of micro milling. The residual stress on the surface of the machined workpiece is the local high temperature of the workpiece caused by the cutting heat in the milling process, which forms an uneven temperature gradient on the surface of the workpiece, thus forming thermal stress. When the milling cutter exerts extrusion and ploughing action on the workpiece, which will lead to the

compressive stress of the workpiece material perpendicular to the workpiece direction, and the two stress states are mutually influenced and superimposed. In other words, the calculation of thermal-structural coupling stress field is to solve the structural deformation of the workpiece under the action of both heat and cutting force, and then remove the influence of load to allow enough time for the workpiece to rebound and cool down, and the obtained stress state is the residual stress of the workpiece. There are two methods for calculating thermal structure coupling field in ANSYS finite element simulation: sequential coupling method and direct coupling method

The direct coupling method applies to the interaction between two fields, which is highly nonlinear, and the two fields interact with each other. When using the direct coupling method, it requires high requirements on computer hardware, large amount of calculation and long calculation time. The milling temperature field has a large direct influence on the workpiece stress field, while the workpiece stress field has a small influence on the temperature field, which is suitable for using the sequential coupling method, so the workpiece temperature field can be analyzed first, if the temperature field is incorrect. Relevant parameters can be modified to ensure the correct temperature field, and then the workpiece stress field analysis, so the selection of sequential coupling field can save calculation time and improve efficiency.

2.4 Statistic method of monitoring point selection

2.4.1 Multiple Linear Regression (MLR)

Multiple linear regression (MLR) method [24] was proposed to establish the formula between two or more explanatory (independent) variables and a response (dependent) variable by fitting a linear equation. The normal form of the MLR model is calculated as follow:

$$Y_i=\beta_0+\beta_1 X_{1,i}+\beta_2 X_{2,i}+\cdots+\beta_k X_{k,i}+\varepsilon_i$$

Where Y_i is stand for the i_{th} measured dependent variable of Y. $X_{1,i}$, $X_{2,i}$, …, $X_{k,i}$ is stand for the ith measured independent variables of X_1, X_2, …, X_k respectively. β_0, β_1, β_2, …, β_k are stand for constant parameters, which are

calculated by the least square method. ε_i is stand for a random variable, which is normal distribution.

2.4.2 Akaike's Information Criterion (AIC)

Akaike's Information Criterion (AIC) provides a measure of model quality obtained by simulating the situation where the model is tested on a different data set. According to Akaike's theory, the most accurate model has the smallest AIC. If you use the same data set for both model estimation and validation, the fit always improves as you increase the model order, therefore, the flexibility of the model structure. Raw AIC is defined as follow [25]:

$$\mathrm{AIC}=\mathrm{N}^{*}\log\left(\det\left(\frac{1}{\mathrm{N}}\sum_{1}^{\mathrm{N}}\varepsilon\left(\mathrm{t},\hat{\theta}_{\mathrm{N}}\right)\left(\varepsilon\left(\mathrm{t},\hat{\theta}_{\mathrm{N}}\right)\right)^{\mathrm{T}}\right)\right)$$

$$+2n_p+N*\left(n_y*(\log(2\pi)+1)\right)$$

Where N is stand for the number of values in the estimation data set. $\varepsilon(t)$is stand for a ny-by-1 vector of prediction errors. θ_N is stand for the estimated parameters. n_p is stand for the number of estimated parameters. n_y is stand for the number of model outputs.

2.4.3 *p*-value in *t*-test

The one-sample t-test is a parametric test of the location parameter when the population standard deviation is unknown. The test statistic is defined as follow：

$$t=\frac{\bar{x}-\mu}{s/\sqrt{n}}$$

Where $\bar{x}$ is stand for the sample mean. μ is stand for the hypothesized population mean. s is stand for the sample standard deviation. *n* is stand for the sample size. *p*-value of the test, returned as a scalar value in the range [0,1]. *p* is the probability of observing a *t*-test statistic as extreme as, or more extreme than, the observed value under the null hypothesis[26]. Small values of p cast doubt on the validity of the null hypothesis. Consequently, the *p*-value is corresponding to the *t*-test value in Correlation Coefficient Boundary Table (CCBT). Finally, the procedure of proposed and optimized

statistic based selection model are conducted as shown in **Fig**. 2.11.

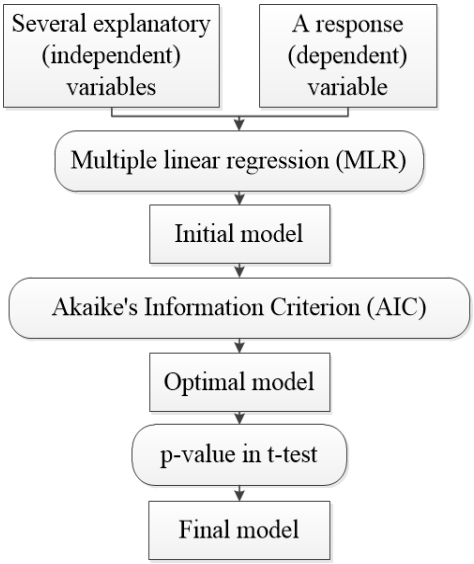

Figure 2.11 Flowchart of estimated model proposed and optimized

2.5 Summary

This chapter detailed introduces the development of thermal analysis models in machining. Most of analytical modeling work are proposed basing on the initial moving heat source method, including thermocouple method, optical/thermal radiation method, thermophysical effect method. During the grinding heat conduction research, the moving heat source method was firstly introduced. Then the grinding heat converted to the workpiece, grinding wheel, chip and coolant are quantitatively analyzed and the boundary of thermal damage to the workpiece was accurately predicted. Meanwhile, lots of systematic and extensive temperature field modeling for right-angle cutting are researched to analysis the temperature distribution of workpiece, chip and tool. In order to reveal cutting heat transfer law of two-dimensional cutting processes, the moving heat source method is introduced. The heat source is regards as a milling tool to manufacture the workpiece, which is separated into the rotation angle and instantaneous cut thickness corresponding to moving line. In addition, the thermocouple method is proposed to validate the thermal model. In fact, the thermal variation is important physical phenomena in cutting process, which has the very heavy effect on not only

directly affect the tool wear and service life, cause the workpiece temperature rise, also directly affect the machining precision of workpiece and the surface quality of the parts. The boundary element method, finite difference method and finite element method are proposed to analysis the cutting heat and temperature during the machining manufacture, which is systematically and scientifically discussed and analyzed by many international researchers. So far, the finite element method is most widely used in machining manufacture process, especially 3D finite element method, which is possible for predicting temperature distribution of tools, the contact surface between the workpiece and the tool, the whole workpiece during the process of high-speed milling. The FEM simulation of thermal-structure in machining is based on heat conductive classic theory and Stress-strain field theory of thermal elastic-plastic deformation. The ANSYS software is a commonly useful business software to calculate thermal structure coupling field by FEM code which could offer the two method, such as sequential coupling method and direct coupling method, which is mean that the temperature and thermal deformation distribution of tools, chips and workpiece could be directly displayed in the software. Hence, it is highly efficient method to research machining manufacture by ANSYS software, especially end-milling. According to literature review, the method of timely combine numerical simulation predict and experiment validation during the machining manufacture process is not proposed, especially in-process of end-milling, which is the basic outline for numerical twinning. Therefore, after introduce the theories of MLR, AIC and *p*-value, the main research content in this project is proposed the statistic-based model for monitoring the thermal deformation of workpiece by combing ANSYS software, MLR, AIC and *p*-value.

3 Procedure of FEM simulation in end-milling process

According to **Fig.** 3.1, the 3D additive manufacture simulation by ANSYS is consist of elements selection, model building, mesh generation, material properties, boundary condition and postprocessing.

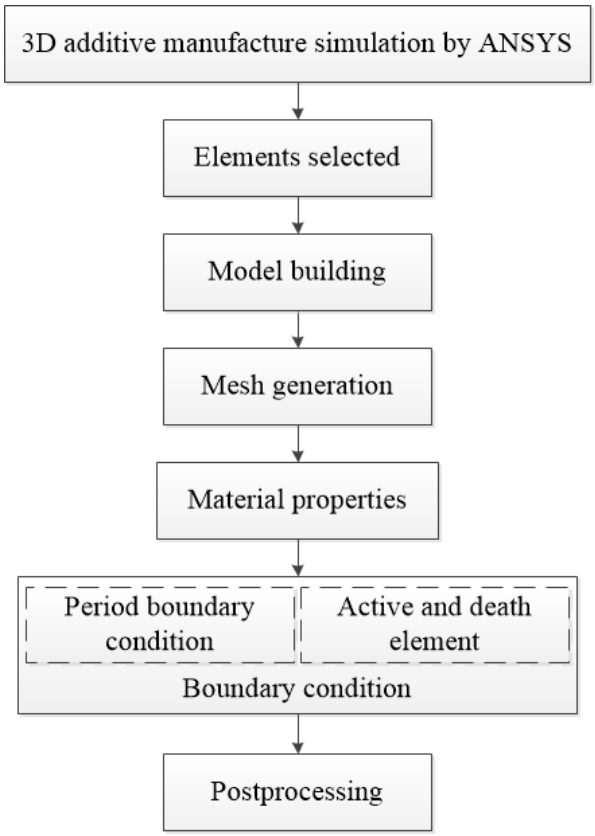

Figure 3.1 Procedure of FEM simulation

There are several steps in this paper to finish the end-milling thermal structure numerical simulation, which mainly contain the element selected, material properties definition, geometric model building, meshing, boundary condition transferring and APDL code and so on.

First, the mechanical-APDL programming method was conducted to establish model of workpiece under end milling process which had not an extremely influence to propose the new method about predict the sensitive points during cutting process.

3.1 Element selected

SOLID 70 has thermal conductivity in three directions, as shown in **Fig**. 3.2. The unit element has 8 nodes and only one temperature degree of freedom on each node, which can be used for 3d static or transient thermal analysis. The unit element can realize the transfer of uniform heat flow. After this option is selected, the thermal parameters of the element will be converted into similar fluid flow parameters, such as temperature degrees of freedom will be transformed into equivalent pressure degrees of freedom.

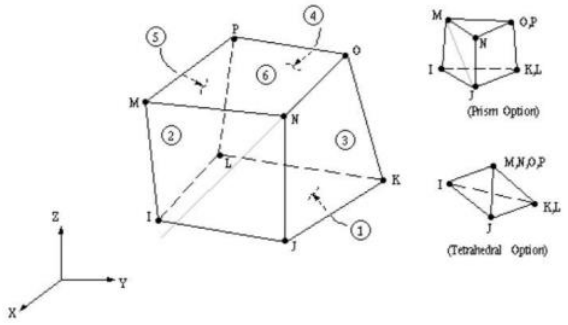

Figure 3.2 Solid 70 illustration schematic

3.2 Material properties definition

The basic constants, variations limited conditions and detail different boundary condition of carbon steel S45C (JIS) in end-milling process by FEM simulation are totally listed in the **Table** 1, **Table** 2 and **Table** 3 respectively. The surface shape of workpiece is rectangle. The diameter and feed rate of end-milling tool are φ16 mm and 0.00125 m/s respectively. The interval distance between tool paths is 10 mm.

Table 1 Basic constants of carbon steel S45C(JIS)

Name	Value
Density	7850 kg/m^3
Initial temperature	10.8℃
Environment temperature	10.8℃

3.3 Geometric model building

The simulation target is a block workpiece, as shown in **Fig.** 3.3 and the machining case for investigation is illustrated as **Fig**.3.4

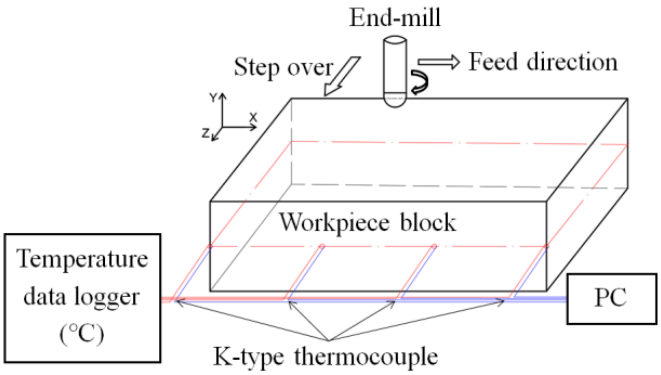

Figure 3.3 Schematic of test block, tool and monitoring arrangement

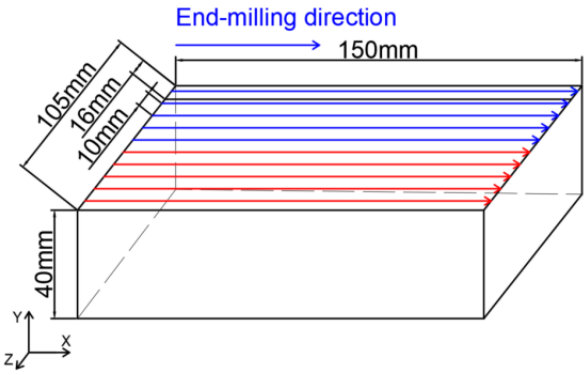

Figure 3.4 End-milling process of workpiece, blue line is stand for half machining tool path, tool path of full machining is combined blue line and red line

As an example case of the four temperature monitoring points at same side surface, the schematic of the end-milling operation system and thermocouple assemblage are shown in Fig.3.3. In this way, the temperature record is systematically conducted by combining temperature data logger and connected personal computer.

3.4 Meshing

Before the mesh division of the overall structure field structure, it is necessary to ensure that there are no single points, unconnected lines and curves in the geometric structure which the elements will make it impossible to form continuous areas in the "Mesh", increase the complexity of Mesh division at the boundary and even lead to mesh division failure. After that, mesh division and mesh optimization can be carried

out for the overall structure field structure, where the Mesh module is called. Through this module, we can set the specific parameters to get the optimized grid. Note that the grid here is a non-structural grid. The optimal mesh should not only ensure reasonable mesh size and density, but also save calculation time as much as possible. Parameter settings include k_0、k_{inf}、R related to one-dimensional mesh density and Amin, Smax/Smin related to two-dimensional mesh density. The calculation formula of one-dimensional mesh density is as follows (4-1).

$$d = \frac{k_0+k_{inf}R^2\rho^2}{1+R^2\rho^2} \qquad (4\text{-}1)$$

k_0、k_{inf}、A_{min}、S_{max}/S_{min} represent the node density on the straight line, the node density on the curve (with infinite curvature), the minimum Angle of the spatial grid triangle, and the ratio of the area of the largest triangle to the smallest triangle, respectively. By changing these parameters we can get meshes of different sizes and densities. Attention should be paid to avoid excessive mesh density at the intersection and corner of line segment, which makes it difficult to converge the calculation results. Therefore, in the finite element analysis, the type of element, the way of grid division and the number of element determine the accuracy of the calculation results. It is particularly important to select the appropriate element and the way of grid division and the reasonable number of element.

The FEM model of the workpiece with heat flux boundary condition is shown in **Fig**. 3.5, which is consist of 79500 elements.

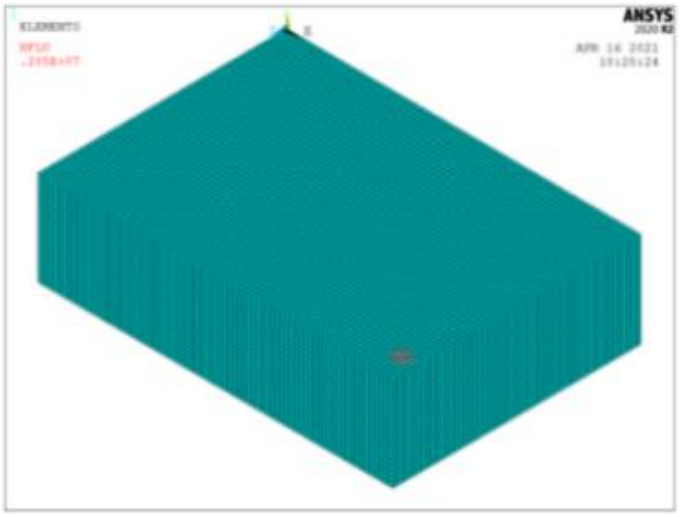

Figure 3.5 FEM model of workpiece

3.5 Boundary condition transferring

The finite element simulation calculation of workpiece thermal deformation involved in this paper belongs to coupling field analysis. Coupling field analysis refers to the interaction and influence of two or more physical fields in the process of finite element analysis, including thermal-stress coupling analysis, thermal-electric coupling analysis, fluid-structure coupling analysis, magnetic-thermal coupling analysis, etc.

ANSYS provides two methods to analyze the coupling field: direct coupling method and indirect coupling method.

(1) Direct coupling method

The coupling element of the direct coupling method contains all the necessary degrees of freedom related to the corresponding coupling field. This method is actually implemented by computing the element matrix or element load vector containing all the necessary terms.

(2) Indirect coupling method

Indirect coupling method, also known as sequential coupling method, mainly realizes the coupling of two fields by using the results of the first field analysis as the load of the second field analysis. For example, thermal-stress coupling analysis means that the node temperature obtained from thermal analysis is applied as a load in the subsequent stress analysis to achieve coupling.

According to the actual working conditions of workpiece in end milling process, the finite element simulation is calculated by indirect coupling method. The finite element simulation model was loaded with boundary conditions according to the specific end milling process. In thermal analysis and calculation, the frictional heat between the cutter and workpiece and the heat transformed form the plastic work are simplified as circular heat source for loading in end milling process of workpiece, as well as the boundary of convective heat transfer between the workpiece and air was considered. In structural analysis and calculation, according to the actual clamping condition of workpiece, the bottom of workpiece was fixed constrained. At the same

time, the temperature field of each time point in the thermal analysis and calculation process of workpiece is taken as initial temperature condition of structural calculation, finally, the finite element simulation process of whole thermal structural coupling of workpiece in end milling process was completed.

Because there are some errors in the process of boundary condition transformation, it is necessary to revise and perfect the material parameters and boundary conditions in the process of workpiece end milling by the method of inverse operation. Response surface method is to use polynomial function to approximate implicit limit state function through a series of deterministic experiments. By selecting test points and iteration strategy reasonably, the polynomial function can be guaranteed to converge to the failure probability of the real implicit limit state function. When the real limit state function is not very nonlinear, the linear response surface has high approximate accuracy. The basic idea of quadratic polynomial without cross terms: similar to linear response surface method, it only selects quadratic polynomial without cross terms to approximate implicit functional functions. There is no nonlinear analysis in the process of workpiece's deformation simulation analysis and calculation, mainly contains the linear analysis and calculation, therefore, the material parameters and boundary conditions in the finite element simulation analysis and calculation of workpiece thermal deformation in the process of machining were calculated by using linear surface response method. Material parameters and boundary conditions calculated by finite element analysis of thermal deformation in the process of workpiece end milling modified by response surface method are shown in **Table** 2 and **Table** 3 respectively.

Table 2 Variations limited conditions of carbon steel S45C(JIS)

Factor	Factor levels			Change limit
	-1	0	1	
A-Heat source ($\times 10^3$ W)	286.5	573	859.5	50%
B-Heat conduct coefficient (W/(m×°C))	29	58	87	50%
C-Convective heat transfer coefficient (W/(m^2×°C))	275	550	825	50%

Table 3 Detail boundary conditions of carbon steel S45C(JIS) for varied situation

Factors No.	A-Heat source ($\times 10^3$ W)	B-Heat conduct coefficient (W/(m×℃))	C-Convective heat transfer coefficient (W/(m^2×℃))
1	286.5	29	550
2	859.5	29	550
3	286.5	87	550
4	859.5	87	550
5	573	29	275
6	573	87	275
7	573	29	825
8	573	87	825
9	286.5	58	275
10	859.5	58	275
11	286.5	58	825
12	859.5	58	825
13	573	58	550

3.6 Temperature result

Temperature field calculation results of workpiece in end milling process are shown as below in **Fig.**3.6. Due to the transient analysis method is adapted in the FEM calculation of thermal analysis of workpiece in the end milling process, therefore, the temperature distribution results of workpiece at different time points in end-milling process can be viewed. According to the figure, with the passage of the time, the heat source moves according to the set trajectory on the surface of workpiece. As well as the process of heat source movement is the same as the process of cutting tool workpiece movement. When the cutting tool contact with the workpiece, there would be friction and plastic transformation work in the corner of workpiece, which could be transformed into heat source to affect the temperature distribution of whole workpiece. According to the calculation results of temperature field, with the progress of end-milling, the temperature is a little higher at the contact location between the surface of workpiece and cutting tool, and the maximum temperature will reach to 200℃, the temperature influence range mainly concentrated at the contact area between the tool and workpiece surface, the temperature influence is lower in other areas. It indicates that the area was

influenced by temperature mainly concentrated in the contact area between tool and workpiece surface in the process of end-milling.

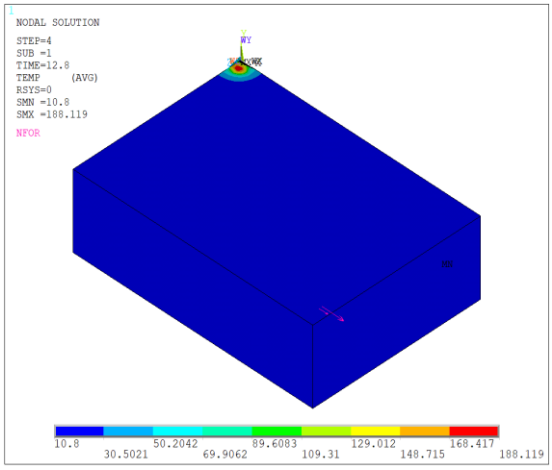

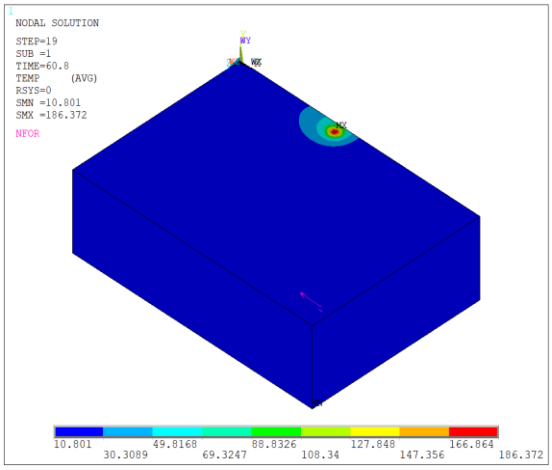

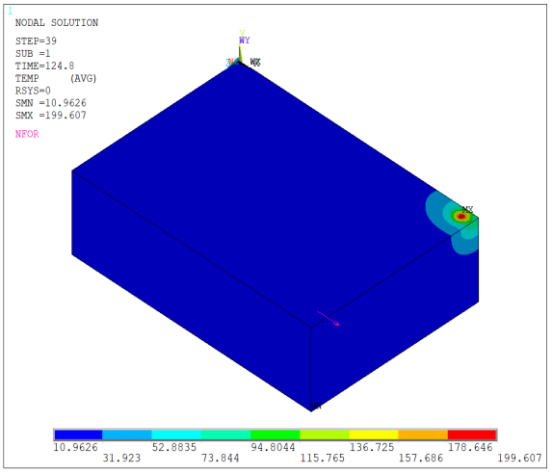

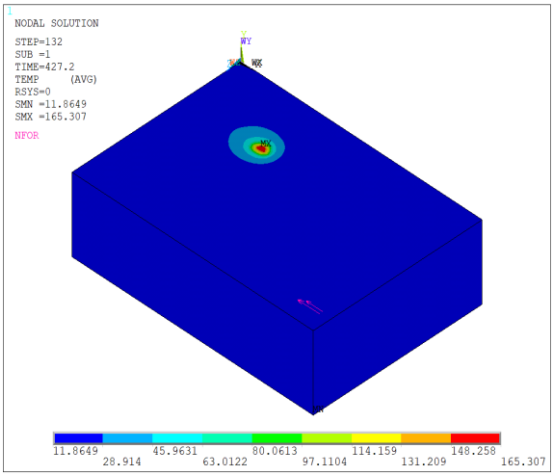

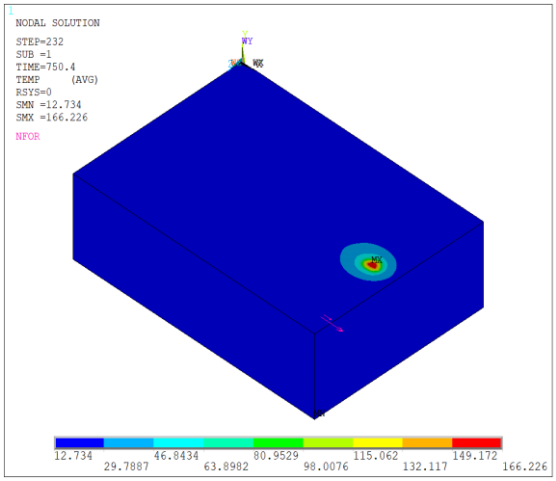

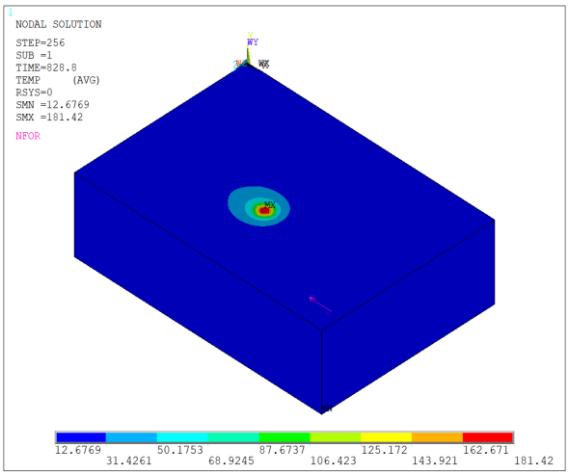

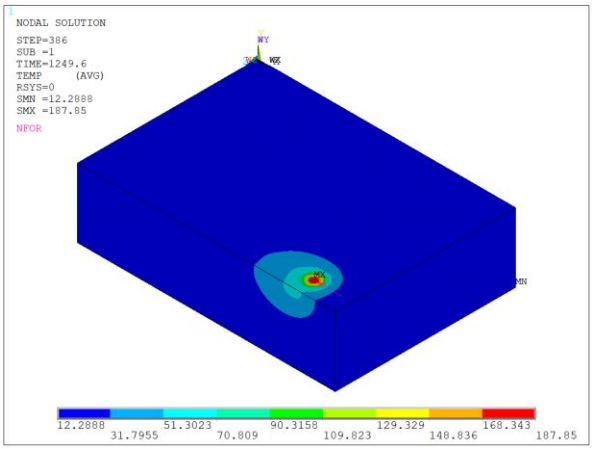

Figure 3.6 Temperature calculation results of workpiece in end milling process at different time

3.7 Thermal deformation result

The study of thermal stress of objects includes two following parts

(1)Research in heat transfer to determine the temperature field；

(2)Research in thermal stress, that is, to determine stress-strain under the situation with known temperature field.

The above two parts affect and couple each other. The temperature determined by heat transfer issue would affect the thermal stress of object directly, while thermal stress has little influence on the temperature. Therefore, the thermal issue of object can be regarded as unidirectional coupled process, which can be divided into two processes to calculate, that is, the physical equation of thermal stress issue is listed firstly, and then the virtual work equation is variated in combination with the virtual work principle to obtain the finite element analysis formula. It is assumed that there is distribution of temperature difference inner the object $\Delta T(x,y,z)$, which cause thermal expansion, $\alpha_T \cdot \Delta T(x,y,z)$, α_T is the coefficient of thermal expansion, due to the thermal expansion increased, the physical equation of object is transformed as

$$\left.\begin{aligned}\varepsilon_{xx}&=\frac{1}{E}\left[\sigma_{xx}-\mu\left(\sigma_{yy}+\sigma_{zz}\right)\right]+\alpha_T\cdot\Delta T\\ \varepsilon_{yy}&=\frac{1}{E}\left[\sigma_{yy}-\mu(\sigma_{xx}+\sigma_{zz})\right]+\alpha_T\cdot\Delta T\\ \varepsilon_{zz}&=\frac{1}{E}\left[\sigma_{zz}-\mu\left(\sigma_{xx}+\sigma_{yy}\right)\right]+\alpha_T\cdot\Delta T\\ \gamma_{xy}&=\frac{1}{G}\gamma_{xy},\gamma_{yz}=\frac{1}{G}\gamma_{yz},\gamma_{xz}=\frac{1}{G}\gamma_{xz}\end{aligned}\right\} \quad (3.1)$$

Rewrite the above equation into the index form:

$$\varepsilon_{ij} = D_{ijkl}{}^{-1} + \varepsilon_{ij}{}^{0} \quad (3.2)$$

Or:

$$\sigma_{ij}=D_{ijkl}(\varepsilon_{kl}-\varepsilon_{ki}{}^{0}) \quad (3.3)$$

$$\varepsilon_{ij}{}^{0} = [\alpha_T\Delta T\alpha_T\Delta T\alpha_T\Delta T000]^T \quad (3.4)$$

The equilibrium equations, geometric equations and boundary conditions of thermal stress problems are the same as those of ordinary elastic problems, and the general virtual work principle of elastic problems is $\delta U - \delta W = 0$,

$$\int_\Omega \sigma_{jj}\,\delta\varepsilon_{ij}d\Omega - \left(\int_\Omega \overline{b_\iota}\,\delta u_i d\Omega + \int_{s_p}\overline{p_\iota}\,\delta u_i dA\right) = 0 \quad (3.5)$$

Substituting the physical equation (3.3) into equation (3.5), the following equation can be obtained:

$$\int_\Omega D_{ijkl}\,(\varepsilon_{kl}-\varepsilon_{ki}{}^{0})\delta\varepsilon_{ij}d\Omega - \left(\int_\Omega \overline{b_\iota}\,\delta u_i d\Omega + \int_{s_p}\overline{p_\iota}\,\delta u_i dA\right) = 0 \quad (3.6)$$

Further, it can be written as follows:

$$\int_\Omega D_{ijkl}\varepsilon_{kl}\,\delta\varepsilon_{ij}d\Omega - \left(\int_\Omega \overline{b_\iota}\,\delta u_i d\Omega + \int_{s_p}\overline{p_\iota}\,\delta u_i dA + \int_\Omega D_{ijkl}\varepsilon_{ki}\,\delta\varepsilon_{ij}d\Omega\right) = 0 \quad (3.7)$$

The above equation is the virtual work equation of the thermal stress problem.

Assumed that node displacement array of the element is

$$q^e = [u_1v_1w_1 \ldots . u_nv_nw_n]^T \quad (3.8)$$

The mechanical parameters in the element are expressed as the relation of node displacement, which can be expressed as follows:

$$\begin{aligned}u &= Nq^e\\ \varepsilon &= Bq^e\\ \sigma &= D(\varepsilon-\varepsilon^0)\\ &= DBq^e - \mathrm{D}\varepsilon^0\\ &= Sq^e - \mathrm{D}\alpha_T\cdot\Delta T[111000]^T\end{aligned} \quad (3.9)$$

Where, N, B, D and S are the shape function matrix, geometric matrix, elastic coefficient matrix and stress matrix of the element respectively, which are the same as the corresponding matrices in general elastic problems. Equation (3.9) is the analytical column of thermal stress, which includes the influence of temperature strain. It can be seen that the last term in Equation (3.9) indicates that temperature change only affects normal stress, but has no influence on shear stress. By calculating the variation of equation (3.9) (that is, calculating the virtual displacement and strain), we can obtain the virtual displacement and strain:

$$\begin{aligned} \delta u &= N * \delta q^e \\ \delta \varepsilon &= B * \delta q^e \end{aligned} \tag{3.10}$$

Substituting it into the virtual work equation, since the variational increment of node displacement δq^e is arbitrary, after eliminating this term, we can get:

$$K^e q^e = P^e + {P_0}^e \tag{3.11}$$

$$K^e = \int_{\Omega^e} B^T D B d\Omega$$

$$\begin{cases} K^e = \int_{\Omega^e} B^T D B d\Omega \\ P^e = \int_{\Omega^e} N^T \bar{b} d\Omega + \int_{{s_p}^e} N^T \bar{p} d\mathrm{A} \\ {P_0}^e = \int_{\Omega^e} B^T D \varepsilon^0 d\Omega \end{cases} \tag{3.12}$$

In the above equation, ${P_0}^e$ is called temperature equivalent load. Compared with the finite element formula of the general elastic problem, the load section of the finite element equation has a temperature equivalent load term ${P_0}^e$.

Thermal deformation FEM calculation results of workpiece in end milling process at different time were shown as below,

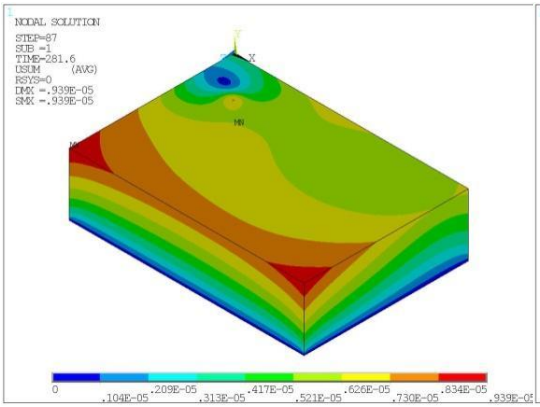
NODAL SOLUTION
STEP=87
SUB =1
TIME=281.6
USUM (AVG)
RSYS=0
DMX =.939E-05
SMX =.939E-05
0
.104E-05
.209E-05
.313E-05
.417E-05
.521E-05
.626E-05
.730E-05
.834E-05
.939E-05

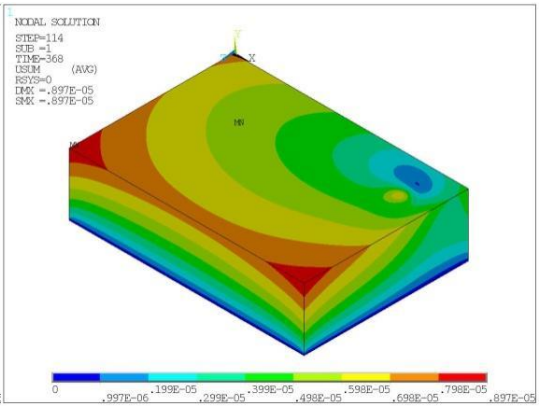
NODAL SOLUTION
STEP=114
SUB =1
TIME=368
USUM (AVG)
RSYS=0
DMX =.897E-05
SMX =.897E-05
0
.997E-06
.199E-05
.299E-05
.399E-05
.498E-05
.598E-05
.698E-05
.798E-05
.897E-05

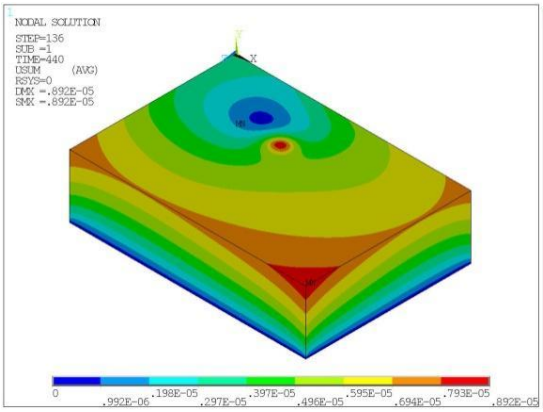
NODAL SOLUTION
STEP=136
SUB =1
TIME=440
USUM (AVG)
RSYS=0
DMX =.892E-05
SMX =.892E-05
0
.992E-06
.198E-05
.297E-05
.397E-05
.496E-05
.595E-05
.694E-05
.793E-05
.892E-05

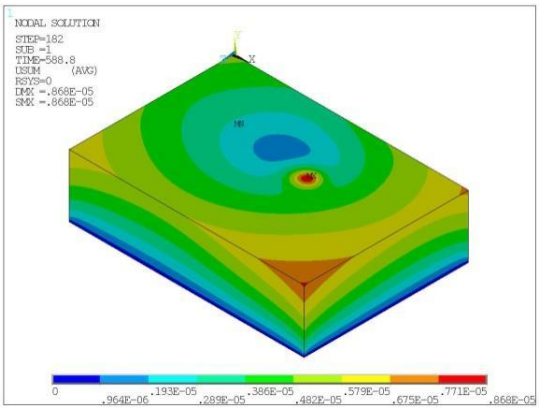
NODAL SOLUTION
STEP=182
SUB =1
TIME=588.8
USUM (AVG)
RSYS=0
DMX =.868E-05
SMX =.868E-05
0
.964E-06
.193E-05
.289E-05
.386E-05
.482E-05
.579E-05
.675E-05
.771E-05
.868E-05

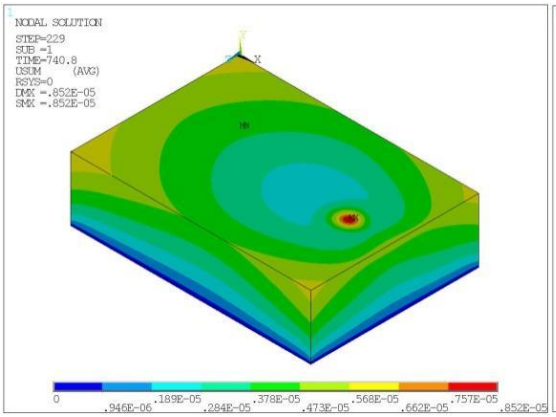
NODAL SOLUTION
STEP=229
SUB =1
TIME=740.8
USUM (AVG)
RSYS=0
DMX =.852E-05
SMX =.852E-05
0
.946E-06
.189E-05
.284E-05
.378E-05
.473E-05
.568E-05
.662E-05
.757E-05
.852E-05

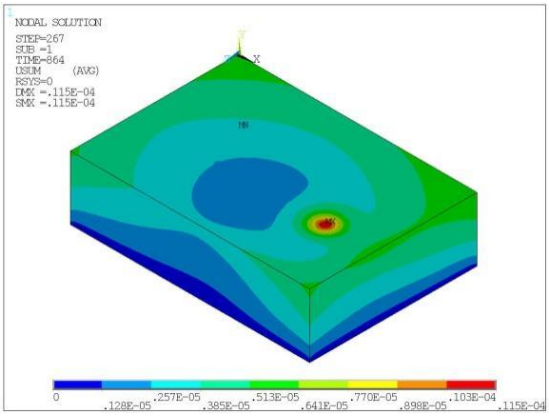
NODAL SOLUTION
STEP=267
SUB =1
TIME=864
USUM (AVG)
RSYS=0
DMX =.115E-04
SMX =.115E-04
0
.128E-05
.257E-05
.385E-05
.513E-05
.641E-05
.770E-05
.898E-05
.103E-04
.115E-04

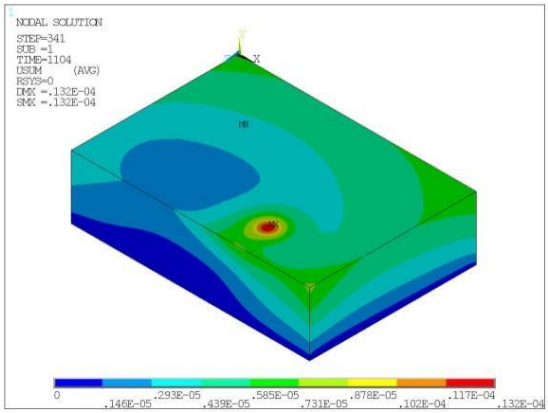

Figure 3.7 Temperature calculation results of workpiece in end milling process at different time

3.8 Numerical simulation result and experiment validate

Under different boundary condition of FEM simulations were extracted, As the measuring points was located in different position, which was shown in **Fig**. 3.8, the time, correspondingly to the maximum temperature, was completely different. In addition, the tendency of temperature-time curves in the measuring points were unchanged under different boundary condition. Only the value range of temperature was changed. Hence, the suitable temperature would be accurately obtained, which was similarly to the actual temperature of workpiece.

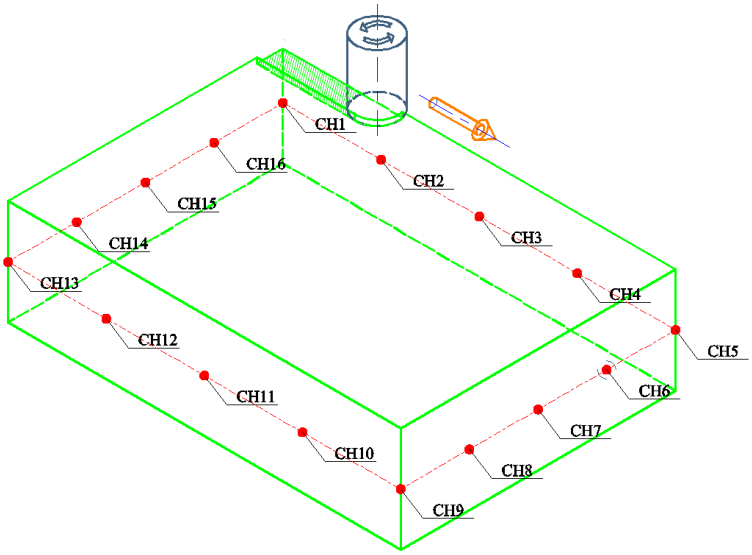

Figure 3.8 Measurement points location

The temperature time-series curve of 16 monitoring points with different material parameters and boundary conditions set under response surface conditions were shown

in **Fig**.3.9. We can obtain numbers of time-series curves with big range according to the material parameters and boundary conditions set by response surface method, meanwhile, there are big shape difference between the time-series curves at different locations of monitoring points. In addition, it is worth to pay attention on the periodic movement of the tool to the workpiece machining path, the temperature time history curve of each monitoring point also shows obvious fluctuation, it indicates that the temperature time history curve of each monitoring point is greatly affected by the tool to the workpiece processing path, and it can comprehensively reflect the tool to the workpiece processing.

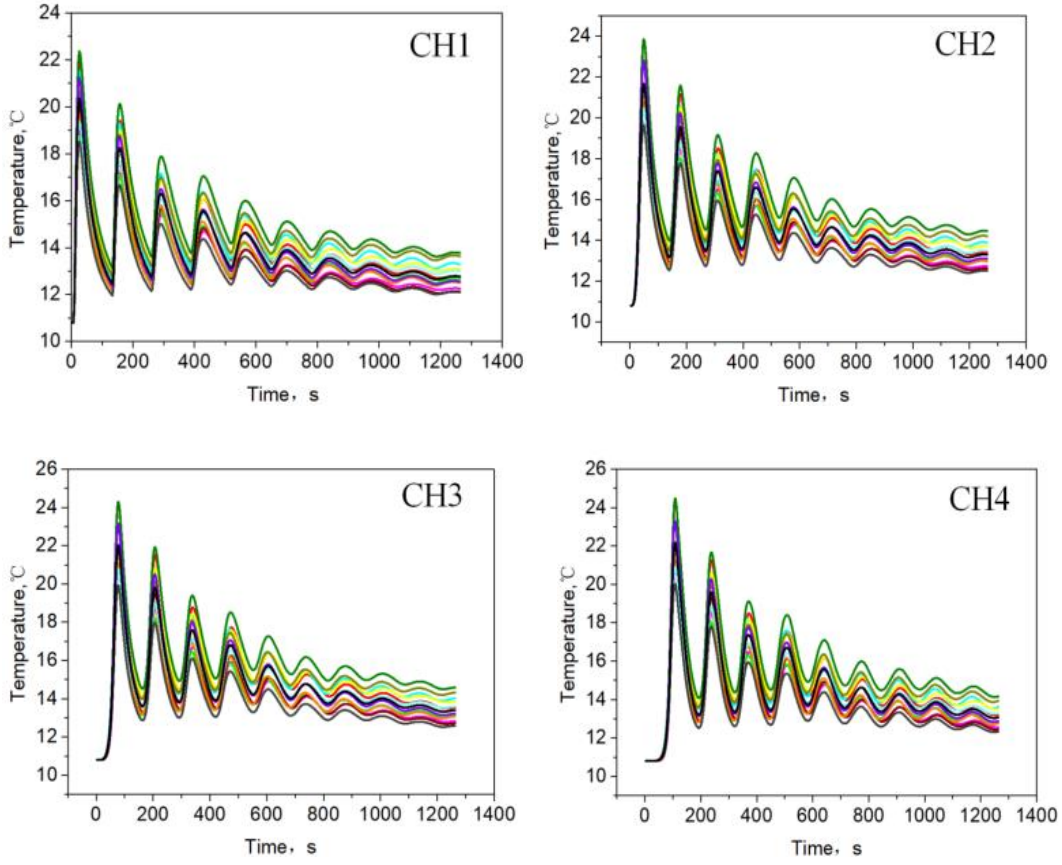

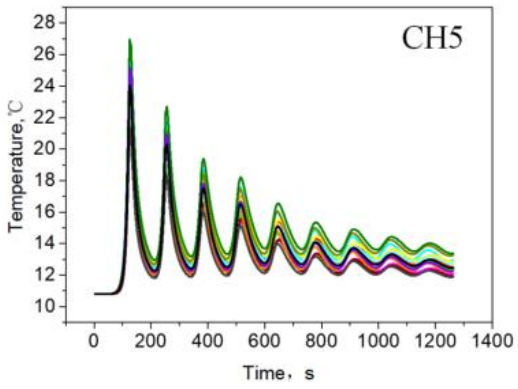
CH5
Temperature,℃
Time，s

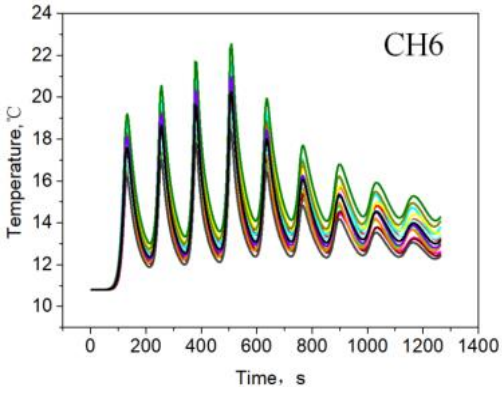
CH6
Temperature,℃
Time，s

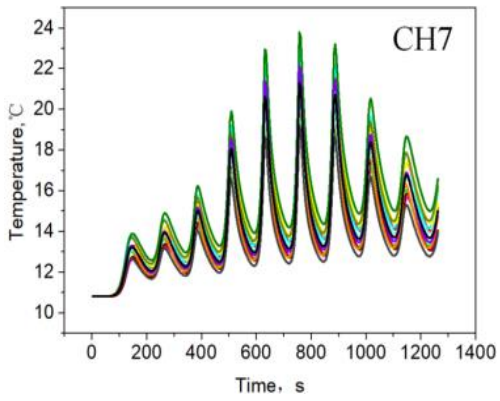
CH7
Temperature,℃
Time，s

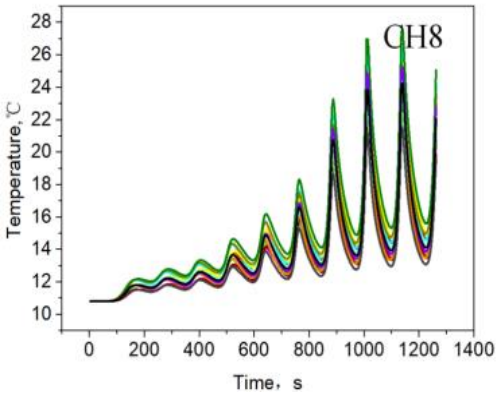
CH8
Temperature,℃
Time，s

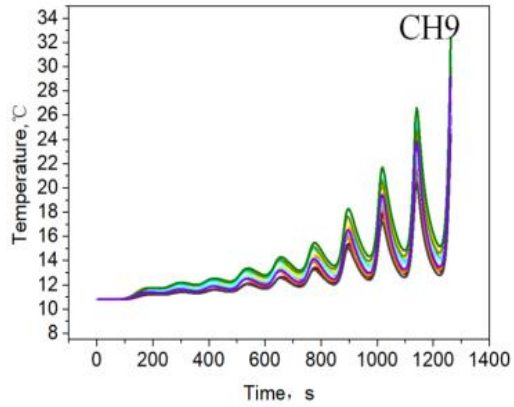
CH9
Temperature,℃
Time，s

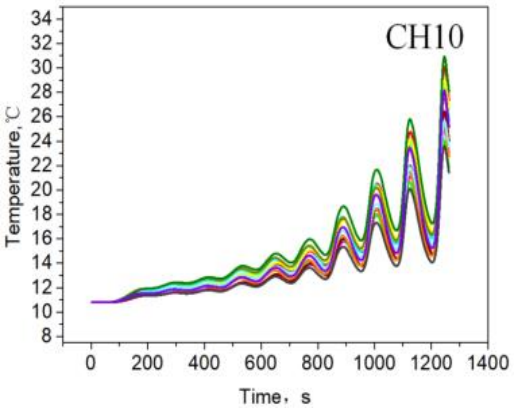
CH10
Temperature,℃
Time，s

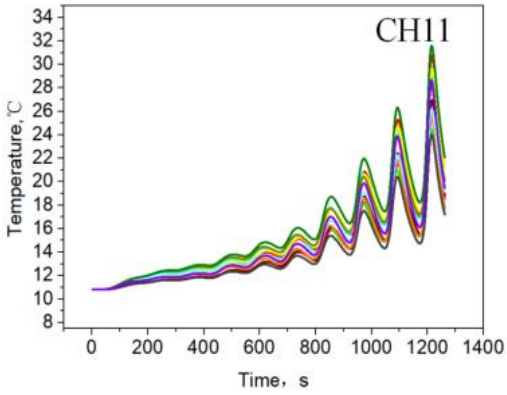
CH11
Temperature,℃
Time，s

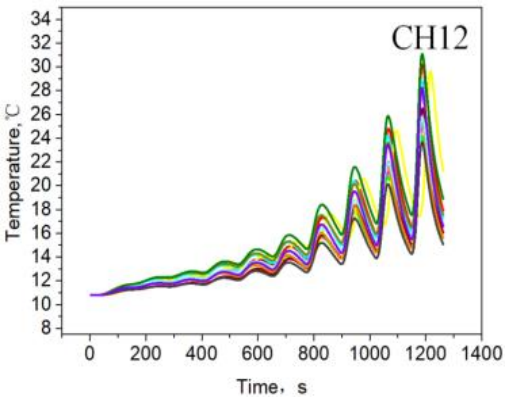
CH12
Temperature,℃
Time，s

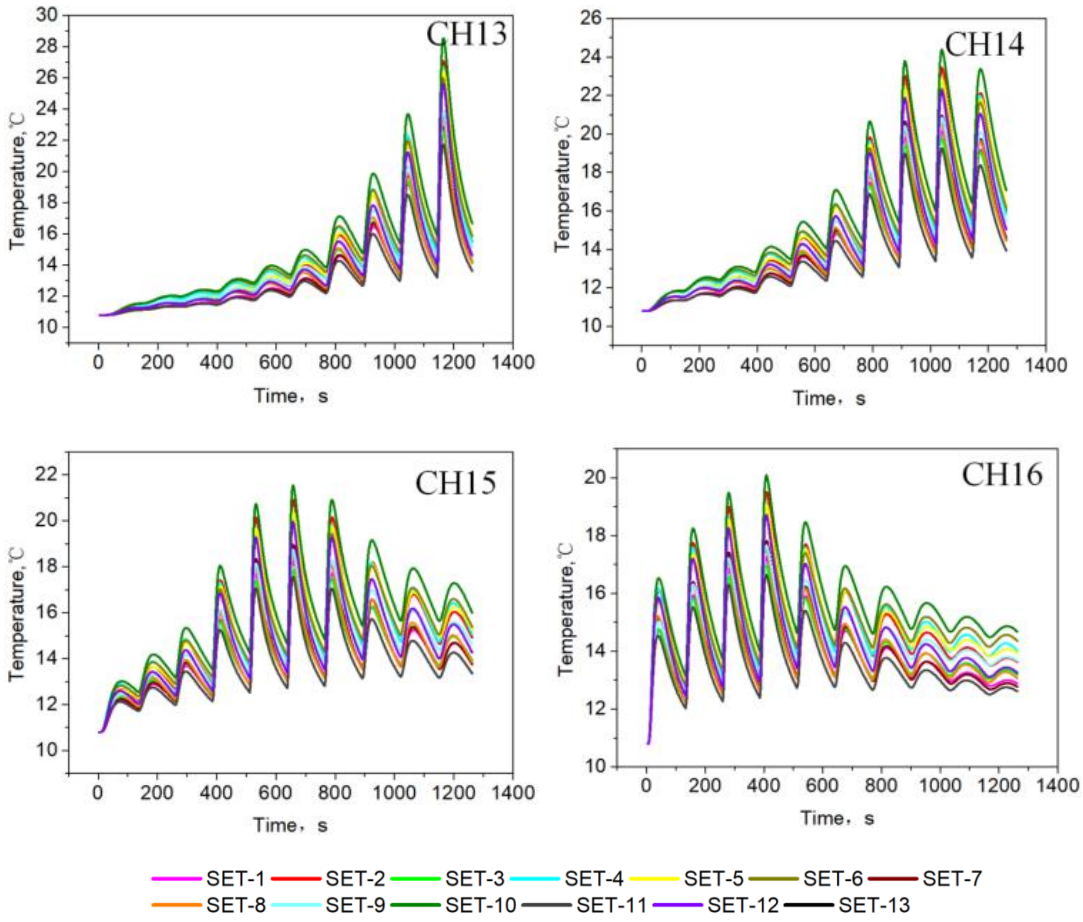

Figure 3.9 Temperature-time curve of 16 measuring points under different boundary condition

Because of multiple temperature time history curves can be extracted from 16 monitoring measurement points to determine which group of process parameter is most close to actual processing situation. Therefore, the most sensitive points can be determined by EOP method, and the most accurate simulation parameters can be obtained by comparing the results of FEM analysis of most sensitive points with actual temperature monitoring results.

The EoP formula[90] is introduced to select sensitive measuring points of temperature monitoring, which is shown as follow,

$$\begin{cases} EoP_i = \frac{\Delta T_{i,n}}{\max\limits_{j\in\{1,N\}}(\Delta T_{j,n})} + \frac{\delta T_i}{\max\limits_{j\in\{1,N\}}(\ \delta T_j)} \\ \delta T_i = \max\limits_{k\in\{1,M\}}(\Delta T_{i,k} - \Delta T_{i,n}) \\ \Delta T_{i,n} = \max\{T_{i,n}\} - \min\{T_{i,n}\} \\ \Delta T_{i,k} = \max\{T_{i,k}\} - \min\{T_{i,k}\} \end{cases} \tag{3.13}$$

Where $T_{i,n}$ is the temperature data series of reference measuring point with normal model parameters. i is stand for the number of measuring point, which is

belong form 1 to N (the total number of measuring point candidate). $T_{i,k}$ is stand for the temperature data series of i measuring point under k FEM simulation boundary condition group. k is stand for the number of FEM simulation boundary condition group, which is belong form 1 to M (the total number of FEM simulation boundary condition groups). In addition, the normal part of EoP shown as following is also calculated to confirm the tendency of the criterion:

$$\begin{cases} nEoP_i = \frac{\Delta T_{i,n}}{\max\limits_{j\in\{1,N\}} \Delta T_{j,n}} \\ \Delta T_{i,n} = \max\{T_{i,n}\} - \min\{T_{i,n}\} \end{cases} \tag{3.14}$$

The calculation results of EOP are shown in **Fig**. 3.10, the most sensitive point of monitoring points is CH11 on the workpiece. Therefore, comparing the temperature time-series calculation results of CH11 under the condition with different material parameters and boundary conditions with experimental results which was shown in **Fig**. 3.11. Finally, the finite element simulation analysis parameters with highest matching degree with the experimental monitoring results can be obtained, as shown in below table.

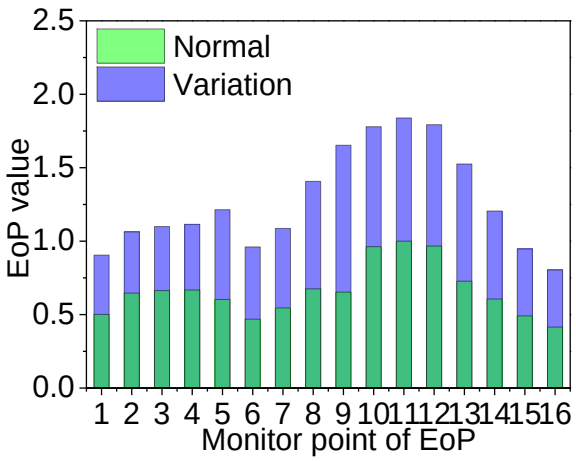

Figure 3.10 EoP of 16 measuring points during end-milling process

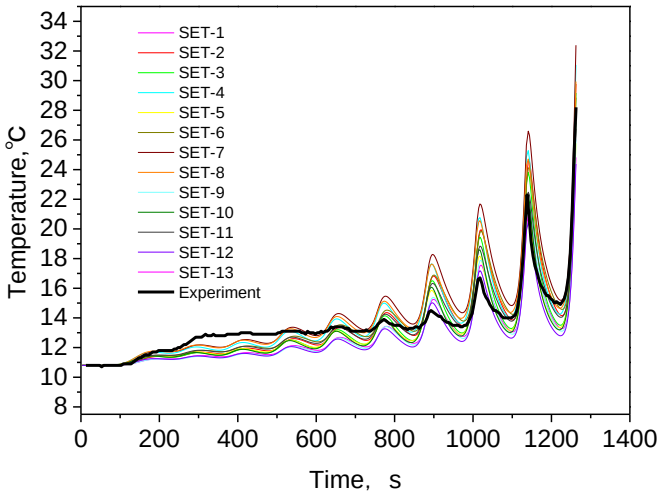

Figure 3.11 CH11 temperature FEM results compared with experiments

Table 4 Workpiece material parameters of S45C

Workpiece material parameters	Carbon steel S45C (JIS)
Heat conduct coefficient	58 W/(m•℃)
Heat transfer coefficient	550W/(m^2•℃)
Heat flux	2850000 W/m^2

In order to further investigate the accuracy and reliability of the selected finite element simulation analysis parameters and boundary condition set, the comparative analysis was proceeded between temperature finite element calculation results and experimental results of new selected 10 monitoring points on the workpiece, which was shown in **Fig**. 3.12. Obviously, the finite element calculation results of 10 monitoring points are quite consistent with the actual experimental results, which indicates that the selected parameters can reflect accurately the temperature field distribution and variation of workpiece in end-milling process.

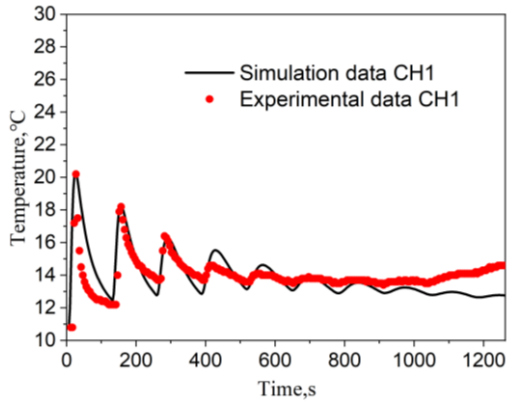
Simulation data CH1
Experimental data CH1
Temperature, °C
Time,s

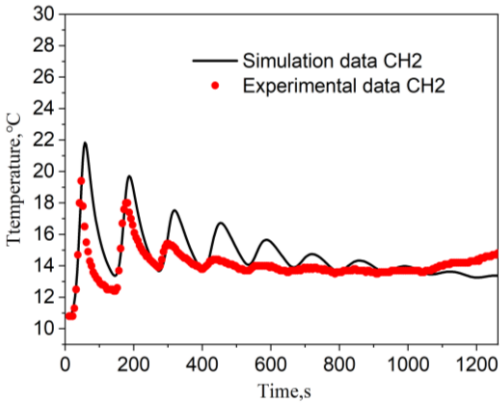
Simulation data CH2
Experimental data CH2
Ttemperature, °C
Time,s

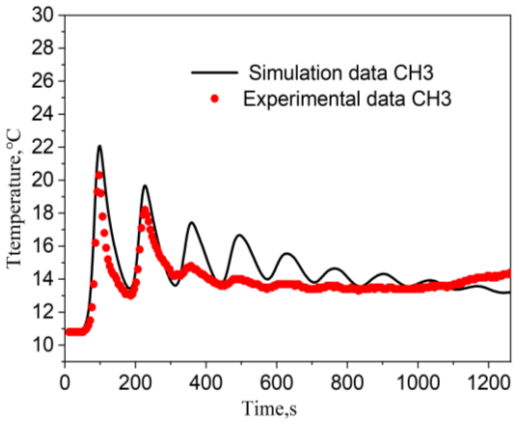
Simulation data CH3
Experimental data CH3
Ttemperature, °C
Time,s

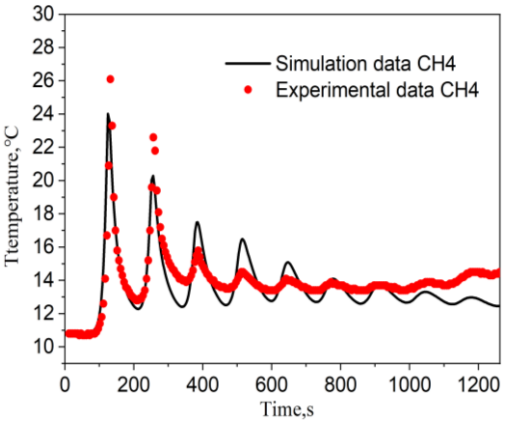
Simulation data CH4
Experimental data CH4
Ttemperature, °C
Time,s

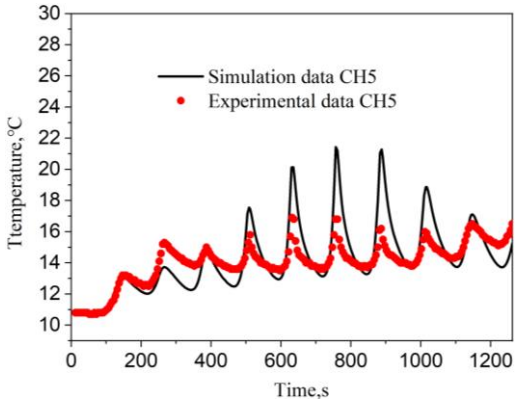
Simulation data CH5
Experimental data CH5
Ttemperature, °C
Time,s

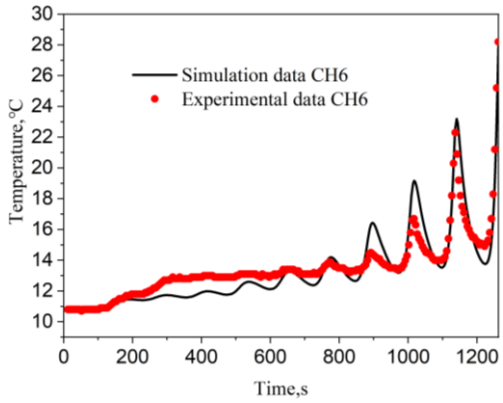
Simulation data CH6
Experimental data CH6
Temperature, °C
Time,s

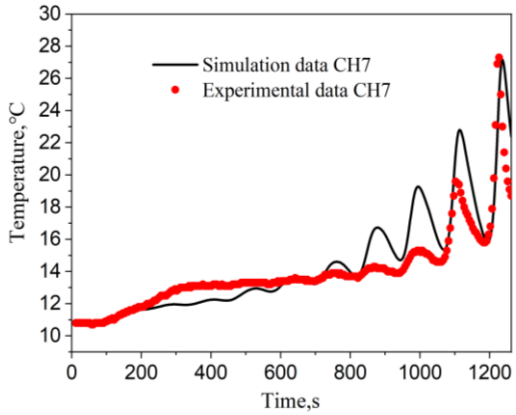
Simulation data CH7
Experimental data CH7
Temperature, °C
Time,s

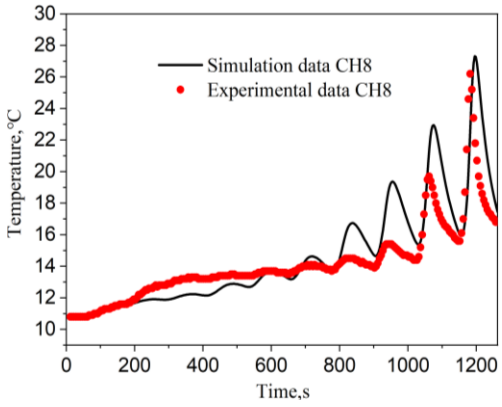
Simulation data CH8
Experimental data CH8
Temperature, °C
Time,s

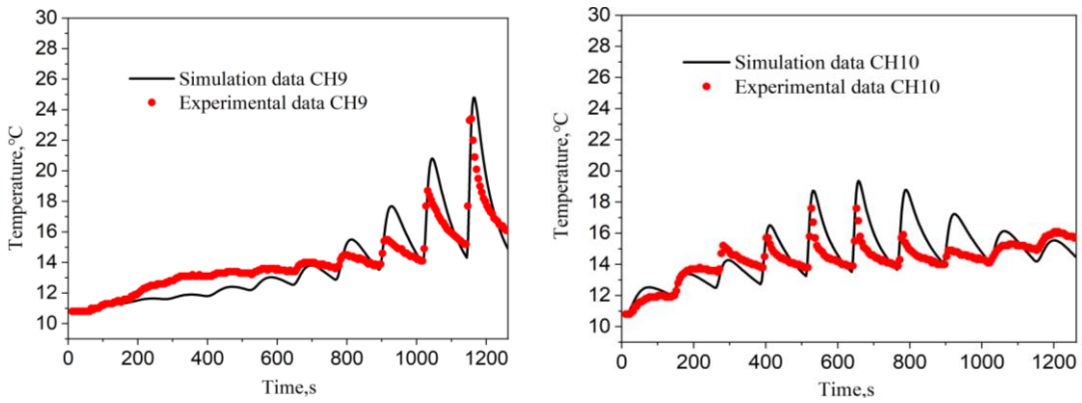

Figure 3.12 10 monitoring point's temperature finite element calculation results were compared with the experimental results

3.9 Summary

This chapter detailed introduces the thermal structural coupling FEM calculation process in end-milling machining in detail, the in-direct coupling method is adapted to calculate the temperature field and thermal deformation in the end-milling process. The results of temperature and thermal deformation finite element simulation analysis indicate that the temperature affected area and thermal deformation area mainly concentrate in the contact area between tool and workpiece surface in the end-milling process. The most sensitive points among 16 measurement points on the workpiece is selected using EOP method, the material parameters and boundary conditions are selected which can calculate workpiece's temperature field accurately based on the comparison between the temperature time-series curves of most sensitive point and actual temperature experimental results. Finally, 10 monitoring points are re-selected again on the workpiece, and the accuracy and reliability of the material parameters and boundary conditions set in the finite element calculation were verified by comparing the finite element calculation results of temperature with the monitoring results in the actual machining process.

4. Statistic-Based model proposed for Monitoring of Workpiece's Thermal Deformation on normal parameters

4.1 A framework and research objective

The schematic expression of the outline for the current study are shown in **Fig.4.1**. The end-milling process of workpieces were conducted by FEM simulation software ANSYS, which was simultaneously calculated the temperature evolution and thermal deformation. The different geometry of workpiece, end-milling process and the location of temperature monitoring points were shown in **Fig.4.2** and **Fig4.3,** respectively. The diameter and feed rate of all end-milling tools were φ16 mm and 0.00125 m/s respectively. The interval distance between tool paths is 10 mm. The basic constants, variations limited conditions and detail different boundary condition of carbon steel S45C(JIS) in end-milling process by FEM simulation are totally listed in the **Table 1**. The temperature distribution and evolution of FEM simulation about carbon steel S45C(JIS) workpiece in the end-milling process is conducted by using ANSYS/APDL. For thermal FEM numerical simulation, the upside surface was loaded area, the others were heat convection boundaries. For structural FEM numerical simulation, the downside surface is the constraint area. After solving the numerical simulation, the time history temperature of monitoring points can be extracted. And the time history deformation of heat source can be also extracted. Then the new model of simple workpiece were firstly proposed and optimal by combining MLR, AIC and *p*-value, which were accurately mathematical relationship between time history temperatures and deformations. Finally, in order to validate the reliability and feasibility of combining MLR, AIC and *p*-value, the same optimal proposed model process was applied in new model of asymmetric complex workpiece established.

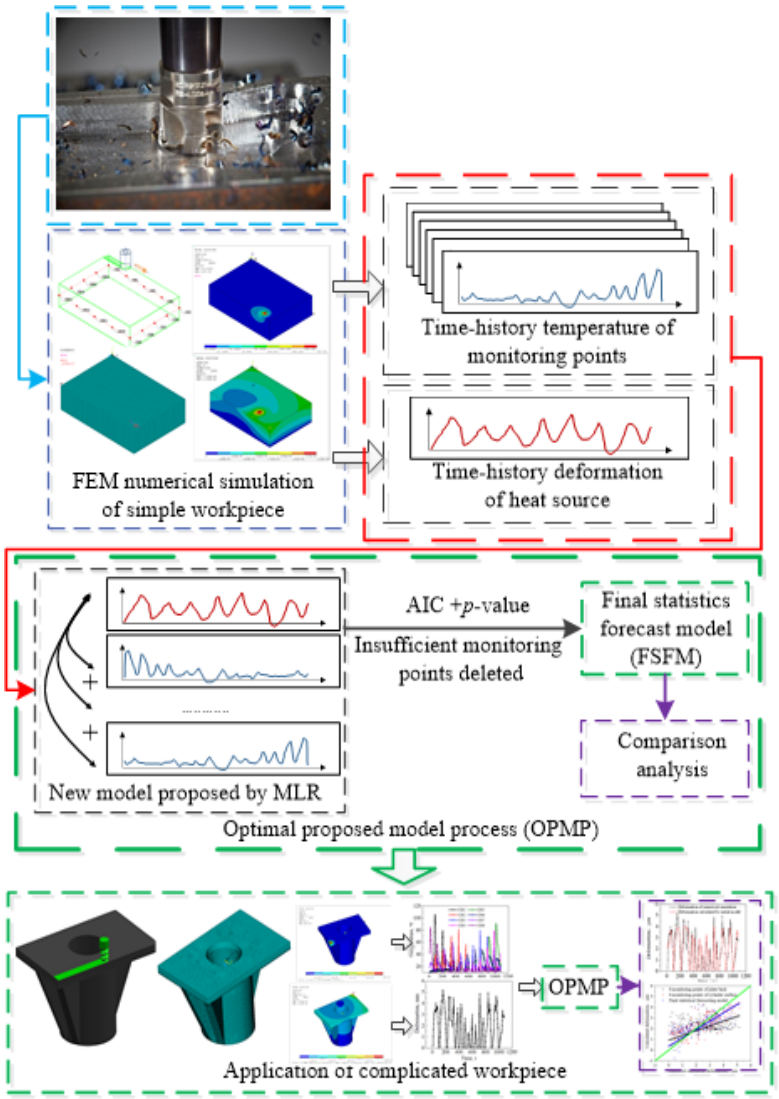

Figure 4.1 Outline of the research

(a)

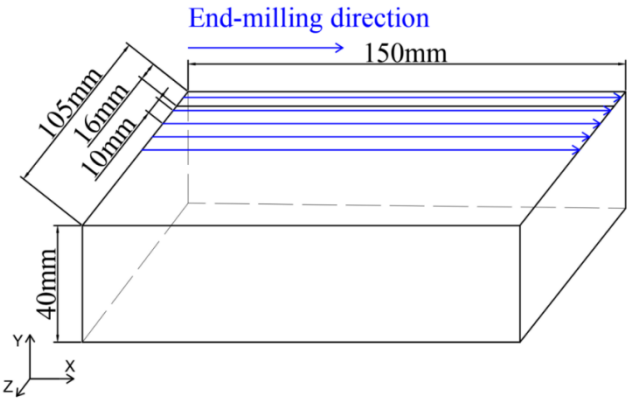

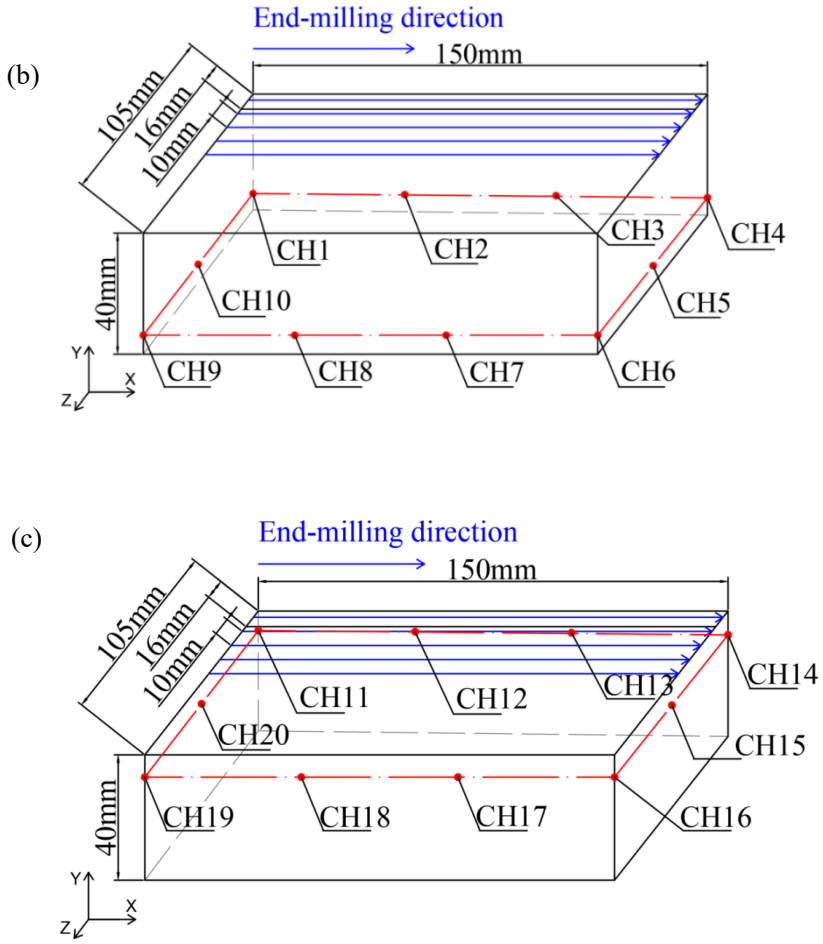

Figure 4.2 End-milling process of workpiece and monitoring points location, (a) blue line is stand for half machining tool path, (b) the location of upper monitoring points, (c) the location of down monitoring points.

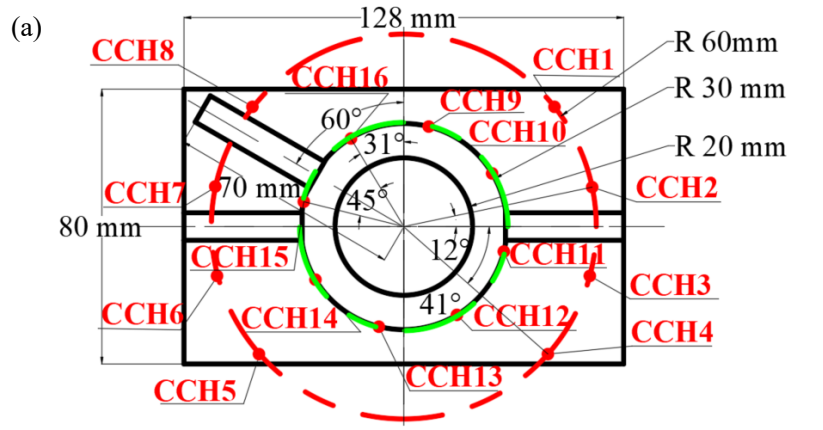

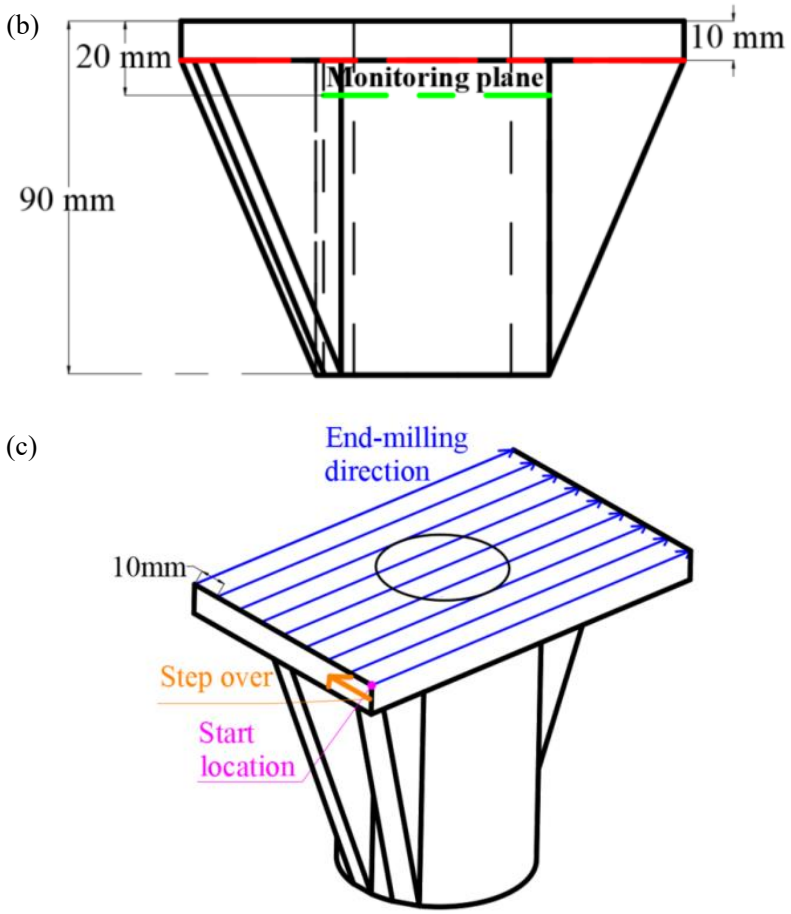

Figure 4.3 Schematic of end-milling process and location of temperature monitoring points: (a) top view, (b) side view, (c) isometric view and tool path.

4.2 Simple workpiece case research

4.2.1 FEM numerical simulation result

According to the location of monitoring points in **Fig.4.2**， the time history temperature of monitoring points was completely extracted, which was shown in **Fig. 4.4**.As the measuring points were located in different position, the time, correspondingly to the maximum temperature, was completely different. As the distance between the heat source and monitoring points were completely different, the amplitude of temperature in monitoring points of upper part were relatively higher than that of lower part. The time history deformation of heat source was shown in **Fig.4.5**. By comparing the **Fig.4.4** and **Fig.4.5**， the total evolution tendency of time history temperatures and deformations are almost similar. In addition, the relationship type between temperature and deformation was linear. Hence, the time history deformation

of heat source could be express by time history temperature of monitoring points.

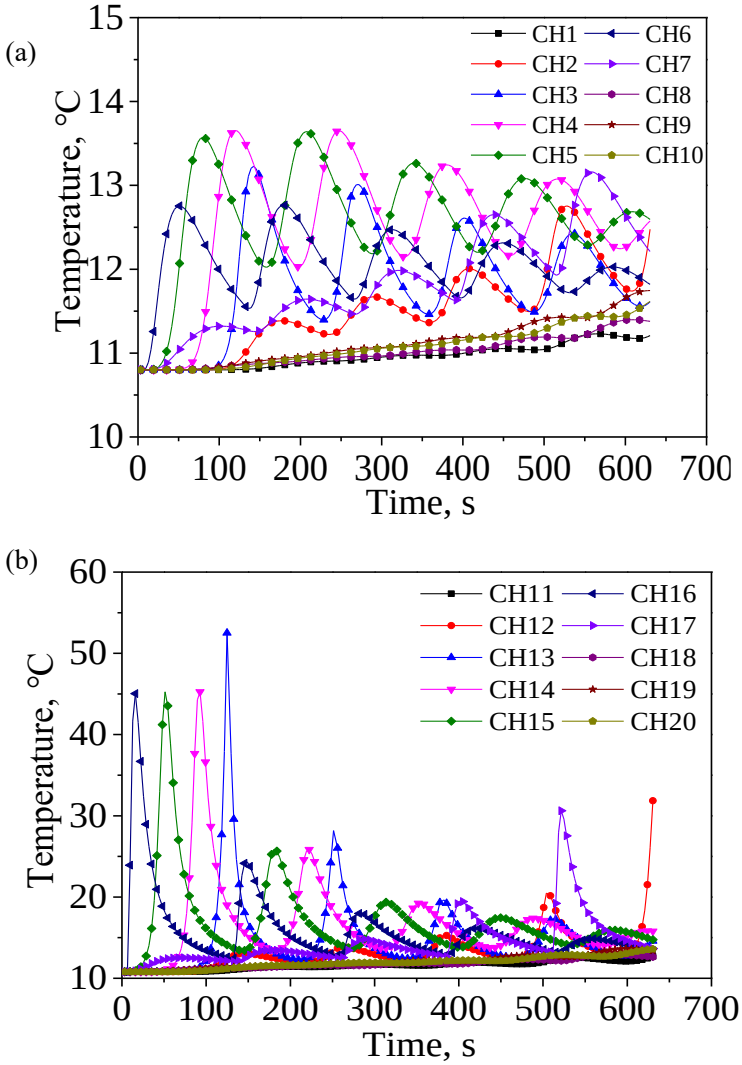

Figure 4.4 Time-series of temperatures at 20 monitoring points: (a) CH1~CH10, (b) CH11~CH20

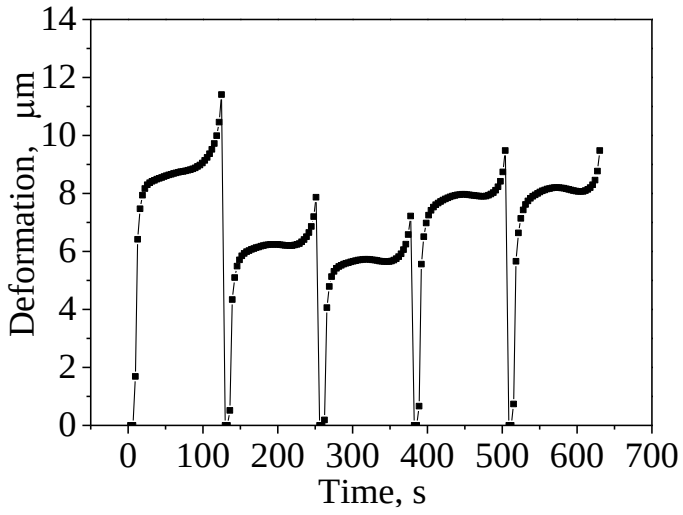

Figure 4.5 Time history of deformation in center of heat source

4.2.2 Statistic based selection model proposed

A simple empirical statistics-based monitoring point selection model is proposed by combining MLR, AIC, and the *p*-value. The time-series temperatures of 20 measuring points (all measuring point candidates) were regarded as input variables ($T_{ch1}(t)$, $T_{ch2}(t)$, …, $T_{chn}(t)$ are the independent variables). The time-series deformations of the heat source were regarded as output variables ($D_{heat\text{-}source}(t)$ is the dependent variable). In addition, the coefficient of multiple determination (R^2) was used to match the level of the MLR method, which represents the proportion of the dependent variable's total variations [35]. The dependent variable was accounted for or described by independent variables. The initial result of the statistical forecasting model is expressed by Eq. (4), as shown in **Table 5**. Here, i is the number of measured temperature monitoring points. In this case, the R^2 value of the initial statistics-based selection model was 0.7381.

$$D_{\text{heat}-\text{source}}(t) = \beta_0 + \beta_1 T_{CH1}(t) + \beta_2 T_{CH2}(t) + \cdots + \beta_n T_{CHn}(t) \text{…….} \quad (4)$$

According to the results of the MLR method, most *p*-values were larger than 0 (here, equal to 1×10^{-4} [36]). Furthermore, the input quantity of the collinearity problem was not considered in the MLR method [37]. The collinearity problem occurs when the changing tendency of the independent variables is similar, which is the major reason for the initial model being inefficient. The AIC is commonly used to solve the collinearity problem [91]. To eliminate the collinearity problem of the initial model, the time-series temperatures of the measuring points were individually deleted, while the other measuring points were used to calculate the AIC value. The AIC values of the candidate models are shown as below. It is worth mentioning that 'None' in **Table 6** indicates the case where no independent variable is deleted.

Table 5 Result of initial model

Coefficient	Estimated value	*t*-test	*p*-value
β_0	-1505.00	-4.541	1.04E-05
β_1	80.15	2.537	0.012069
β_2	-8.39	-2.672	0.008246
β_3	-1.23	-3.507	0.000576
β_4	2.35	5.174	6.27E-07
β_5	1.28	2.838	0.005078
β_6	2.91	5.323	3.12E-07
β_7	13.38	5.290	3.64E-07
β_8	241.50	3.556	0.000486
β_9	-137.70	-2.371	0.018852
β_{10}	-24.07	-1.067	0.287237
β_{11}	-15.92	-1.296	0.19657
β_{12}	0.69	4.329	2.52E-05
β_{13}	0.03	1.067	0.287456
β_{14}	0.01	0.170	0.865301
β_{15}	-0.06	-1.567	0.119043
β_{16}	0.24	7.598	1.78E-12
β_{17}	0.66	7.487	3.38E-12
β_{18}	-32.19	-3.242	0.001424
β_{19}	-14.70	-3.771	0.000223
β_{20}	30.31	2.249	0.025783

Table 6 AIC value in different groups

Deleted monitoring point	AIC value
14	98.65
13	99.889
10	99.89
11	100.492
None	100.617
15	101.348
20	104.204
9	104.816
1	105.699
2	106.461
5	107.442
18	110.052
3	111.938
8	112.294
19	113.936
12	118.564
4	126.519

7	127.698
6	128.036
17	153.072

Table 7 Result of better suitable model

Coefficient	Estimated value	*t*-test	*p*-value
β_0	-1158.00	-4.885	2.29E-06
β_1	26.49	2.688	0.007863
β_2	-11.90	-7.615	1.50E-12
β_3	-1.08	-3.253	0.001364
β_4	2.71	7.823	4.40E-13
β_5	1.11	2.813	0.005456
β_6	2.79	5.198	5.49E-07
β_7	11.32	5.557	9.89E-08
β_8	188.30	3.859	0.000159
β_9	-88.81	-2.936	0.003764
β_{12}	0.48	5.087	9.16E-07
β_{15}	-0.04	-1.314	0.190613
β_{16}	0.24	7.594	1.69E-12
β_{17}	0.63	7.441	4.11E-12
β_{18}	-25.54	-3.218	0.001535
β_{19}	-11.46	-3.512	0.000563
β_{20}	11.95	2.693	0.007765

By comparing the AIC values, if the AIC value of the model with solely deleted independent variables is larger than the non-deleted model's AIC value (100.617), as shown in **Table 5**, it is illustrated that the process of solely deleting independent variables is beneficial for improving the efficiency of the model. Hence, the measuring points No. 13, No. 14, No. 10, and No. 11 were reasonably deleted in the improved model. The improved model was fitted using MLR, as shown in **Table 7**. The R^2 value of the improved model was 0.7316, which is close to that of the initial model (0.7381). However, some *p*-values of the coefficients are larger than 1×10^{-4}, which illustrates that the model is still inefficient [29, 36]. Hence, the independent variables were deleted to refit the optimal model by MLR, for which the *p*-value was larger than 1×10^{-4}. This optimal process was conducted ten times. During the optimization processes, the larger *p*-values of the measuring point were deleted individually to fit the new model and calculate its R^2 value. Finally, the final model became simpler and more reliable

because it consisted of only six independent variables.

The R^2 values of each point in the improved model were 0.729, 0.7196, 0.7152, 0.7127, 0.7123, 0.7103, 0.676, 0.6177, 0.6047, 0.6038, respectively. The final model consisted of six measuring points to guarantee the accuracy of the statistics-based selection model. The R^2 value was 0.6038, which is larger than the predetermined R^2 value criterion. Finally, the equation of the statistics-based selection model is fitted by MLR, which is expressed as follows:

$$D_{heat\text{-}source}(t)=31.4-11.74T_{CH2}(t)+1.36T_{CH6}(t)+5.76T_{CH7}(t)+$$
$$0.75T_{CH12}(t)+0.18T_{CH16}(t)+0.89T_{CH17}(t)\ldots\ldots\ldots\ldots\ldots\ldots\ (3)$$

Table 8 Result of first optimal model

Coefficient	Estimated value	*t*-test	*p*-value
β_0	-1082.00	-4.697	5.23E-06
β_1	24.24	2.493	0.01357
β_2	-11.72	-7.513	2.65E-12
β_3	-1.15	-3.498	0.000592
β_4	2.71	7.784	5.43E-13
β_5	1.02	2.619	0.009564
β_6	2.35	5.567	9.34E-08
β_7	11.23	5.501	1.29E-07
β_8	178.40	3.692	0.000295
β_9	-84.80	-2.812	0.00547
β_{12}	0.48	5.081	9.39E-07
β_{16}	0.25	8.162	5.68E-14
β_{17}	0.63	7.443	3.99E-12
β_{18}	-24.44	-3.09	0.002319
β_{19}	-10.59	-3.308	0.001137
β_{20}	11.54	2.603	0.010011

Table 9 Result of second optimal model

Coefficient	Estimated value	*t*-test	*p*-value
β_0	-732.34	-3.951	0.000112
β_2	-9.47	-7.336	7.25E-12
β_3	-1.37	-4.287	2.95E-05
β_4	2.35	7.308	8.52E-12
β_5	0.60	1.69	0.092796
β_6	2.33	5.429	1.81E-07
β_7	9.23	4.847	2.69E-06
β_8	132.29	2.922	0.003924
β_9	-52.62	-1.903	0.058575
β_{12}	0.41	4.466	1.41E-05
β_{16}	0.24	7.768	5.86E-13
β_{17}	0.62	7.161	1.97E-11
β_{18}	-12.51	-1.958	0.051735
β_{19}	-12.51	-3.969	0.000104
β_{20}	8.21	1.914	0.057206

Table 10 Result of third optimal model

Coefficient	Estimated value	*t*-test	*p*-value
β_0	-529.11	-	0.000254
β_2	-9.74	-	1.87E-12
β_3	-1.43	-	1.25E-05
β_4	2.26	7.093	2.86E-11
β_6	2.67	7.001	4.80E-11
β_7	7.88	4.536	1.04E-05
β_8	89.90	2.373	0.018682
β_9	-31.35	-	0.206694
β_{12}	0.45	5.057	1.04E-06
β_{16}	0.22	7.627	1.32E-12
β_{17}	0.66	8.039	1.14E-13
β_{18}	-7.43	-	0.191428
β_{19}	-10.51	-	0.000442
β_{20}	5.43	1.363	0.174436

Table 11 Result of final model

Coefficient	Estimated val	*t*-test	*p*-value
β_0	31.40	5.041	1.08E-06
β_2	-11.74	-13.965	<2E-16
β_6	1.36	4.586	8.22E-06
β_7	5.76	14.549	<2E-16
β_{12}	0.75	9.788	<2E-16
β_{16}	0.18	7.362	5.49E-12
β_{17}	0.89	12.181	<2E-16

4.2.3 Error analysis of proposed model

An error analysis was performed on the proposed model to analyze the effectiveness and reliability of the statistics-based selection model. A comparison between the results of the FEM numerical simulation and the statistics-based selection model is shown in **Fig.4.6**. The comparison with the proposed models shows that the time-series deformations of the heat source were accurately and efficiently predicted by the final statistics-based selection model. The number of measuring points was successfully decreased from 20 to only six, namely CH2, CH6, CH7, CH12, CH16, and CH17. To further discuss the advantages of the final statistics-based selection model, it is necessary to conduct a comparison between the fitted results of ten measuring points in the lower location of the simple workpiece using MLR, fitted results of ten measuring points in the upper location of the simple workpiece using MLR, and final statistics-based selection model. The R^2 values of the ten measuring points in the lower and upper locations were 0.4056 and 0.5189, respectively, which were smaller than the R^2 of the statistics-based selection model (0.6038). The comparison results are shown in **Fig. 4.7**. The black, blue, and red lines are linearly fitted by the corresponding color point groups. The green line indicates that the deformation calculated by the different measuring point groups is equal to that calculated using the numerical simulation. It is clear that the red line is closer to the green line. In addition, the number of input variables in the final statistics-based selection model was only six. Therefore, it can be concluded that the final statistics-based selection model is more reliable than other models. Moreover, it is clear that differences in the candidate point sets affect the final estimation quality. Therefore, it is necessary to consider all the possible measurable points as the initial candidate set.

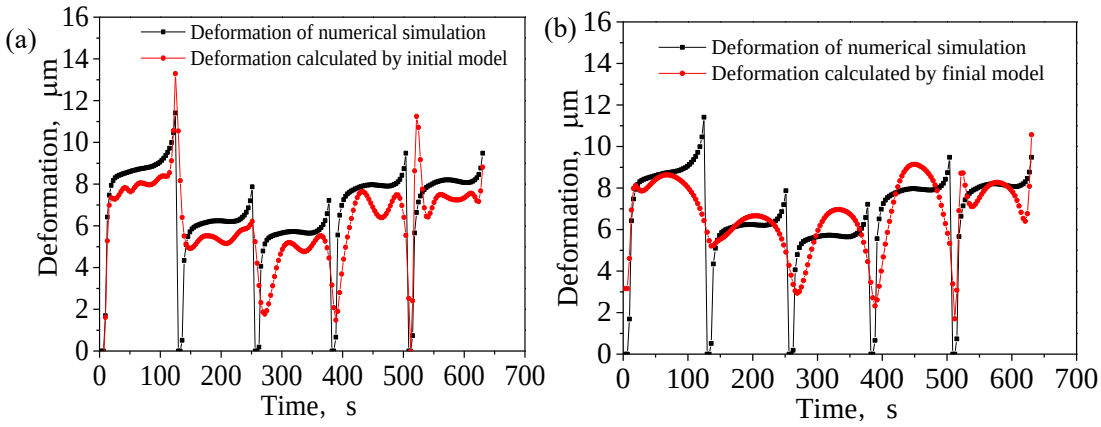

Figure 4.6 Comparison between time history deformation of numerical simulation and other models, (a) initial model, (b) final model

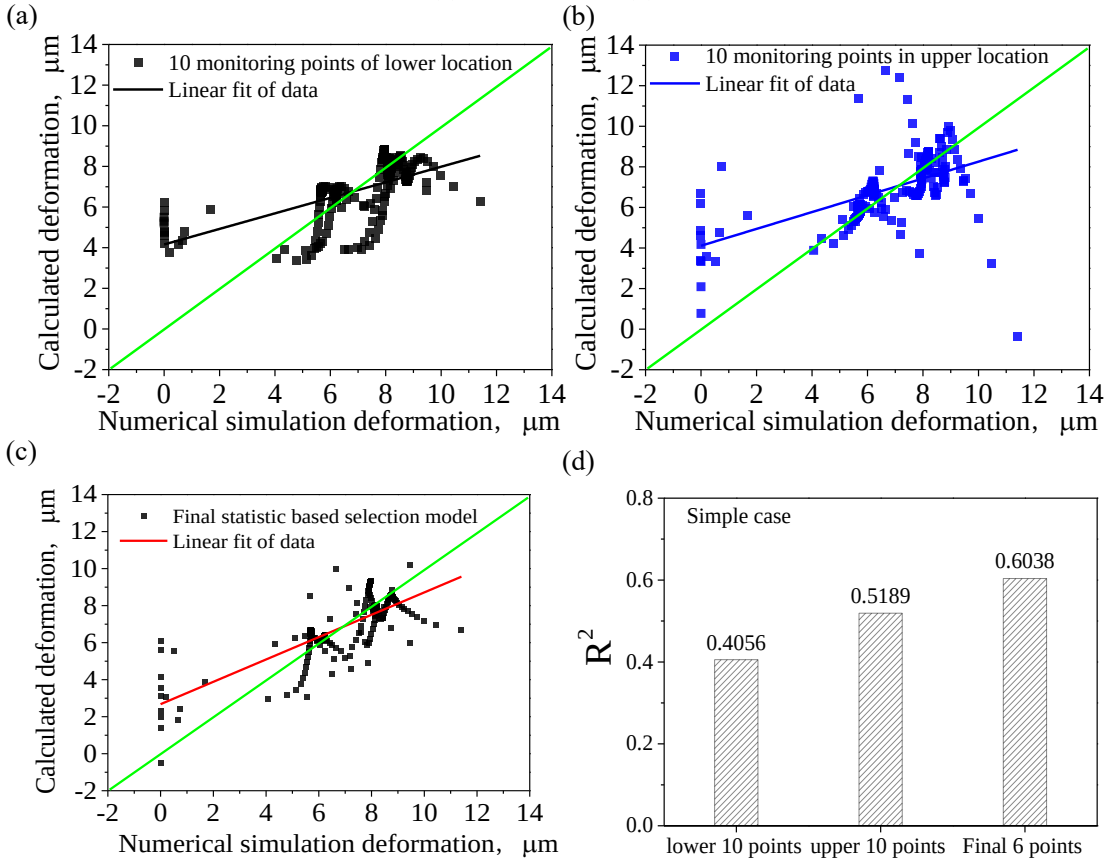

Figure 4.7 Comparison in different monitoring points group, (a) 10 monitoring points of lower location, (b) 10 monitoring points of upper location, (c) Six measuring points of the final statistics-based selection model, (d) Compared of R^2 values different points selection

4.3 Complex workpiece case research

4.3.1 Statistic based selection model proposed and optimal

To confirm the applicability of the proposed method in an actual situation, a machining case of a complex workpiece was investigated.

The workpiece geometry of the second case study and the outline of the end-milling process are illustrated in **Fig.4.3**. The machining of the entire top surface of the workpiece is assumed. The candidate locations of the temperature measuring points are shown in **Fig.4.3** (a) and (b). CCH1, CCH2, CCH3, CCH4, CCH5, CCH6, CCH7, and CCH8 are located along the red dotted line, whose radius was 60 mm. CCH1 and CCH2 had transverse symmetries with CCH4 and CCH3, respectively. CCH1, CCH2, CCH3, and CCH4 had longitudinal symmetry with CCH8, CCH7, CCH6, and CCH5, respectively. The angle between the CCH2 and the transverse axis was 12°. The angle between the CCH4 and the transverse axis was 41°. CCH9, CCH10, CCH11, CCH12, CCH13, CCH14, CCH15, and CCH16 are located on the green dotted line on average, whose radius was 30 mm. The angle between them was 45°. The angle between the CCH16 and the longitudinal axis was 31°.

The workpiece material and all machining conditions were the same as those in the first case. Therefore, the simulation conditions, except for the workpiece shape, are the same as in the first simulation.

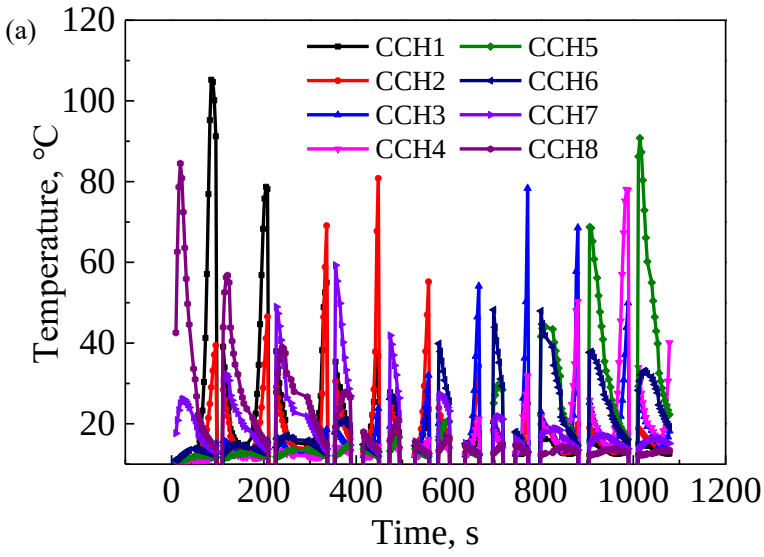

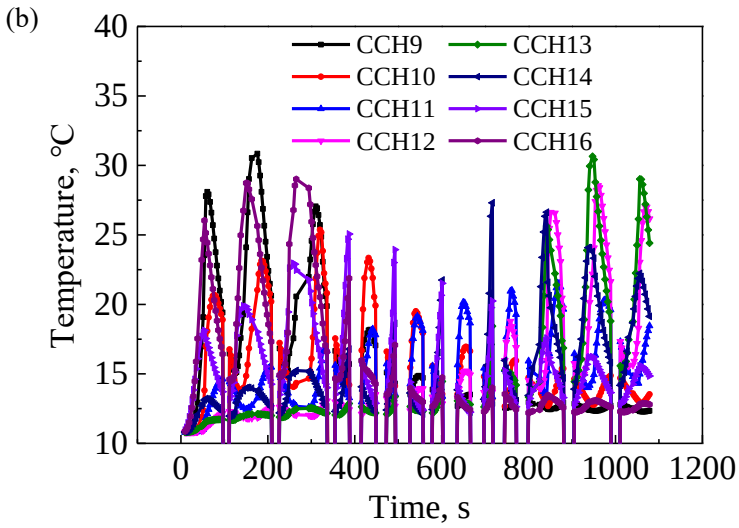

Figure 4.8 Time-series of temperatures in 16 monitoring points

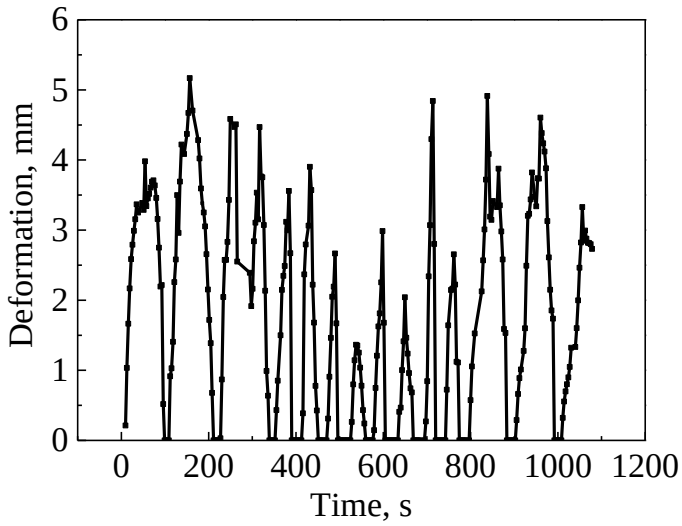

Figure 4.9 Time-series of deformations in the center of the heat source

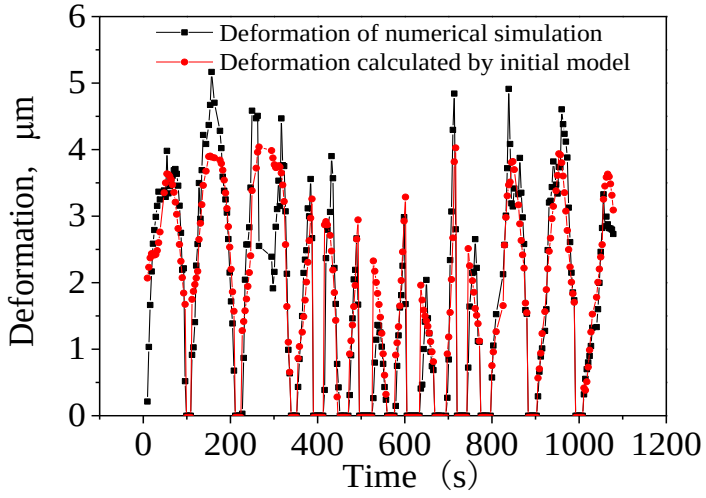

(a) Initial model

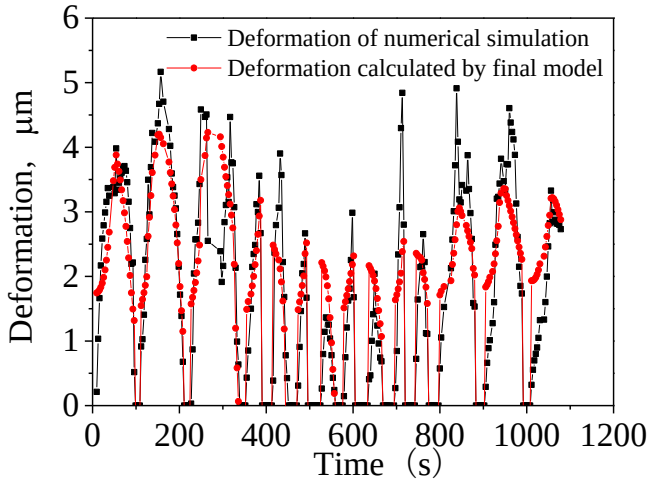

(b) Final model

Figure 4.10 Comparison between time-series deformations of numerical simulation and other models

According to the location of the measuring points in **Fig.4.3**, the time-series temperatures of the measuring points and time-series deformations at the moving heat source were extracted, as shown in **Fig.4.8** and **Fig.4.9**, respectively. The same procedure as in the first case was applied to determine a simple empirical model of the workpiece deformation. The R^2 value for the initial model was 0.8483. After evaluating the AIC and *p*-values, the R^2 value of the final model was 0.8083. Notably, all *p*-values were lower than 1×10^{-4}. Finally, the equation of the statistics-based selection model was fitted using MLR, which is expressed as follows:

$$D_{heat\text{-}source}(t)=0.059-0.045T_{CH2}(t)-0.025T_{CH5}(t)+0.138T_{CH14}(t)+$$

$$0.106T_{CH16}(t)\ldots\ldots\ldots\ldots\ldots\ldots\ldots\ldots\ (4)$$

Table 12 Result of initial model

Coefficient	Estimated value	*t*-test	*p*-value
β_0	-0.0247	-0.39	0.696628
β_1	-0.0005	-0.15	0.881207
β_2	-0.0338	-5.687	3.19E-08
β_3	-0.0025	-0.378	0.705844
β_4	-0.0090	-2.108	0.035875
β_5	-0.0163	-3.74	0.000222
β_6	-0.0139	-1.574	0.116687
β_7	-0.0163	-2.417	0.016252
β_8	0.0103	2.672	0.007975
β_9	-0.0382	-0.985	0.325345
β_{10}	0.1142	2.864	0.004495
β_{11}	-0.1950	-4.609	6.09×10^{-6}

β_{12}	0.1793	4.438	1.30×10^{-5}
β_{13}	-0.1072	-2.497	0.013098
β_{14}	0.2184	4.965	1.18×10^{-6}
β_{15}	-0.0379	-0.852	0.395131
β_{16}	0.1220	3.016	0.00279

Table 13 AIC value in different groups

Deleted monitoring point	AIC value
1	-298.99
3	-298.86
15	-298.24
9	-297.98
none	-297.01
6	-296.4
4	-294.34
7	-292.88
13	-292.48
8	-291.54
10	-290.44
16	-289.52
5	-284.54
12	-278.83
11	-277.3
14	-273.96
2	-266.55

Table 14 Result of better suitable model

Coefficient	Estimated value	*t*-test	*p*-value
β_0	-0.0184	-0.273	0.78537
β_2	-0.0373	-7.025	1.51×10^{-11}
β_4	-0.0095	-2.413	0.016458
β_5	-0.0209	-4.627	5.59×10^{-6}
β_6	0.0112	1.321	0.18738
β_7	-0.0164	-2.465	0.014275
B_8	0.0104	2.57	0.010663
β_{11}	-0.1051	-3.382	0.000817
β_{12}	0.0465	1.406	0.160885
β_{13}	0.1095	4.728	3.54×10^{-6}
β_{14}	0.0643	3.084	0.00224
β_{16}	0.1153	9.757	$<2\times10^{-16}$

Table 15 Result of optimal model

Coefficient	Estimated value	*t*-test	*p*-value
β_0	-0.05866	-0.857	0.392
β_2	-0.0446	-11.115	<2E-16
β_5	-0.02453	-7.451	1.00E-12
β_{14}	0.13838	13.632	<2E-16
β_{16}	0.106249	13.425	<2E-16

Table 16 Result of final model

Coefficient	Estimated value	*t*-test	*p*-value
β_0	-0.07508	-1.01	0.313
β_2	-0.04496	-10.31	<2E-16
β_{14}	0.090017	10.61	<2E-16
β_{16}	0.122581	14.83	<2E-16

4.3.2 Error analysis of proposed model

The measuring points were successfully decreased from 16 to four, namely CCH2, CCH5, CCH14, and CCH16. By comparing different proposed models, it can be concluded that the time-series deformations of the heat source were accurately and efficiently estimated by the final statistics-based selection model, as shown in **Fig. 4.10**. To discuss the advantages of the final statistics-based selection model, the fitted results of eight measuring points on the plate backside using MLR, the fitted results of eight measuring points on the cylinder surface using MLR, and the final statistics-based selection model were compared. The R^2 values of the eight measuring points in the lower and upper locations were 0.4435 and 0.7827, respectively, which were smaller than the R^2 of the final model (0.8083). The comparison results are shown in **Fig.4.13**. The black, red, and blue lines are linearly fitted by the corresponding color point groups in **Fig.4.13**. The green line indicates that the calculated deformations by different measuring point groups are equal to the deformations measured using the FEM-based process simulation. It is evident that the red and blue lines are all closer to the green line. However, the number of input variables in the final model was only four. Consequently, the final model was more suitable than other models.

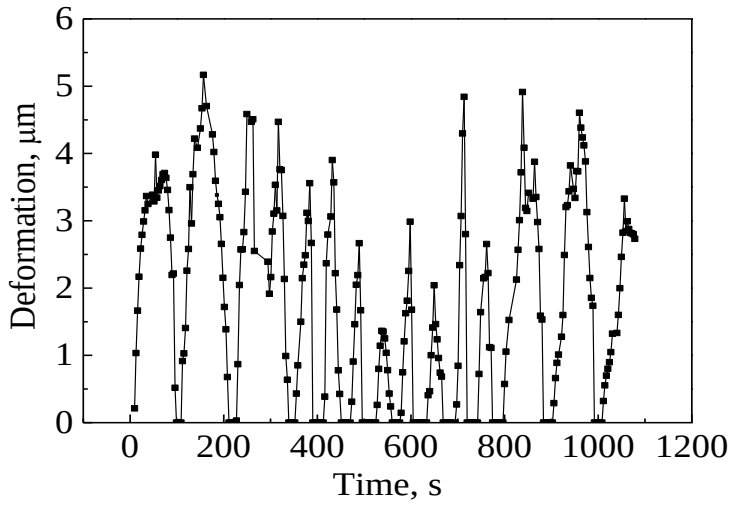

Figure 4.11 Time-series of deformations in the center of the heat source

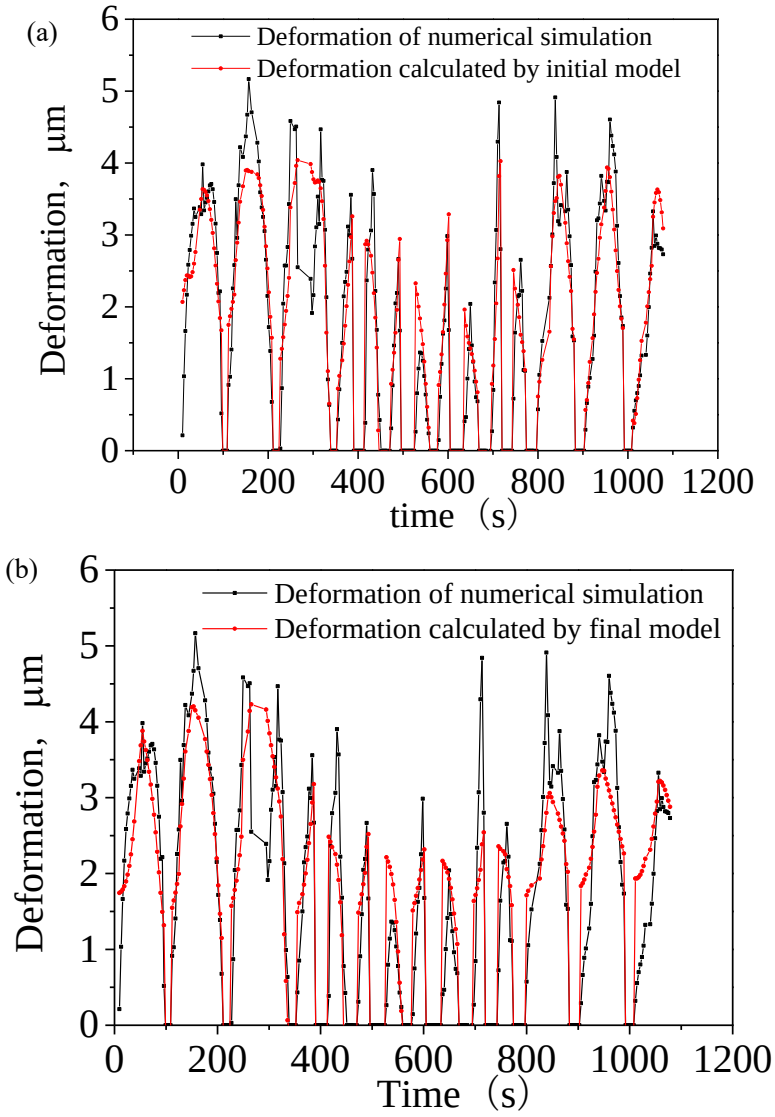

Figure 4.12 Comparison between time history deformation of numerical simulation and other models, (a) initial model, (b) final model

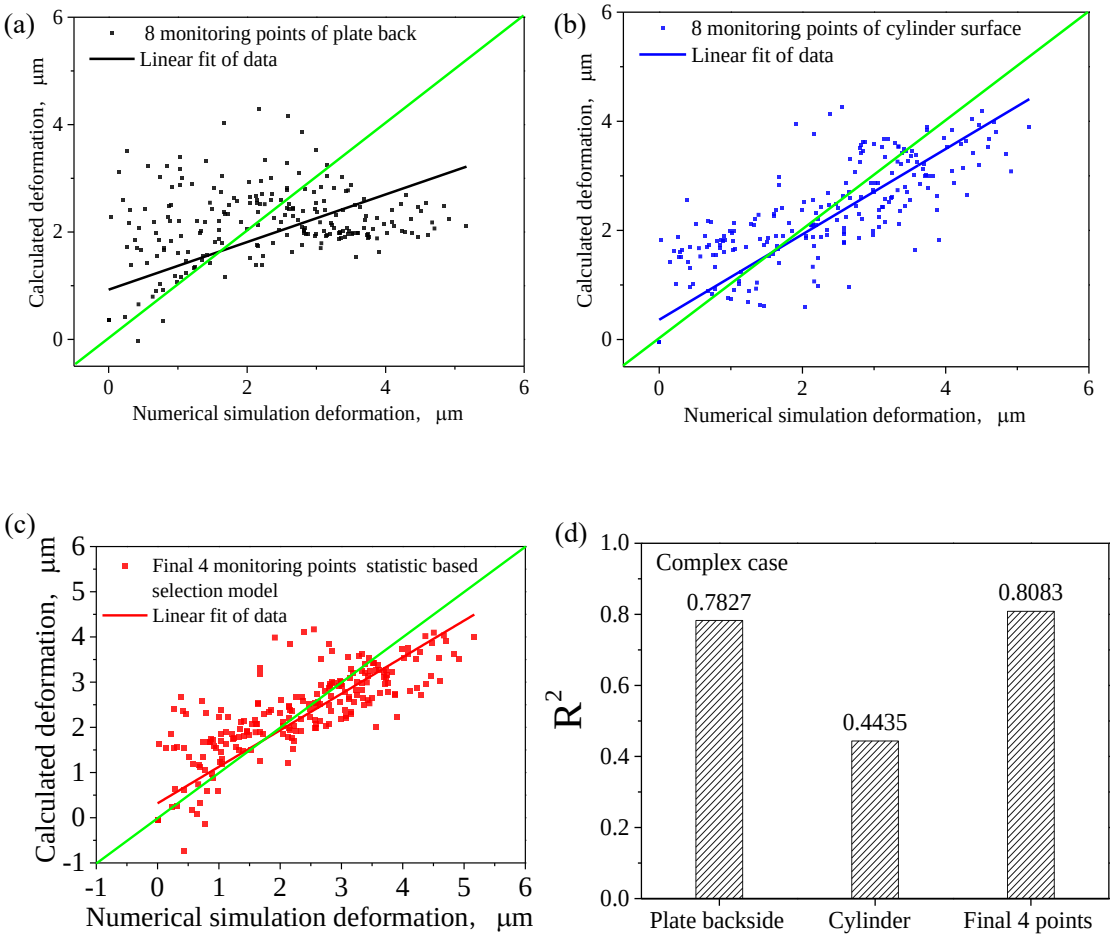

Figure 4.13 Comparison in different monitoring points group, (a) 8 monitoring points of plate back, (b) 8 monitoring points of cylinder surface, (c) 4 monitoring points of final statistic based selection model, (d) R^2 value compared of different points selection for complex workpiece

4.4 Summary

In current chapter, we propose and evaluate a statistics-based method to determine measuring points for the thermal process measurement in end milling. The predicted machining error and measurable temperatures were calculated using FEM process simulation. These predicted values were correlated in the form of the MLR model. The model was simplified based on statistical evaluations, such as AIC and *p*-values. To investigate the applicability of the proposed method for obtaining a simplified model of machining error, case studies for simple and complex workpieces in the end-milling process were conducted. In both cases, the number of measuring points was successfully decreased without deteriorating estimation accuracy. This indicates that the proposed statistics-based selection method enables the systematic determination of appropriate measuring points for the thermal monitoring of the end-milling process.

5. Statistic model comparison based on variation parameters

5.1 Background

End milling is widely used for finishing-cut parts of planar or curved shaped parts by the characteristic as agile production, which plays a significant role in manufacturing[6,7]. During the end-milling process, the generation of heat by friction between machining tool and workpiece is involved to induce excessive temperature[92~98]. Then, thermal deformation of workpiece is enhanced to cause the detriments of the surface integrity and machining quality. As the contact phenomena within the contact area between the workpiece and machining tool is extremely narrow and high-speed movement, it's extremely difficult to measure temperature and thermal deformation, especially in different thermal variations of machining process[99,100]. Therefore, how to accurately monitoring temperature and thermal deformation of workpiece in end-milling is specifically important to improve the end-milling process [101~106].

As the FEM (Finite Element Method)-based process simulation is deeply investigated for many years in thermal measurement, which is indispensable for understanding the actual machining process. An analytical model was proposed by Radulescu and Kapoor for the prediction of tool temperature fields in metal cutting process, which can be applied to any continuous or discontinuous 3D cutting process. The analysis predicts the time-dependent heat fluxes into the cutting tool and requires the cutting force as input to accurately represent the heating and cooling cycles encountered during interrupted cutting. The results show a linearly increasing relationship between tool-chip interface temperature and cutting speed during continuous and interrupted cutting [67]. A prediction of tool and chip temperature fields during continuous machining and time-varying milling is presented by Lazoglu and Altintas, the finite difference method (FDM) was conducted to solve the temperature distribution in their study. To investigate continuous or steady-state machining operations such as orthogonal cutting within the tool rake face contact region, the heat

transfer between the tool and the chip is first simulated. In their work, the time-varying chip was digitized into small elements with different tool rotation angles, and the temperature field of each of these differential elements was modeled as a first-order dynamic system. To evaluate the transient temperature change, a recursive solution was used in the study. The proposed model enables the combination of steady-state temperature prediction in continuous machining with transient temperature assessment in interrupted cutting operations [107]. In W.Grzesik's research, the finite difference methods (finite difference approaches) were conducted to detect the temperature distribution inside the contact area for continuous (turning) and discontinuous (milling) machining processes. Difference equations are used to predict the tool temperature field, defined based on the energy balance produced by all discrete elements of the model. In case of lack of simulation programs for prediction of the temperatures in the cutting zone during machining process, a basic equilibrium method (BEM) was proposed [108]. Currently, the monitoring of temperature variations can be easily and accurately realized based on some methods, while mainly focus on measuring temperature on the rake face and flank face as well as on the cutting tool [109, 110]. All above mentioned literatures are all surrounding with the analysis of temperature distribution on the cutting tool. Meanwhile, many researches also realized the significant of temperature measurement of workpiece in machining processes. During the completely end-milling process, the poor machinability and the consequent limitation on productive, tool life and workpiece integrity are mainly caused by high temperature in the machining system, so the temperature measurement for workpiece during end-milling machining should also be paid attention and investigated. For the measurement of temperature of workpieces, mostly done with the embedded thermocouples and IR systems. Some phenomena can affect production by reducing quality or precision have been described. Therefore, it becomes essential to understand processing phenomena, temperature variation and significance of temperature measurements during the end-milling process. A simple way to identify these phenomena is to monitor the process. In their work, the first step in selecting and defining the various techniques that can be used to monitor

the process is discussed. In addition, they point out the significance of temperature measurements during the end-milling process and outline the techniques for acquiring and processing the signals for monitoring the process. In order to deal with an in-process visualization method of machining support the state recognition in machining, an accurate state estimation technique was proposed, which was associated with series of data in the machine simulation [104,111~113]. For the in-process visualization, many theoretical are conducted in the researches, especially the multiple linear regression (MLR) provided better adaptation in modeling to prediction of temperature variations [114]. Multiple regression analysis is used whenever we wish to model the relationship between one response variable and more than one regressor variable [115]. The MLR theory is conducted in a comparison study to investigate the adaptation in prediction of the significant wave height. It's noted that some meteorological factors with much affection to the model are remained after the analysis of selection. Then the significant wave height models have better performance are proposed, benefiting from nonlinear models with the factors selected by MLR, such as wind speed and wind gust at a previous time step and air pressure, water temperature as well as air temperature at the same time step yield [116]. In Cakmak's research, he presents a theoretical examination, multiple linear regression (MLR) were used for modeling the temperature of water in the cooker. The adaptation abilities of models were investigated comparing the rootsquare of mean square error, mean absolute error and correlation coefficient [117]. On the other hand, for realizing the same function of prediction error and thereby relative quality of statistic models based numerous data, the Akaike information criterion (AIC) [118,119] as an estimator is conducted in researches. For describing model complexity, the effective degrees of freedom are significant, moreover, the number of effective degrees of freedom can be determined by AIC in the mixed effects models with correlated errors [120]. It's obviously that the application of MLR and AIC theories plays a significant role in-process visualizing, especially in selecting or estimating dependent variables by the optimal combination of multiple independent variables. But unfortunately, very few applications of MLR and AIC theories to the

mechanical field in-process visualizing. There are researchers pointed out that thermal expansion of the workpiece during end milling can reduce machining accuracy, so a method was proposed to select the appropriate temperature measurement location based on changes in conscious machining evaluation. By giving temperature distributions corresponding to the parameter combinations, evaluation criteria for selecting measurement points are then calculated. Furthermore, the adaptability of the proposed criteria to different machining situations is evaluated by comparing selected measurement points corresponding to different toolpaths [22,111,120]. However, it remains restrictions for real-time calculation of the FEM analysis. For solving this issue, Y.Sasaki proposed a method with much accuracy for estimating thermal displacement based on FEM. In this work, it was pointed out that machining errors could be caused by the thermal displacement of machine tools due to environmental temperature variations. And the machining errors could decrease a lot after equipped with a simplified model [121].While the heat is transformed from mechanical work during machining process. About 90% in mechanical energy become thermal energy according to the research of Shaw [96]. During the end-milling process, workpiece's thermal changes due to the existence of frictional heating and plastic work convert heating, which can cause the thermal deformation variation. Absolutely, the deformation of the thermal workpiece, which plays a significant role on the accuracy of machining in the end-milling. Although there is not enough literature to study this field, the monitoring and research of thermal deformation variations in the process of end-milling is urgent. In this paper, statistic models based on variation parameters for monitoring workpiece's thermal deformation are proposed, and their relative merits and demerits are discussed by considering precision, ease of use and applicable range, etc. Based the data are completely obtained through finite element numerical simulations, also the MLR and AIC theories are conducted in this research in describing the thermal deformation at machining points by the optimal combination of multiple independent variables.

Various cases of changing the significant parameters of machining process such as heat source, convective heat transfer coefficient is simulated and calculated. Both the

methods proposed in this study have good applicability to the prediction of the deformation of the machining point, even though, the two methods to propose the models have different adaptation ranges and situations. It's selectable for other researches to choose the appropriate statistic model based on vary situation for their own needs.

5.2 Framework of Statistics-based thermal monitoring based on variation parameters

For the previous part of this research, mainly concerned with a selection of statistic-based measuring points for monitoring the thermal deformation of a workpiece in end-milling. Due to the deformation of thermal workpiece plays an important role which can affect the machining accuracy, in this sense, it comes the issue that how to realize the function to direct measure the workpiece deformation in a machining situation with process disturbances. Fortunately, it can be easily and accurately to measure the local temperatures of the workpiece using common measuring methods. With this purpose, a sensor-configured thermal simulation is conducted which combines local temperature measurements with thermal simulations [111].

There are linear relationships between the thermal deformation and thermal states during end-milling process, appropriately, multiple linear regression (MLR) can be applied. For estimating the workpiece deformation with measured temperatures, an empirical modeling method is introduced. In the FEM-based simulations, the predicted time- series of temperature and deformations of the workpiece can be extracted, with these data base, the number of measuring points can be determined using Akaike information criterion (AIC) and effective measuring points are selected using the *p*-value index. Therefore, a monitoring method for workpiece deformations is developed using simulation-based case studies in our previous research, which can represent workpiece deformation with minimum number of measuring points and corresponds well to the FEM simulations. The schematic explanation of this research is shown in **Fig.5.1**.

In my previous research work [122], the proposed model has a good effect in predicting thermal deformation when applied to constant material parameter condition. The following research is aimed at the variable material parameters, which means that the variable range can be adjusted up and down, and thermal deformation can be predicted effectively and with high precision. Because in the actual processing process, some parameters such as heat source and heat conversion coefficient will change due to the influence of gas flow and friction. Then we will discuss and analyze the application of the proposed model after changing the processing parameters in the following research. In the analysis, the temperature field of the finite element simulation results is experimentally verified, and the influence of different material parameters on the model accuracy is studied; On this basis, two new models are proposed, one is the MLR fitting method, and the other is adding a correction coefficient to the equation based on the original model.

In this way, both models have better reliability and accuracy for predicting thermal deformation. Finally, the error analysis of the calculation results of these two models is carried out. The proposed two models can guide the thermal deformation monitoring work in the future end milling process, and provide a preliminary basis for the digital twin work of the end milling process.

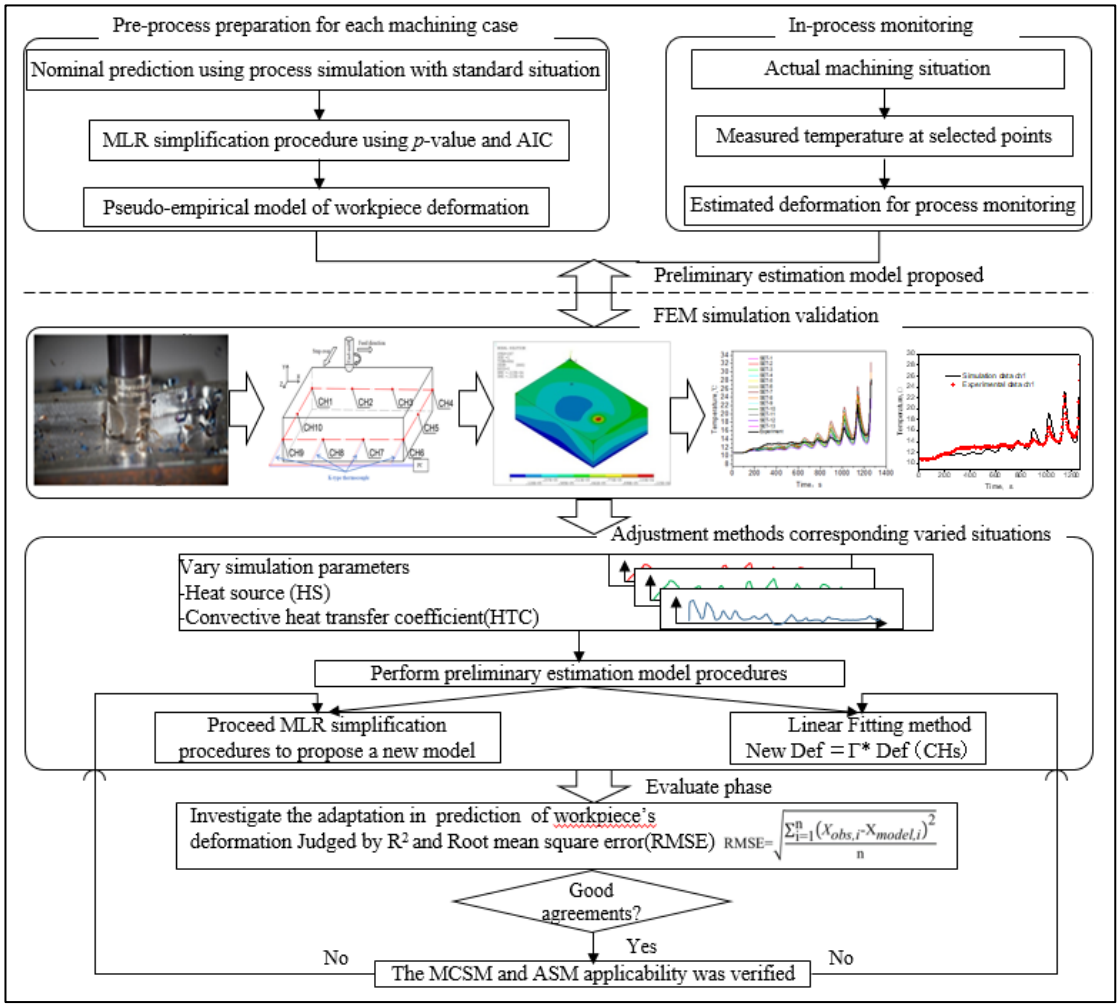

Figure 5.1 Framework of this research

5.3 Statistic-model proposed

5.3.1 Normal statistic-model proposed

The geometry of workpiece, the end-milling process and the locations of measuring points are presented in **Fig.5.2**. In this study, the workpiece is assumed under full machining with φ16 mm diameter end-milling tool at 0.00125 m/s feed rate. There is 10mm distance between adjacent tool paths. By referring to the catalogue of high-speed steel cutting tools for bottom surface finishing, the setting conditions mentioned above are determined. The machining process is modeled as a heat conduction problem with a moving heat source, since the volume reduction of the workpiece during machining is ignored. Furthermore, the machining error due to the thermal expansion of the

workpiece is approximated by the opposite value of the deformation at machining point corresponding to the position of the end-milling. **Table 1** shows the basic constants and detailed boundary conditions of carbon steel S45C (JIS) which obtained by FEM simulations in the end-milling process.

Table 1 Basic constants of carbon steel S45C (JIS)

Name	Value
Density	7850 kg/m^3
Heat source (W)	573
Heat conduct coefficient (W/(m×°C))	58
Convective heat transfer coefficient (W/(m^2×°C))	550
Initial temperature (°C)	10.8
Environment temperature (°C)	10.8
Elasticity modulus (GPa)	206
Poisson ratio	0.3
Coefficient of linear expansion (°C^{-1})	14.8×10^{-6}

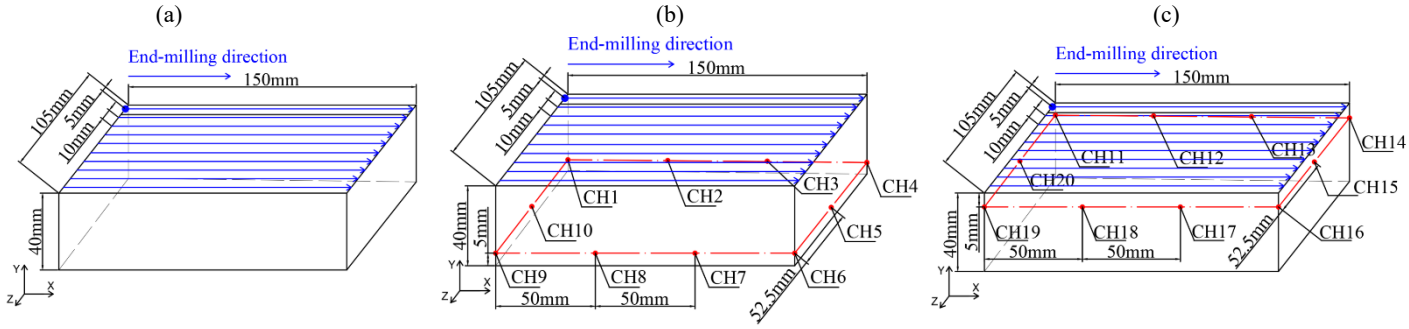

Figure 5.2 End-milling process of the workpiece and locations of the measuring points. (a) The straight lines on the top indicate the machining tool path. (b) Location of lower measuring points. (c) Location of upper measuring points.

Firstly, an empirical model for monitoring thermal expansion would be proposed referring the procedures described in previous research [122] combining MLR, AIC and *p*-value, while the block workpiece in this study is in a different full machining than before. After the simulation conducted by ANSYS/APDL, the time-series temperatures of 20 measuring points and time-series deformation of heat source are extracted, which represent input variables ($T_{ch1}(t)$, $T_{ch2}(t)$, … $T_{chn}(t)$ are stand for independent variable)and output variable respectively($D_{heat\text{-}source}(t)$ is stand for dependent variable). In addition, for matching the level of MLR method considering the determination of coefficient of multiple determined (R^2) [123]. The independent

variables are used to illustrate or describe the dependent variable. The whole optimizing procedures to obtain the statistic-model is shown in **Fig.5.5**, in which The R^2 values of each improved model are 0. 0.7663, 0.762, 0.7527, 0.7508, 0.743, 0.7394, 0.7233, 0.7114, 0.7001, 0.6849, 0.666, 0.6382, respectively. The AIC terms and *p*-value (should lower than 1×10^{-4}[124]) with high value would be eliminated during optimizations. The initial result of statistics forecasting model is expressed as Eq. (1), in which *i* is stand for number of measuring monitoring points of temperature.

$$D_{heat-source}(t) = \beta_0 + \sum \beta_i T_{CHi} \quad \ldots\ldots\ldots\ldots\ldots\ldots\ldots\ldots\ldots\ldots \text{(1)}$$

As described the function of MLR and AIC in this study as well as based on data base extracted from simulations, the number of measuring points can be determined effective measuring points can be selected using the *p*-value index. Finally, the equation of statistic-based selection model is simpler and more reliable by only consisting of 6 independent variables is fitted by MLR with the R^2 value of 0.6382. For the consideration of the effectiveness and reliability of the proposed statistic-model, a comparison between time-series deformation of numerical simulation with the proposed statistic-model was conducted. The comparison results show that the statistic-model with few measurement points can accurately and efficiently predict the thermal deformation. The statistic-model is expressed as follow:

$$D_{heat-source}(t) = [7.81494\text{-}1.39202T_{CH1}(t)\text{-}0.76221T_{CH3}(t)+1.25265T_{CH8}(t)+ 0.35316T_{CH10}(t)+0.31799T_{CH11}(t)+0.17424T_{CH17}(t) \ldots\ldots\ldots \text{(2)}$$

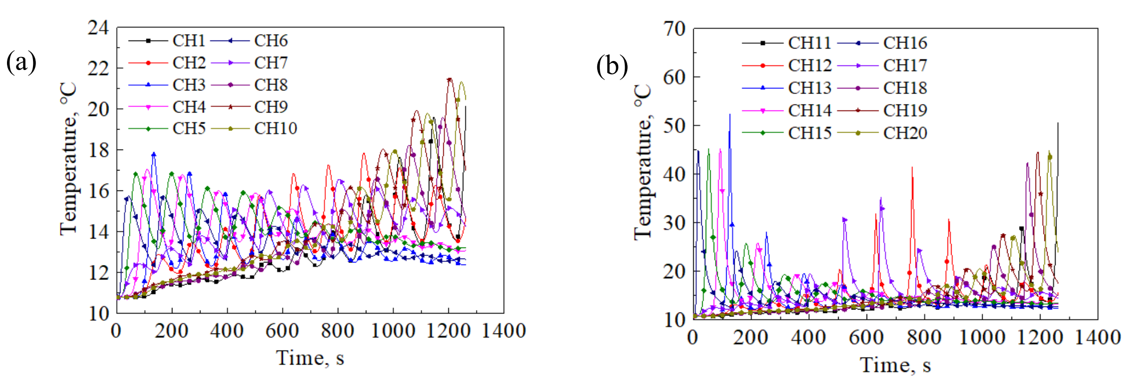

Figure 5.3 Time-series of temperature in 20 monitor points, (a) CH1~CH10, (b) CH11~CH20

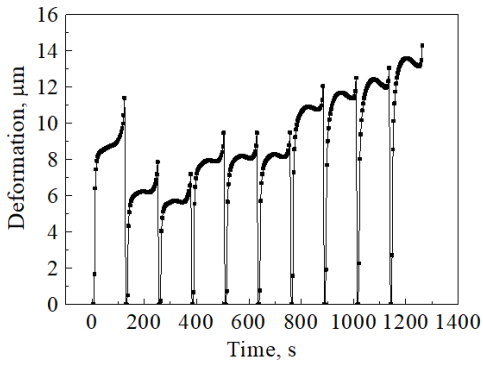

Figure 5.4 Time-series of deformation in center of heat source

Coefficient	Estimated value	*p*-value
β_0	-16.24001	8.42E-05
β_1	-1.54612	2.66E-06
β_2	-0.92882	0.001197
β_3	-1.2943	1.34E-11
β_4	0.85195	2.54E-05
β_5	-0.60719	0.000742
β_6	0.73186	0.000318
β_7	0.77544	5.49E-07
β_8	1.12942	7.72E-09
β_9	-0.34284	0.038378
β_{10}	1.22419	2.04E-09
β_{11}	0.29736	6.23E-05
β_{12}	0.18315	0.003942
β_{13}	0.26268	5.45E-09
β_{14}	0.05917	0.128163
β_{15}	0.15125	0.000187
β_{16}	0.19924	3.63E-06
β_{17}	0.29122	1.01E-10
β_{18}	0.22828	6.63E-06
β_{19}	0.03584	0.465629
β_{20}	-0.12099	0.016449

(**a**) Result of initial model

Deleted measuring point	AIC value
19	403.89
none	
14	405.77
9	407.86
20	409.42
12	412.12
2	414.43
5	415.37
6	417.04
15	418.1
11	420.29
4	422.09
18	424.81
16	426.03
1	426.66
7	429.87
8	438.61
13	439.33
10	441.36
17	447.56
3	451.75

(**b**) AIC value in different groups

Eliminate low AIC term

Coefficient	Estimated value	*p*-value
β_0	-16.72689	4.06E-05
β_1	-1.50432	3.39E-06
β_2	-0.94993	0.000865
β_3	-1.28142	1.65E-11
β_4	0.85159	2.53E-05
β_5	-0.60413	0.00078
β_6	0.74858	0.00021
β_7	0.73105	2.61E-07
β_8	1.182	8.61E-11
β_9	-0.27126	0.041517
β_{10}	1.17268	8.38E-10
β_{11}	0.29517	6.86E-05
β_{12}	0.18617	0.003306
β_{13}	0.261	6.29E-09
β_{14}	0.05952	0.125657
β_{15}	0.15069	0.000195
β_{16}	0.19874	3.77E-06
β_{17}	0.29663	2.50E-11
β_{18}	0.22026	8.19E-06
β_{20}	-0.11957	0.017587

(**c**) Result of improved model

Eliminate large *p*-value term

Coefficient	Estimated value	*p*-value
β_0	7.81494	3.55E-08
β_1	-1.39202	<2.00E-16
β_3	-0.76221	<2.00E-16
β_8	1.25265	<2.00E-16
β_{10}	0.35316	3.22E-05
β_{11}	0.31799	6.16E-07
β_{17}	0.17424	2.36E-07

(**d**) Result of tenth improved model

Figure 5.5 Tables in MLR simplification

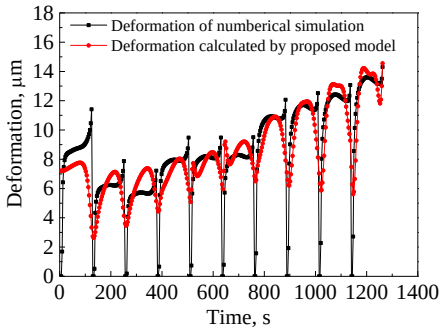

Figure 5.6 Comparison between time-series deformation of numerical simulation and statistic-model

5.3.2 Statistic-model applied in the situation of variation parameters

In order to analysis the reliability of proposed model, the variation parameters of numerical simulation in end-milling process were conducted. The different boundary condition was listed in **Table 14.** According to the **Table 14**, the changing range of heat source and convective heat transfer coefficient were from 50% to 150%. The different boundary conditions were embedded in the FEM numerical simulation of simple workpiece end-milling process. Therefore, the time series of temperature in monitoring points and thermal deformation in the center of heat source were extracted respectively. In addition, according to the time series of temperature monitoring points, predict thermal deformation of workpiece was correspondingly calculated by proposed model. Finally, the comparison between FEM simulation result and proposed model calculated result were shown in **Fig.5.7**, **Fig.5.8** and **Fig.5.9**. According to the **Fig.5.7**, with the heat source value changing from 50% to 150%, the tendency of FEM numerical simulation and proposed model calculation are shown as the linear changing. The proposed model calculated thermal deformation are firstly bigger than FEM numerical simulation thermal deformation and then smaller than that of FEM numerical simulation. By comparing **Fig.5.7** and **Fig.5.8**, the changing tendency of comparison between proposed models calculated result and FEM numerical simulation result by the convective heat transfer coefficient changing are completely opposite to the heat source changing. By comparing **Fig.5.7**, **Fig.5.8** and **Fig.5.9**, the changing tendency of comparison between proposed models calculated result and FEM numerical simulation result by heat source and convective heat transfer coefficient simultaneous changing are closely similar to the result of heat source solo changing, which is opposite to the result of convective heat transfer coefficient changing. Hence, it is illustrate that the temperature and thermal deformation changing of workpiece during end-milling process are mainly determined by heat source changing. Meanwhile, the changing tendency of FEM numerical simulation result and proposed model calculated result are obviously shown as the linear relationship, including heat source solo changing, convective heat transfer coefficient solo changing and two factors simultaneous

changing.

Table 17 Factors and detailed simulation design

No.	A-Heat source (W)		B-Convective heat transfer coefficient (W/(m²×℃))	
	Change limit	Value	Change limit	Value
Normal	100%	573	100%	550
1	50%	286.5	100%	550
2	75%	429.75	100%	550
3	105%	601.65	100%	550
4	110%	630.3	100%	550
5	115%	658.95	100%	550
6	125%	716.25	100%	550
7	150%	859.5	100%	550
8	100%	573	50%	275
9	100%	573	75%	412.5
10	100%	573	105%	577.5
11	100%	573	110%	605
12	100%	573	115%	632.5
13	100%	573	125%	687.5
14	100%	573	150%	825
15	50%	286.5	50%	275
16	75%	429.75	75%	412.5
17	125%	716.25	125%	687.5
18	150%	859.5	150%	825

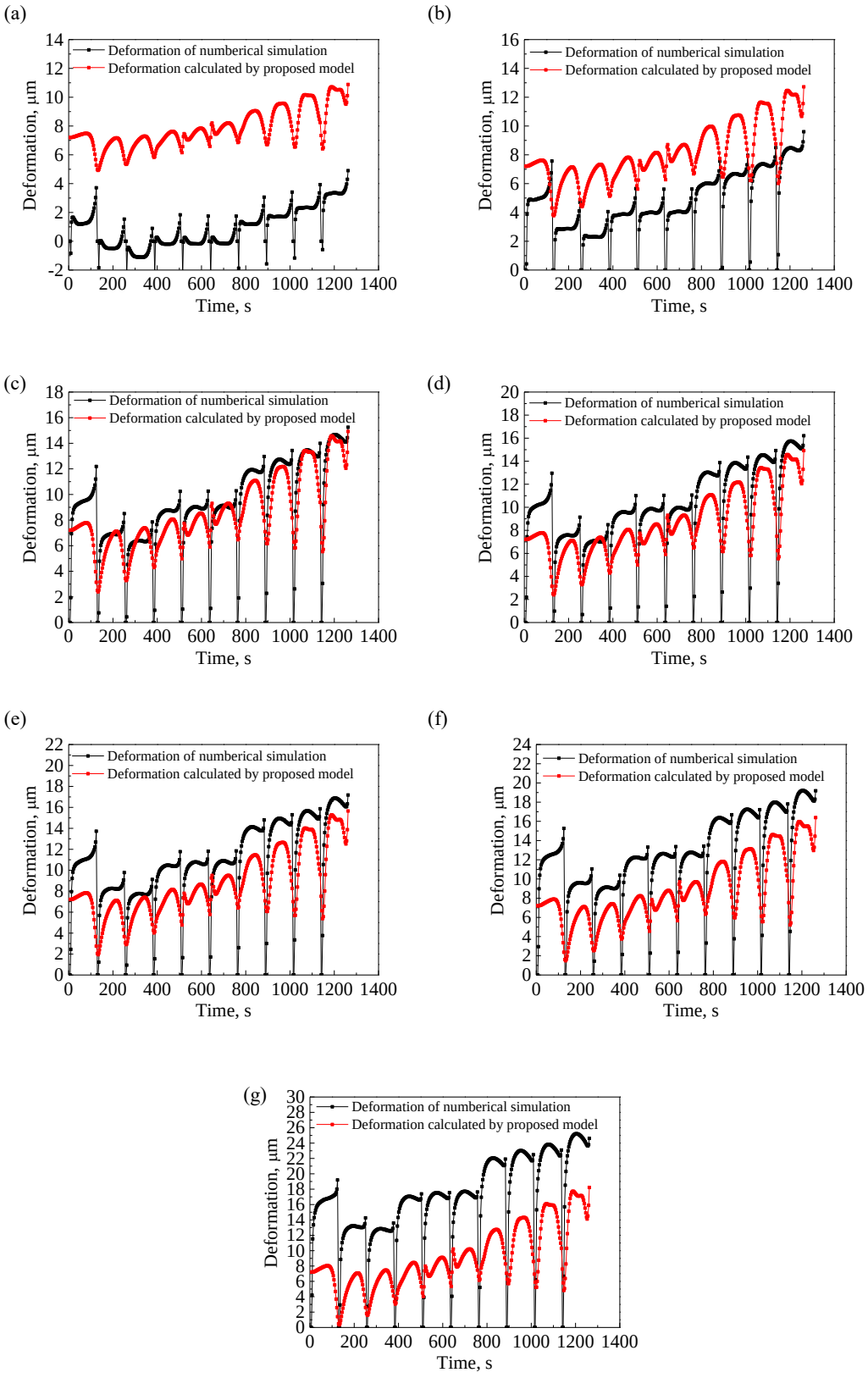

Figure 5.7 Comparison between time-series deformation of numerical simulation and statistic-model in different heat source: (a)50%, (b)75%, (c)105%, (d)110%, (e)115%, (f)125%, (g)150%

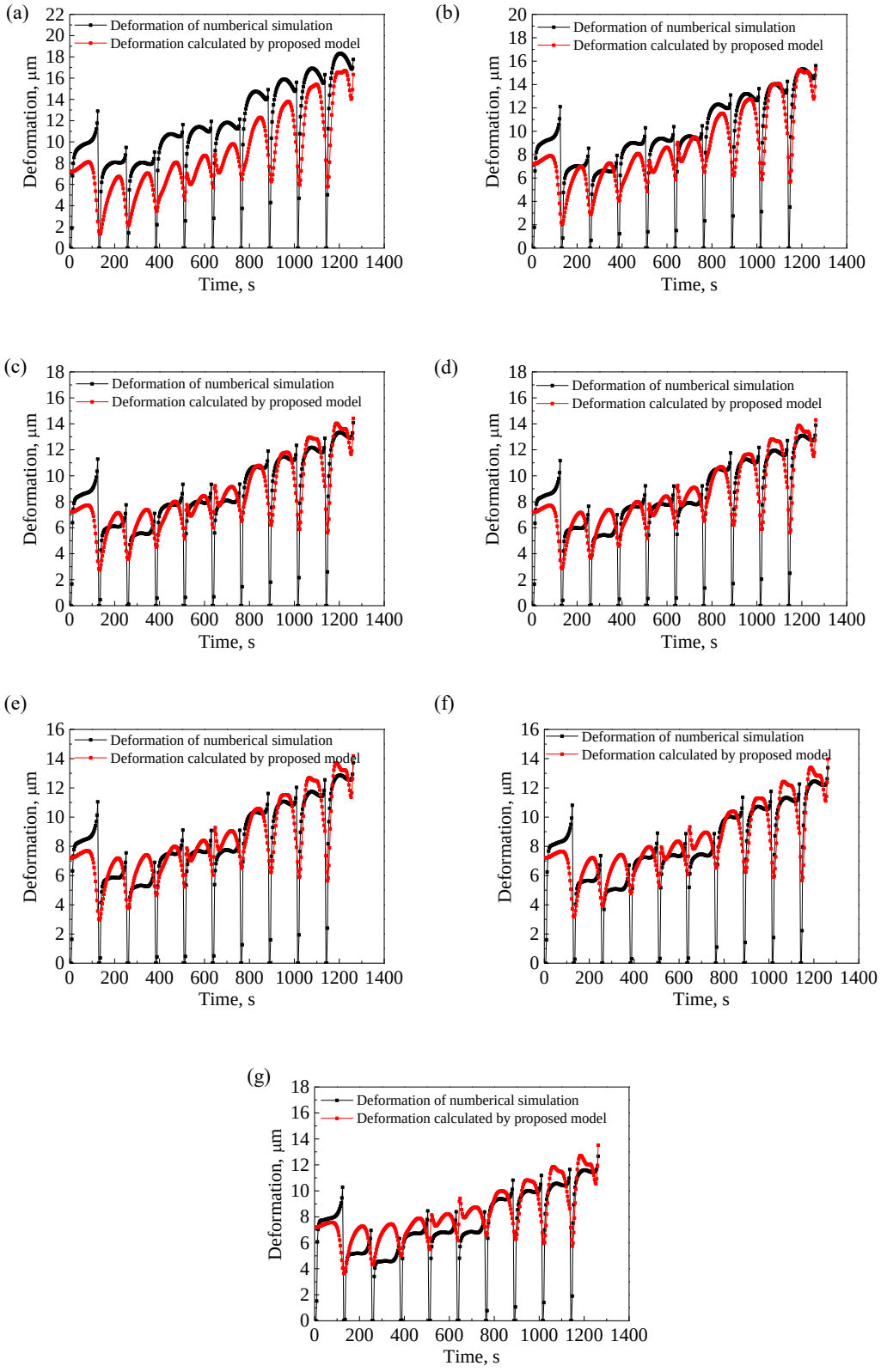

Figure 5.8 Comparison between time-series deformation of numerical simulation and statistic-model in different convective heat transfer coefficient: (a)50%, (b)75%, (c)105%, (d)110%, (e)115%, (f)125%, (g)150%

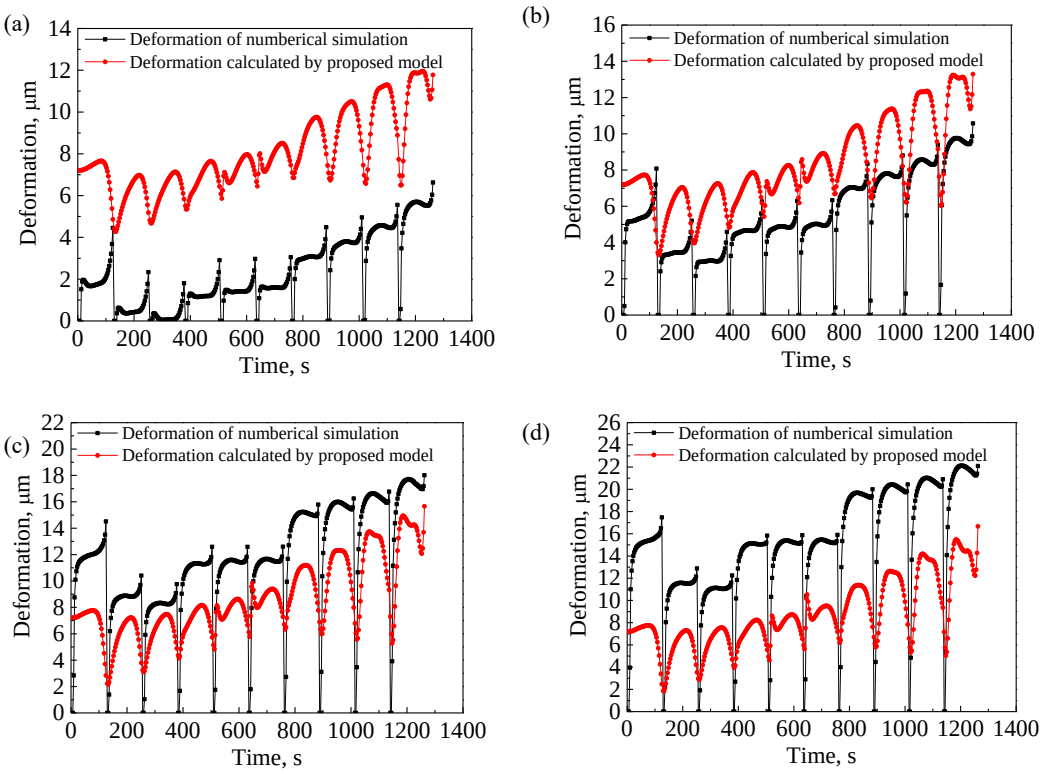

Figure 5.9 Comparison between time-series deformation of numerical simulation and statistic-model in different heat source and convective heat transfer coefficient: (a)50%, (b)75%, (c)125%, (d)150%

5.3.3 Adjusted statistic-model proposed based on variation parameters

When the machining situations are changed, the FEM numerical result of thermal deformation hardly correspond to those calculated by the normal model. The thermal deformation changing rate (δ_{TDC}) is used to describe the relationship between FEM numerical result of thermal deformation and proposed model calculated result, which is expressed as follow:

$$\delta_{TDC} = \frac{D_{FEM\ simulated}}{D_{model\ calculated}} \tag{3}$$

According to the Eq. (3), the thermal deformation change rate after the heat source and convective heat transfer coefficient are changed individually are shown in **Fig. 5.10** and **Fig.5.11** respectively. Therefore, the relationship between thermal deformation changing result and heat source solo changing could be expressed as following:

$$\alpha = 2.38254\mathrm{e}^{\frac{\mu_{HS}}{2.0305}} - 2.95399 \tag{4}$$

Where, δ_{α} is thermal deformation changing coefficient depending on heat source solo

changing. μ_{HS} is the change rate of heat source. Meanwhile, the relationship between thermal deformation changing result and convective heat transfer coefficient solo changing could be expressed as following:

$$\beta = 1.52563e^{\frac{\mu_{HTC}}{-0.47939}} + 0.80008 \quad (5)$$

Where, δ_β is thermal deformation changing coefficient which varies depending on the HTC alone. μ_{HTC} the change rate of convective heat transfer coefficient. Then, by combining δ_α, δ_β and the thermal deformation changing rate of heat source and convective heat transfer coefficient simultaneous changing, the thermal deformation changing coefficient δ_γ depends on the simultaneous change of HS and HTC could be expressed by MLR method, which is written as following:

$$\delta_\gamma = 0.98892\alpha + 0.85962\beta - 0.86279 \quad (6)$$

Consequently, the adjusted proposed model could be obtained by combining Eq.(2), Eq.(4), Eq.(5) and Eq.(6), modified coefficient statistic model (MCSM) is expressed as following:

$$\begin{aligned} D_{\text{heat-source}}(t) = &\left(2.35614e^{\frac{\mu_{HS}}{2.0305}} + 1.31146e^{\frac{\mu_{HTC}}{-0.47939}} - 3.09629\right) \\ &* [7.81494 - 1.39202T_{CH1}(t) - 0.76221T_{CH3}(t) + 1.25265T_{CH8}(t) + \\ &0.35316T_{CH10}(t) + 0.31799T_{CH11}(t) + 0.17424T_{CH17}(t)] \end{aligned} \quad (7)$$

On the other hand, the adjusted statistic-model (ASM) was introduced as the second method utilizing MLR simplifications to offer operators more options, which could also adjusted to varied parameters correspond to variation of actual machining process in end-milling. In the case of varied parameters, compared with normal model equation (2) scheme, more databases were additionally considered including the normal database, databases with HS and HTC simultaneously changed within ±25%. Then the equation of ASM could also be obtained by combining MLR, AIC and p-value, the insufficient measurement candidates with same changing tendencies would be eliminated one by one referring the procedures for normal model proposed. Consequently, the equation of ASM is expressed as following:

$$\begin{aligned} &D_{\text{heat-source}}(t) \\ &= -11.94278 - 3.68748T_{CH1}(t) + 0.72531T_{CH2}(t) - 2.21636T_{CH3}(t) + 0.92495T_{CH4}(t) \end{aligned}$$

$$+ 1.99685T_{CH7}(t)+1.07628T_{CH10}(t)+0.75046T_{CH11}(t)+0.41957T_{CH13}(t)+0.38645T_{CH16}(t)+ 0.68189T_{CH18}(t) \quad (8)$$

The R^2 of the adjusted statistic-model is 0.6762.. All the *p*-value are smaller than 2×10^{-16}.

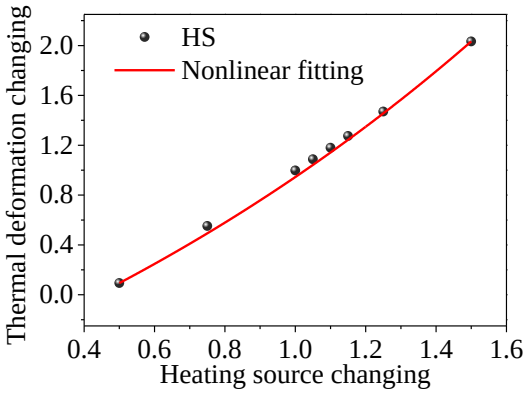

Figure 5.10 Thermal deformation changing result of heat source solo changing

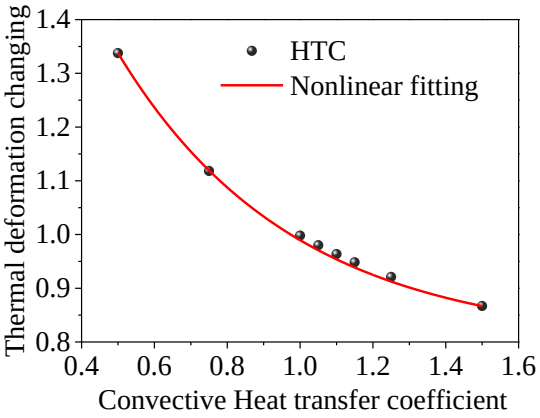

Figure 5.11 Thermal deformation changing result of convective heat transfer coefficient solo changing

5.4 Error analysis of modified statistic-model

5.4.1 Error analysis of MCSM

The comparison between time-series deformation of numerical simulation and MCSM calculation by heating source solo changing, convective heat transfer coefficient solo changing and two factors simultaneous changing are shown in **Fig. 5.12**, **Fig.5.13** and **Fig.5.14**, respectively. The black line is the thermal deformation of FEM

numerical simulation. The red and blue line are the thermal deformation of proposed normal model and MCSM respectively. According to the **Fig. 5.12**, when the range of heating source solo changing is from 50% to 150%, the thermal deformation of MCSM is more closely to the thermal deformation of FEM numerical simulation. Meanwhile, when the range of two factors simultaneous changing is from 50% to 150%, the thermal deformation of MCSM is also more accurate, which is shown in **Fig. 5.14**. In addition, according to the **Fig. 5.13**, when the range of convective heat transfer coefficient solo changing is from 50% to 150%, the thermal deformation of MCSM is closely to the thermal deformation of FEM numerical simulation, which is similar to that of thermal deformation calculated by proposed normal model. Consequently, rather than proposed normal model, MCSM is more accuracy to describe the relationship between temperature of monitoring points and thermal deformation of end-milling center.

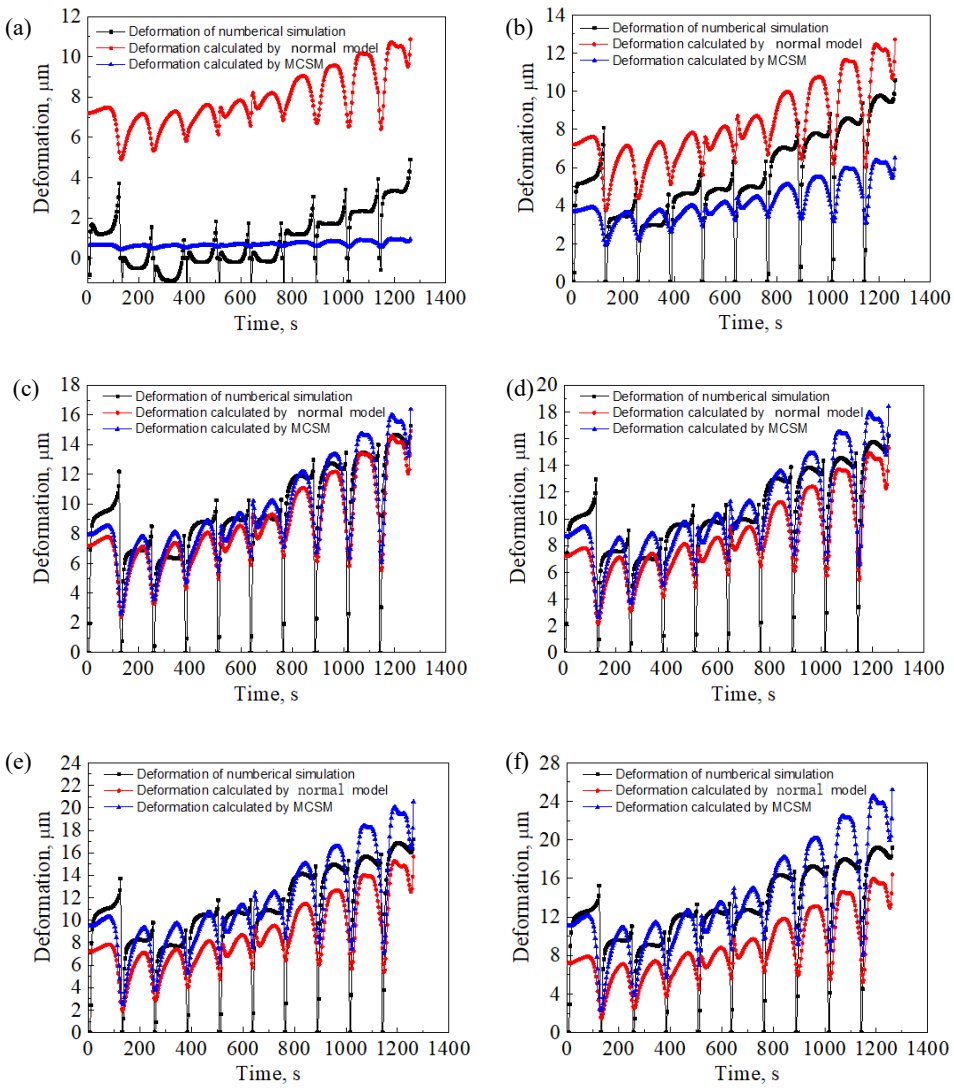

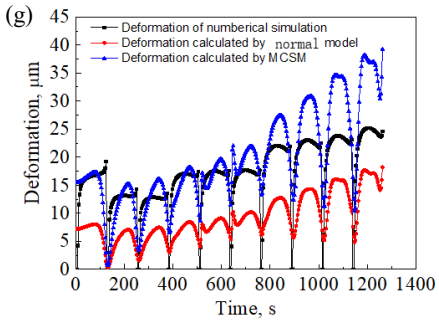

Figure 5.12 Comparison between time-series deformation of numerical simulation and MCSM in different heat source: (a)50%, (b)75%, (c)105%, (d)110%, (e)115%, (f)125%, (g)150%

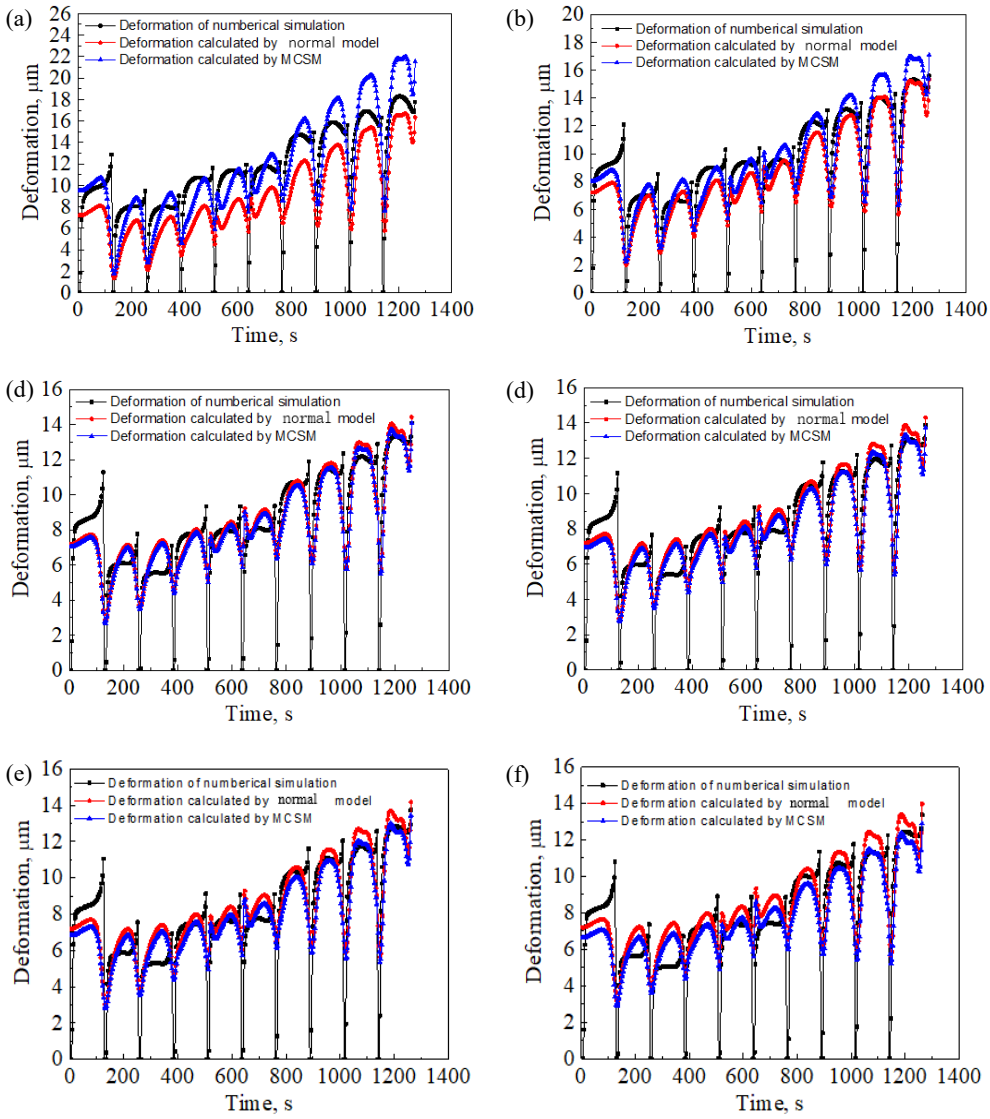

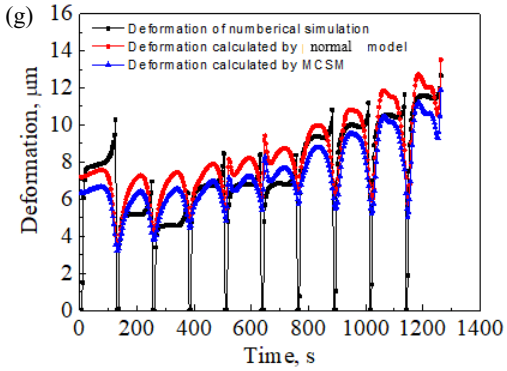

Figure 5.13 Comparison between time-series deformation of numerical simulation and MCSM in different convective heat transfer coefficient: (a)50%, (b)75%, (c)105%, (d)110%, (e)115%, (f)125%, (g)150%

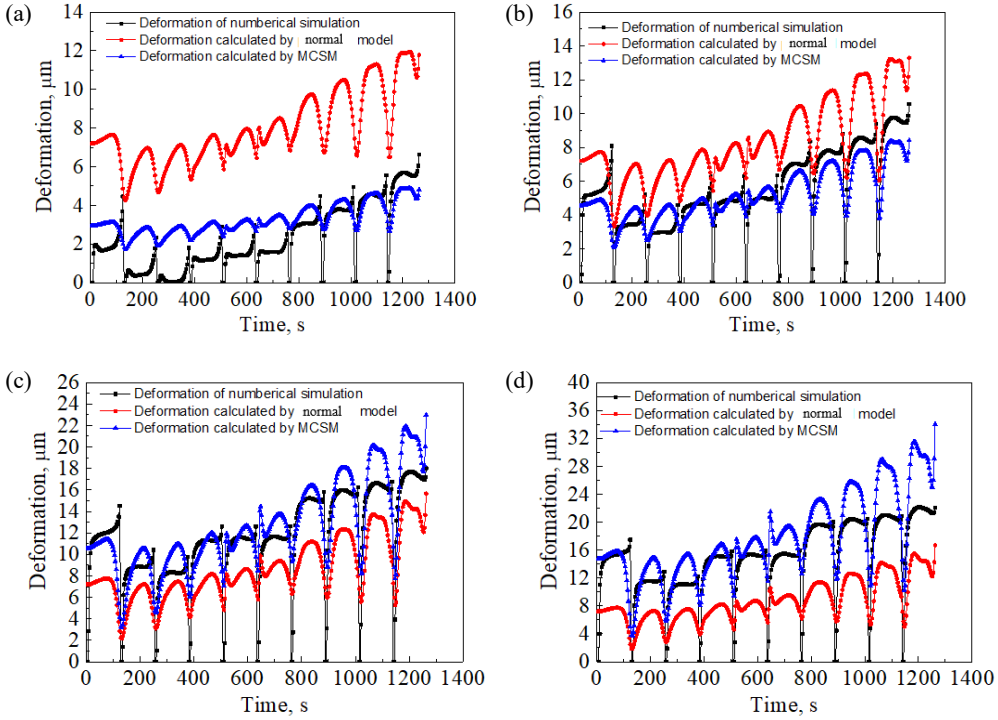

Figure 5.14 Comparison between time-series deformation of numerical simulation and MCSM in different heat source and convective heat transfer coefficient: (a)50%, (b)75%, (c)125%, (d)150%

The error analysis is calculated by root-mean-square error (RMSE), which is expressed as follow:

$$RMSE = \sqrt{\frac{\sum_{i=1}^{n}\left(X_{cal,i}-X_{model,i}\right)^2}{n}} \tag{9}$$

Where $X_{cal,i}$ is the observed value, $X_{model,i}$ is e model value. The closer the RMSE value is to 0, the more similar the observed result is to the model result. The comparison between time-series deformation of numerical simulation and MCSM

calculation by HS changes alone, HTC changes alone and two factors simultaneous change are shown in **Fig.**5.15, **Fig**.5.16 and **Fig**.5.17, respectively. The purple color is stand for MCSM result, the green color is stand for proposed normal model. According to the **Fig.**5.15, when the range of HS is changed alone from 50% to 150%, the thermal deformation of MCSM is more closely to the thermal deformation of FEM numerical simulation. Meanwhile, when the range of two factors are simultaneously changed from 50% to 150%, the thermal deformation of MCSM is also more accurate, which is shown in **Fig**.5.17. In addition, according to the **Fig**.5.16, when the range of HTC is changed alone from 100% to 115%, the thermal deformation of MCSM is closely to the thermal deformation of FEM numerical simulation, which is similar to that of thermal deformation calculated by proposed normal model. Consequently, rather than proposed normal model, MCSM is more accuracy to describe the relationship between temperature of monitoring points and thermal deformation of end-milling center.

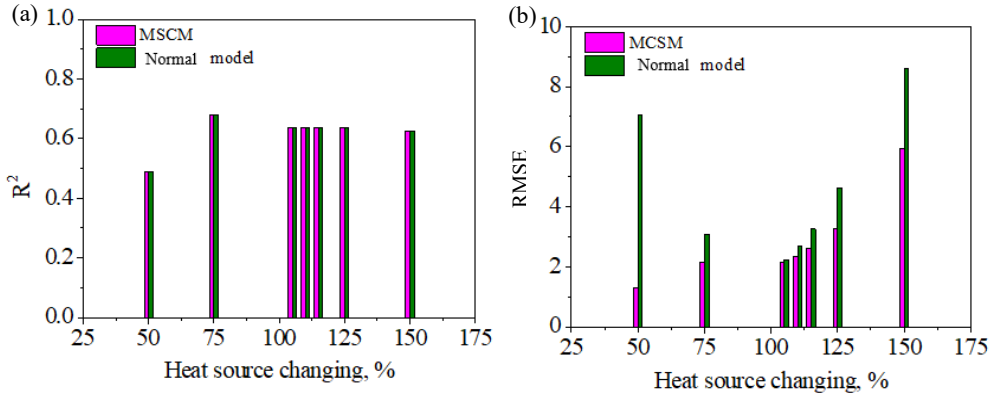

Figure 5.15 Comparison between time-series deformation of normal model and MCSM in different HS: (a) R^2, (b)RMSE

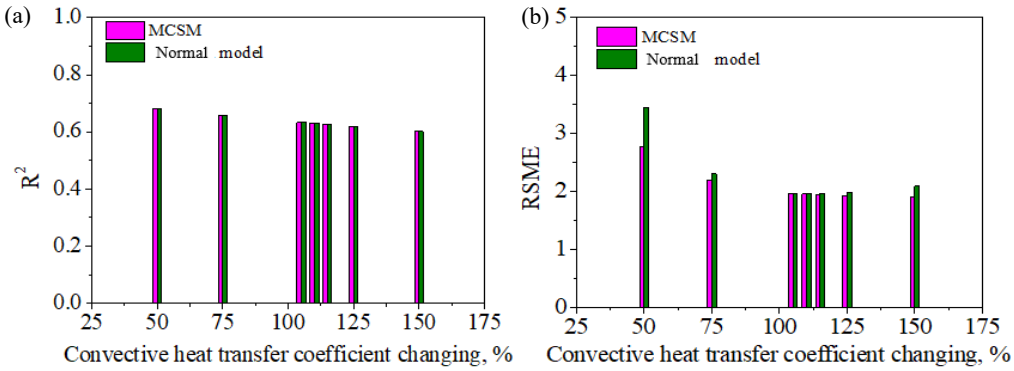

Figure 5.16 Comparison between time-series deformation of normal model and MCSM in different HTC: (a) R^2, (b) RMSE

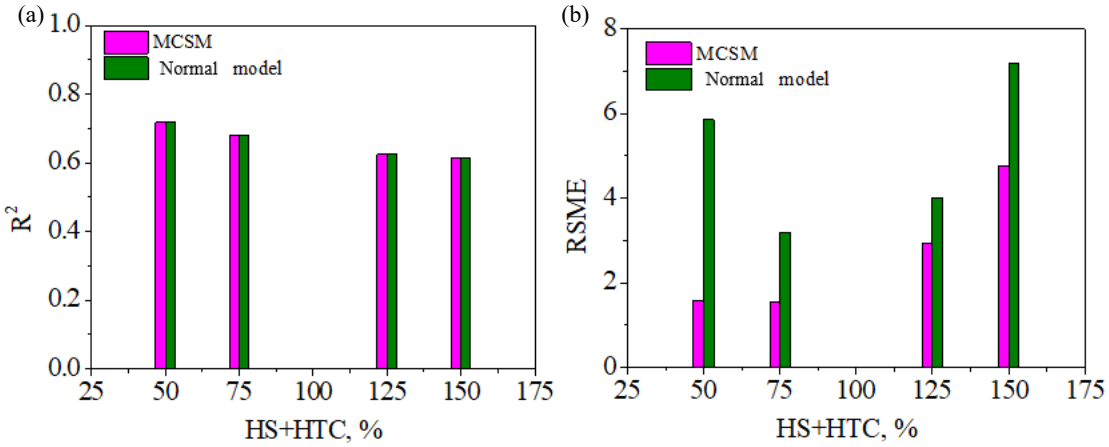

Figure 5.17 Comparison between time-series deformation of normal model and MCSM in different HS and HTC: (a) R^2, (b) RMSE

5.4.2 Error analysis of ASM

The comparison between time-series deformation of numerical simulation and ASM calculation by heating source solo changing, convective heat transfer coefficient solo changing and two factors simultaneous changing are shown in **Fig.5.18**, **Fig.5.19** and **Fig.5.20**, respectively. The black line is the thermal deformation of FEM numerical simulation. The red and green line are the thermal deformation of proposed normal model and ASM respectively. According to the **Fig.5.18**, when the range of HS is changed alone from 50% to 150%, most of the thermal deformation of ASM is more closely to the thermal deformation of FEM numerical simulation. However, when the range of HTC is changed alone from 50% to 150%, the thermal deformation of ASM is not closely to the thermal deformation of FEM numerical simulation by comparing with that of thermal deformation calculated by proposed normal model. When the range of two factors are simultaneously changed from 50% to 150%, the thermal deformation of ASM is accurate in range from 50% to 150%, but excluding the unchanged 100%. Consequently, only when range of HS changes alone, HTC changes alone and two factors simultaneous change are located in 50% to 150% respectively, ASM is more accuracy to describe the relationship between temperature of monitoring points and thermal deformation at machining point rather than proposed normal model.

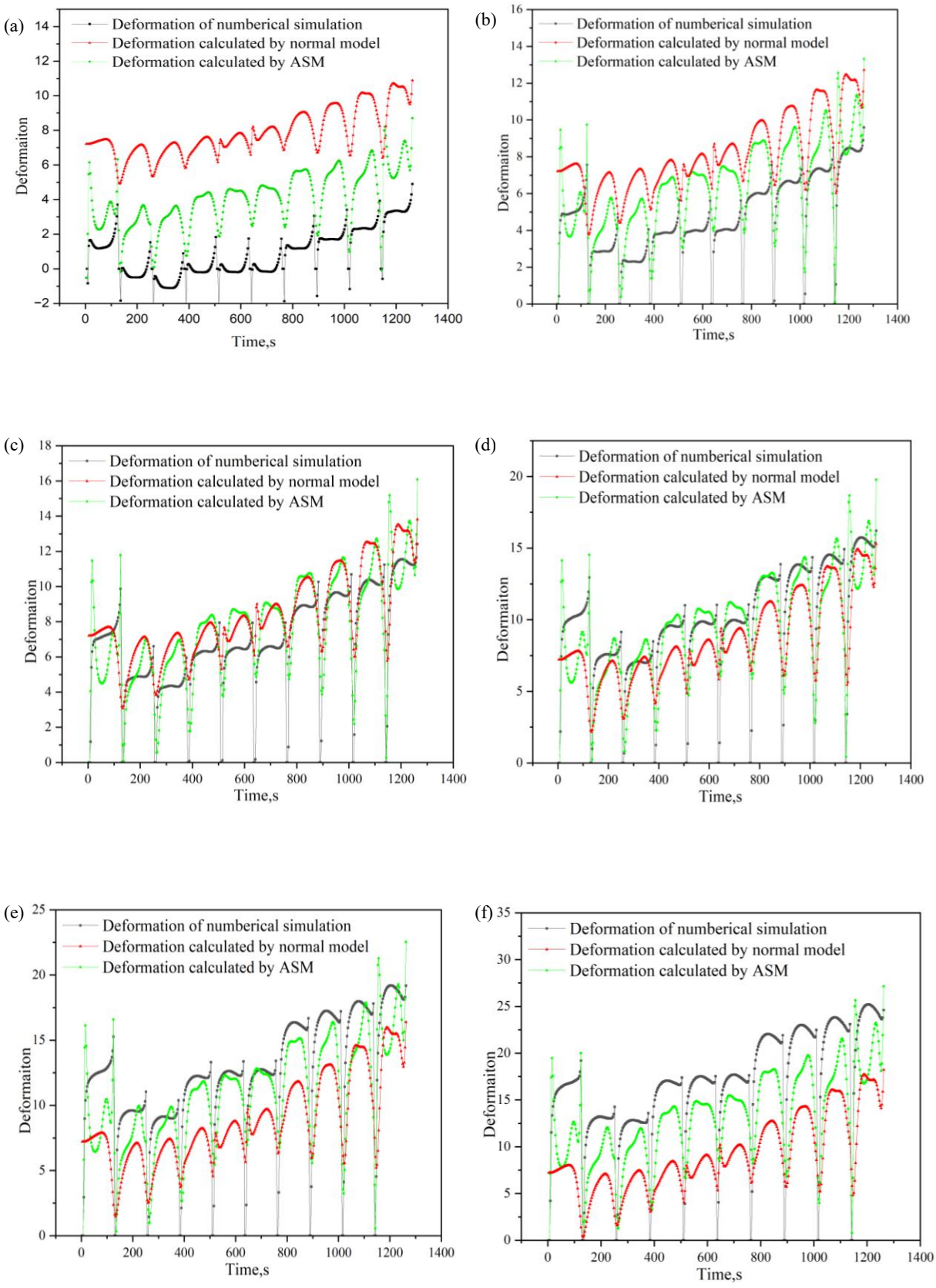

Figure 5.18 Comparison between time-series deformation of numerical simulation and ASM in different HS : (a)50%, (b)75%, c)90%, (d)110%, (e)125%, (f)150%,

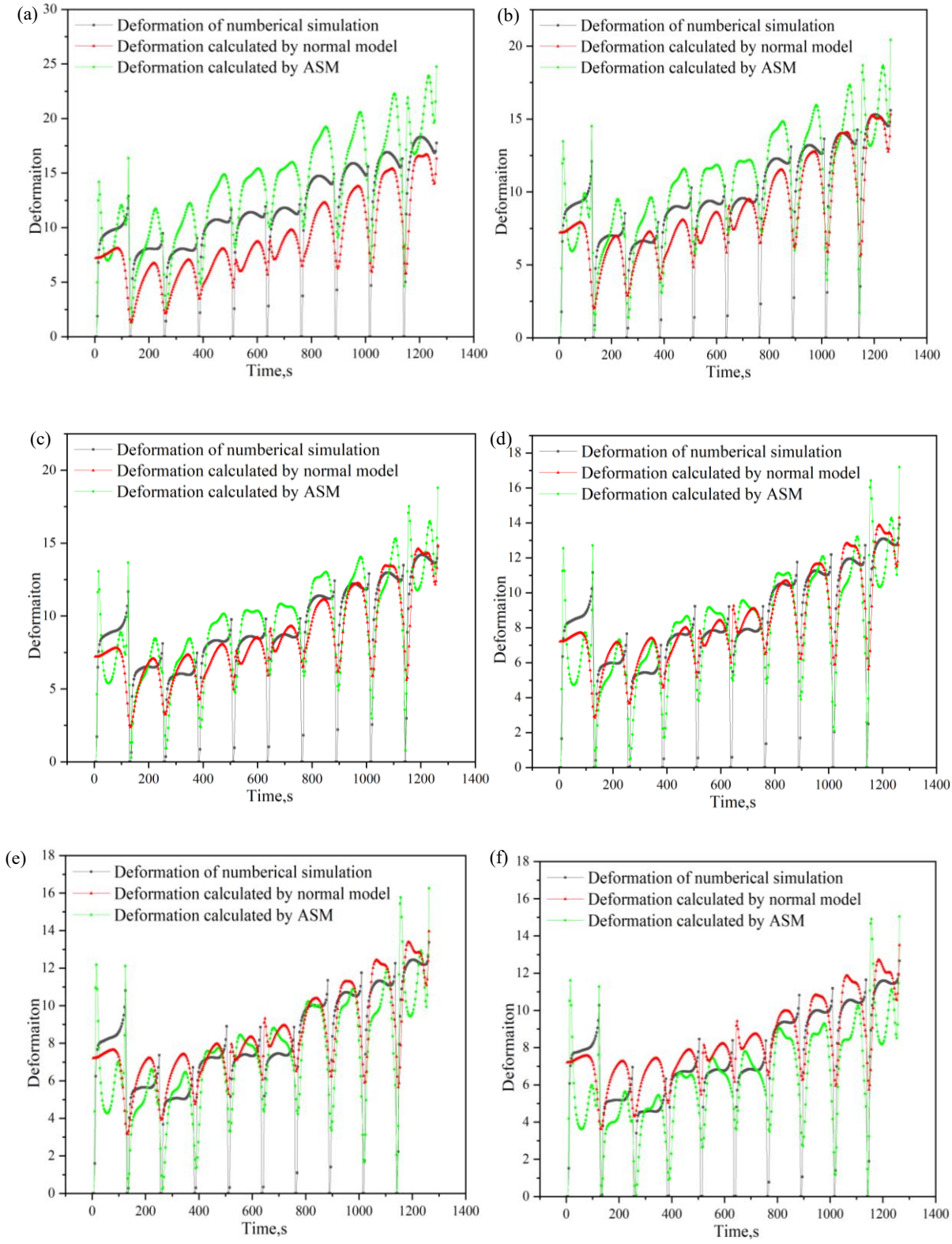

Figure 5.19 Comparison between time-series deformation of numerical simulation and ASM in different HTC: (a)50%, (b)75%, c)90%, (d)110%, (e)125%, (f)150%,

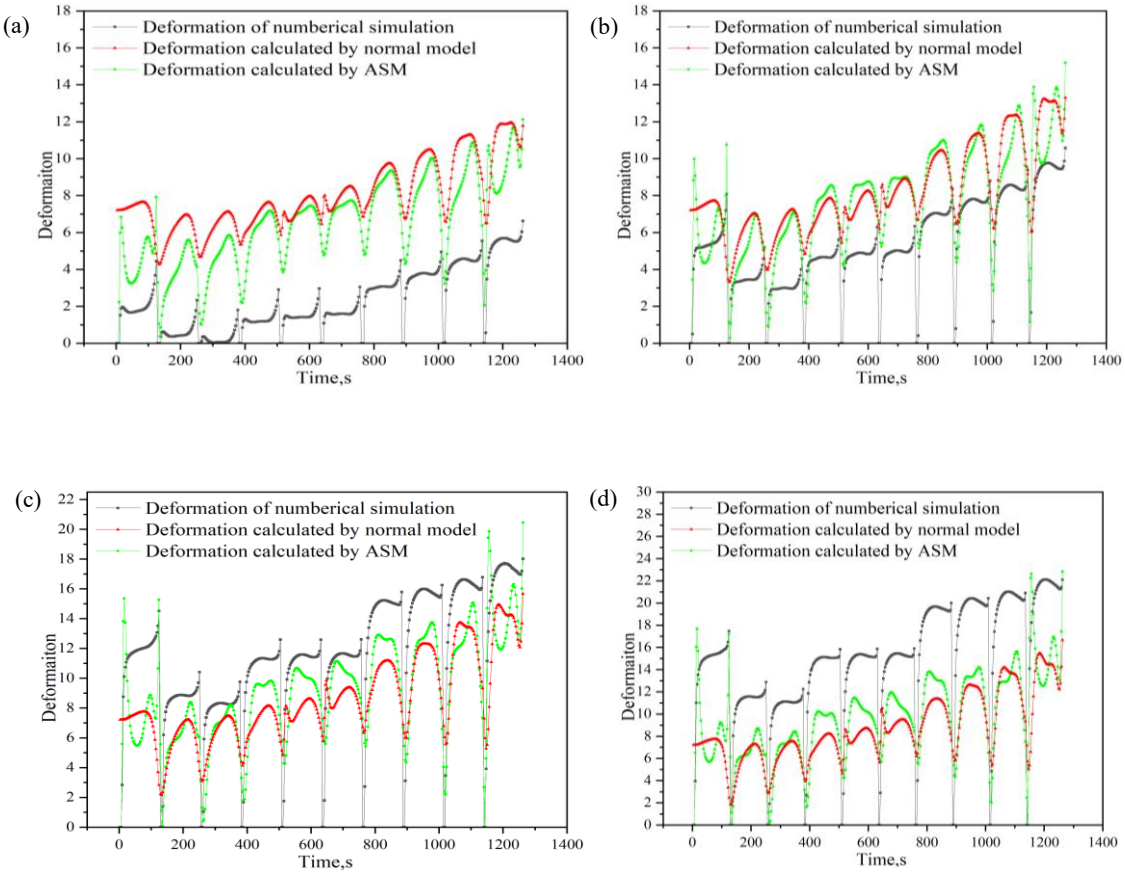

Figure 5.20 Comparison between time-series deformation of numerical simulation and ASM in different HS and HTC:(a)50%, (b)75%, c)125%, (d)150%

Almost the similar comparisons with the error analysis of MCSM were carried out to verify the effectiveness and reliability of the ASM. Since the ASM was proposed on the basis of more databases to compare to the normal model. The properly magnifying the parameters to ±50%, and narrowing a certain range within ±10% and ±15% is considered. As the error analysis of ASM proceeded, the comparison between time-series deformation of normal model and ASM calculation by HS changes alone, HTC changes alone and two factors simultaneous change are shown in **Fig.5.21**, **Fig.5.22** and **Fig.5.23,** respectively. The orange color is stand for ASM result, the green color is stand for normal model.

According to the **Fig.5.21**, **Fig.5.22** and **Fig.5.23**, the R^2 value of ASM are almost the same as that of normal model except the situation of 50%. When the range of HS is changed alone from 50% to 150%, the RMSE of ASM is smaller than that of normal

model, which is illustrated that the calculated result of ASM more closely to the thermal deformation of FEM numerical simulation. When the range of two factors are simultaneously changed from 50% to 150%, the RMSE of ASM are also smaller than that of normal model, as shown in **Fig. 5.23(b)**. There is not so much difference between the RMSE of ASM and normal model when the changing rate of HTC from 50% to 150%, shown in **Fig. 5.21(b)**. Consequently, When range of HS changes alone, HTC changes alone and two factors simultaneous change are located in 50~150% respectively, ASM is more accuracy to describe the relationship between temperature of monitoring points and thermal deformation at machining point rather than normal model.

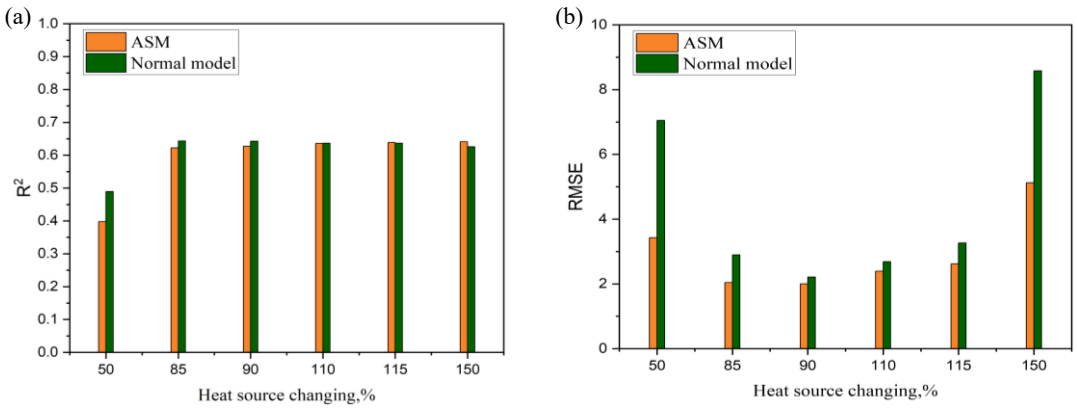

Figure 5.21 Comparison between time-series deformation of numerical simulation and ASM in different HS : (a) R^2, (b) RMSE

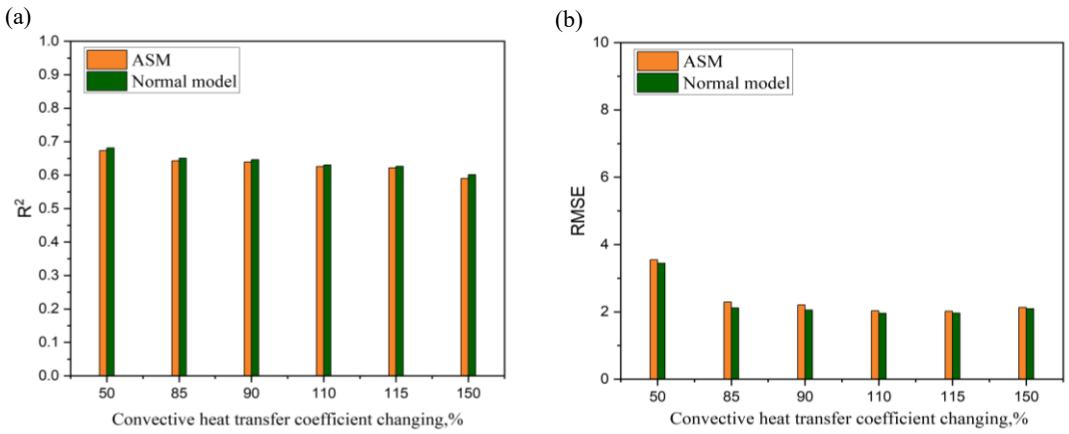

Figure 5.22 Comparison between time-series deformation of numerical simulation and ASM in different HTC: (a) R^2, (b) RMSE

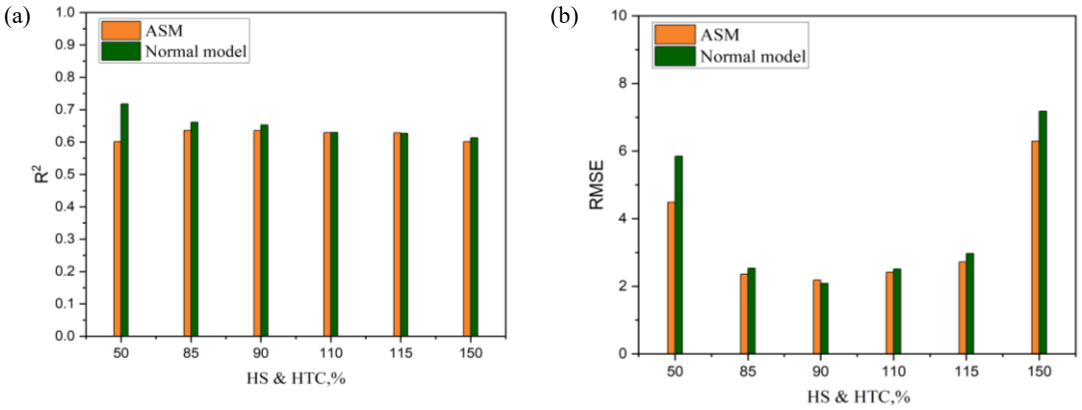

Figure 5.23 Comparison between time-series deformation of numerical simulation and ASM in different HS and HTC: (a) R^2, (b) RMSE

5.5 Summary

In this paper, the finite element method (FEM) numerical simulation of workpiece during end-milling process was systematically conducted, which was scientifically validated by the machining experiment under same boundary condition. A statistic-based temperature monitoring points selection method and statistic model were proposed by using the Multiple Linear Regression (MLR) method, Akaike's Information Criterion (AIC) and *p*-value index. In the statistic model, predicted time-series of deformation at the machining point were regarded as output variable, while time-series of temperature of measuring points were regarded as input variables. The accuracy of proposed statistic model during end-milling process was systematically discussed in various boundary conditions, such as heat source changes alone from 50% to 150%, convective heat transfer coefficient changes alone from 50% to 150% and two factors simultaneous change from 50% to 150%. Finally, two modified statistic model, such as modified coefficient statistic model (MCSM) and the adjusted statistic-model (ASM), were proposed to more suitable expressing the relationship between monitoring points temperature and thermal deformation of friction area between tool and workpiece surface, of which the error analysis were respectively discussed. Consequently, several conclusions were summarized as follow:

(1) The FEM calculation results of 10 monitoring points are quite consistent with

the actual experimental results, which indicates that the selected parameters can reflect accurately the temperature field distribution and variation of workpiece in end-milling process.

(2) The modified coefficient statistic model (MCSM) and adjusted statistic-model (ASM) were successfully proposed by discussed the initially proposed statistic model in different various boundary conditions.

(3) When the range of heat source changes alone, convective heat transfer coefficient changes alone and two factors simultaneous change are located in 50~150%,MCSM and ASM are both more accuracy to describe the relationship between temperature of monitoring points and thermal deformation at machining point in various boundary condition. In addition, only when the ranges of the machining parameters are known in advance, MCSM is preferred to describe the relationship between temperature of monitoring points and thermal deformation at machining point rather than initially proposed statistic model.

6. Conclusion

(1)The thermal structural coupling FEM calculation process was conducted in end-milling machining in detail, the in-direct coupling method is adapted to calculate the temperature field and thermal deformation in the end-milling process. The results of temperature and thermal deformation finite element simulation analysis indicate that the temperature affected area and thermal deformation area mainly concentrate in the contact area between tool and workpiece surface in the end-milling process.

(2)The most sensitive points among 16 measurement points on the workpiece is selected using EOP method, the material parameters and boundary conditions are selected which can calculate workpiece's temperature field accurately based on the comparison between the temperature time-series curves of most sensitive point and actual temperature experimental results. Finally, 10 monitoring points are re-selected again on the workpiece, and the accuracy and reliability of the material parameters and boundary conditions set in the finite element calculation were verified by comparing the finite element calculation results of temperature with the monitoring results in the actual machining process.

(3) The FEM calculation results of 10 monitoring points are quite consistent with the actual experimental results, which indicates that the selected parameters can reflect accurately the temperature field distribution and variation of workpiece in end-milling process.

(4)A statistics-based method was proposed and evaluated to determine measuring points for the thermal process measurement in end milling. The predicted machining error and measurable temperatures were calculated using FEM process simulation. These predicted values were correlated in the form of the MLR model. The model was simplified based on statistical evaluations, such as AIC and *p*-values. To investigate the applicability of the proposed method for obtaining a simplified model of machining error, case studies for simple and complex workpieces in the end-milling process were conducted. In both cases, the number of measuring points was successfully decreased

without deteriorating estimation accuracy. This indicates that the proposed statistics-based selection method enables the systematic determination of appropriate measuring points for the thermal monitoring of the end-milling process.

(5) The modified coefficient statistic model (MCSM) and adjusted statistic-model (ASM) were successfully proposed by discussed the initially proposed normal statistic model in different various boundary conditions. When the range of heat source changes alone, convective heat transfer coefficient changes alone and two factors simultaneous change are located in 50~150%,MCSM and ASM are both more accuracy to describe the relationship between temperature of monitoring points and thermal deformation at machining point in various boundary condition. In addition, only when the ranges of the machining parameters are known in advance, MCSM is preferred to describe the relationship between temperature of monitoring points and thermal deformation at machining point rather than initially proposed statistic model.

Reference

[1] U.T. Tygesen, M.S. Jepsen, J. Vestermark, N. Dollerup, A. Pedersen. The true digital twin concept for fatigue re-assessment of marine structures. ASME 2018 37th International Conference on Ocean, Offshore and Arctic Engineering, American Society of Mechanical Engineers Digital Collection (2018), 10.1115/OMAE2018-77915

[2] P.E. Love, J. Matthews. The 'how' of benefits management for digital technology: from engineering to asset management. Autom. Constr., 107 (2019), Article 102930, 10.1016/j.autcon.2019.102930

[3] M. Grieves, J. Vickers. Digital twin: Mitigating unpredictable, undesirable emergent behavior in complex systems. Transdisciplinary Perspectives on Complex Systems, Springer (2017), pp. 85-113, 10.1007/978-3-319-38756-7_4

[4] E.J. Tuegel, A.R. Ingraffea, T.G. Eason, S.M. Spottswood. Reengineering aircraft structural life prediction using a digital twin. Int. J. Aerospace Eng. (2011), pp. 11-14, 10.1155/2011/154798

[5] E. Glaessgen, D. Stargel, The digital twin paradigm for future NASA and U.S. air force vehicles, 53rd AIAA/ASME/ASCE/AHS/ASC Structures, Structural Dynamics and Materials Conference, AIAA, 2012.

[6] Lazoglu I , Bugdayci B . Thermal modelling of end milling [J]. CIRP Annals - Manufacturing Technology, 2014, 63(1):113-116.

[7] Y. Sun, J. Sun, J. Li, Modeling and experimental study of temperature distributions in end milling Ti6Al4V with solid carbide tool, Proceedings of the Institution of Mechanical Engineers Part B-Journal of Engineering Manufacture 231(2) (2017) 217-227.

[8] Childerhouse T , Jackson M . Near Net Shape Manufacture of Titanium Alloy Components from Powder and Wire: A Review of State-of-the-Art Process Routes [J]. Metals - Open Access Metallurgy Journal, 2019, 9(6):689.

[9] Rauch E , Unterhofer M , Dallasega P . Industry sector analysis for the application of additive manufacturing in smart and distributed manufacturing systems [J]. Manufacturing Letters, 2017:S2213846317300925.

[10] Turner, Brian, N, et al. A review of melt extrusion additive manufacturing processes: II. Materials, dimensional accuracy, and surface roughness. [J]. Rapid Prototyping Journal, 2015, 21(3):250-261.

[11] Reddy N , Kwang-Sup S , Yang M . Experimental study of surface integrity during end milling of Al/SiC particulate metal-matrix composites [J]. Journal of Materials Processing Tech, 2008, 201(1-3):574-579.

[12] Li Yong, Li Zhicheng et al., Zhisheng 21st Century-Overview of The Development Strategy of America's 21st Century Integrated Manufacturing Technology, Beijing Advanced Flexible Manufacturing Technology Consulting Company, 2002

[13] Liu Baicheng. Materials Forming Technology in the 21st century, Aeronautical Manufacturing Technology, 2003, 6:17-21,69

[14] Huang xuemei, Zhao mingyang, Chen shuhong, research on physical simulation technology of machining process, modular machine tool and automatic manufacturing technology,2002,9: 8-11

[15] Chen Xiusheng, Zhang Chengrui, Liu Riliang, LAN Hongbo, Research on Physical Simulation Technology of NC Machining, Modular Machine Tool & Automatic Manufacturing Technology, 2006, 9: 8-11

[16] Vericut Optipath Software, CGTech Corporation, 2003.

[17] Zhou Ji, ZHOU Yanhong, CNC Machining Technology, Beijing: National Defense Industry Press, 2002

[18] Iwata K. A. Modeling and simulation architecture for virtual manufacturing systems. Annals ofthe CIRP, 1995, 44 (1) : 399-402

[19] Huang xuemei, zhao mingyang, wang qiyi, research and development of virtual nc turning physical simulation system, China mechanical engineering, 2002,13(15): 1336-1338

[20] Aha D , Ts D , Ewb D , et al. The development of a digital twin for machining processes for the application in aerospace industry [J]. Procedia CIRP, 2020, 93:1399-1404.

[21] Tansel I N , Ozcelik B , Bao W Y , et al. Selection of optimal cutting conditions by using GONNS[J]. International Journal of Machine Tools & Manufacture, 2006, 46(1):26-35.
[22] Teramoto K , Onosato M . In-process visualization of machining state with sensor-based simulation to support the recognition ability of operators [J]. Human Friendly Mechatronics, 2001, 40(13):389-394.
[23] Dongjin WU and Koji TERAMOTO, An evaluation criterion to select temperature measurement positions in end-milling, International Journal of Automation Technology, Vol.12, No.1, pp. 105-112, 2018
[24] Jaeger J C. Moving sources of heat and the temperature at sliding contacts [J].Journal of the royal society of New South Wales, 1942, 76: 203-224.
[25] Han J, Liu Z, Cao K, Xu L, Shi T, Liao G. Cutting temperature measurement in turning using fiber-optic multi-spectral radiation thermometry and its application in tool wear status recognition. Measurement. 2022;198.
[26] Bhirud NL, Gawande RR. Measurement and prediction of cutting temperatures during dry milling: review and discussions. Journal of the Brazilian Society of Mechanical Sciences and Engineering. 2017;39(12):5135-5158.
[27] Outwater J O, Shaw M C. Surface temperatures in grinding [J]. Transactions of the ASME, 1952, 74(1): 73-78.
[28] Li HN, Axinte D. On a stochastically grain-discretised model for 2D/3D temperature mapping prediction in grinding. International Journal of Machine Tools & Manufacture. 2017;116:60-76.
[29] Dai C, Ding W, Xu J, Xu X, Fu D. Effects of undeformed chip thickness on grinding temperature and burn-out in high-efficiency deep grinding of Inconel718 superalloys. International Journal of Advanced Manufacturing Technology. 2017;89(5-8):1841-1852.
[30] Pang J, Wu C, Shen Y, Liu S, Wang Q, Li B. Heat flux distribution and temperature prediction model for dry and wet cylindrical plunge grinding. Proceedings of the Institution of Mechanical Engineers Part B-Journal of Engineering Manufacture. 2019;233(10):2047-2060.
[31] Komanduri R, Hou ZB. UNIFIED APPROACH AND INTERACTIVE PROGRAM FOR THERMAL ANALYSIS OF VARIOUS MANUFACTURING PROCESSES WITH APPLICATION TO MACHINING. Machining Science and Technology. 2009;13(2):143-176.
[32] Ding Z, Sun J, Guo W, Jiang X, Wu C, Liang SY. Thermal Analysis of 3J33 Grinding Under Minimum Quantity Lubrication Condition. International Journal of Precision Engineering and Manufacturing-Green Technology. 2022;9(5):1247-1265.
[33] Han S, Faverjon P, Valiorgue F, Rech J. Prediction and modeling of thermal distortion in sequential MQL drilling of AlSi7 cylindrical parts. Paper presented at: 8th CIRP Conference on High Performance Cutting; 2018 Jun 25-27, 2018; Budapest, HUNGARY.
[34] Hahn R S. On the temperature developed at the shear plane in the metal cutting process[C]. Journal of applied mechanics - transactions of the ASME. 345 E 47th ST, New York, NY 10017: ASME-AMER soc mechanical eng, 1951, 18(3): 323-323.
[35] Trigger K J, Chao B T. An analytical evaluation of metal cutting temperature [J]. Transactions of ASME, 1951, 73: 57-68.
[36] Campo A, Chang JY, Ridouane EH. HEAT TRANSFER COMPARISON BETWEEN A VERTICAL RECTANGULAR CAVITY AND AN ISOSCELES RIGHT-ANGLED TRIANGULAR CAVITY OF EQUAL CROSS-SECTIONAL AREA. Thermal Science. 2011;15:357-365.
[37] Moon M-A, Park M-J, Kim K-Y. Evaluation of heat transfer performances of various rib shapes. International Journal of Heat and Mass Transfer. 2014;71:275-284.
[38] Komanduri R, Hou Z B. Thermal modeling of the metal cutting process - part III: temperature rise distribution due to the combined effects of shear plane heat source and the tool - chip interface frictional heat source [J]. International joumal of mechanical sciences, 2001, 43(1): 89-107.

[39] Komanduri R, Hou Z B. Thermal modeling of the metal cutting process-part II: temperature rise distribution due to frictional heat source at the tool - chip interface [J]. International journal of mechanical sciences, 2001, 43(1): 57-88.
[40] Komanduri R, Hou Z B. Thermal modeling of the metal cutting process: part I temperature rise distribution due to shear plane heat source [J]. International journal of mechanical sciences, 2000, 42(9): 1715-1752.
[41] Liao Z, Axinte D, Gao D. On modelling of cutting force and temperature in bone milling. Journal of Materials Processing Technology. 2019;266:627-638.
[42] Karpat Y I, özel T R. Analytical and thermal modeling of high-speed machining with chamfered tools [J]. Journal of manufacturing science and engineering transactions of the ASME, 2008, 130(1): 11001.
[43] Zhou F, Wang X, Hu Y, Ling L. Modeling temperature of non-equidistant primary shear zone in metal cutting. International Journal of Thermal Sciences. 2013;73:38-45.
[44] Resendiz-Flores EO, Saucedo-Zendejo FR. Two-dimensional numerical simulation of heat transfer with moving heat source in welding using the Finite Pointset Method. International Journal of Heat and Mass Transfer. 2015;90:239-245.
[45] Shan C, Zhang X, Shen B, Zhang D. An improved analytical model of cutting temperature in orthogonal cutting of Ti6Al4V. Chinese Journal of Aeronautics. 2019;32(3):759-769.
[46] Velaga SK, Ravisankar A. Finite element based parametric study on the characterization of weld process moving heat source parameters in austenitic stainless steel. International Journal of Pressure Vessels and Piping. 2017;157:63-73.
[47] Nasir V, Kooshkbaghi M, Cool J, Sassani F. Cutting tool temperature monitoring in circular sawing: measurement and multi-sensor feature fusion-based prediction. International Journal of Advanced Manufacturing Technology. 2021;112(9-10):2413-2424.
[48] Gottwein K. Measurement of the temperatures in the turning of steels [J]. Maschinenbau technik, 1925, 4: 1129-1135.
[49] Shore H. Thermoelectric measurement of cutting tool temperatures [J]. Journal of the Washington academy of sciences, 1925, 15: 85-88.
[50] Sergeev AS, Tikhonova ZS, Uvarova TV. Method for measuring thermo-emf of a "tool-workpiece" natural thermocouple in chip forming machining. Paper presented at: International Conference on Modern Trends in Manufacturing Technologies and Equipment (ICMTMTE); 2017 Sep 11-15, 2017; Sevastopol, RUSSIA.
[51] Khapachev BS, Voloshin YN, Ivanova DM, Zhilyaev AA. The Determination of Contact Temperature during Mechanical Treatment of Materials. Paper presented at: IEEE International Conference on Quality Management, Transport and Information Security, Information Technologies (IT and QM and IS); 2018 Sep 24-28, 2018; St Petersburg Electrotechn Univ LETI, St Petersburg, RUSSIA.
[52] Wang H, Yang Q, Zhu X, Zhou P, Yang K. Inverse estimation of heat flux using linear artificial neural networks. International Journal of Thermal Sciences. 2018;132:478-485.
[53] Lin B, Zhou K, Guo J, Liu QY, Wang WJ. Influence of grinding parameters on surface temperature and burn behaviors of grinding rail. Tribology International. 2018;122:151-162.
[54] Bezpalova A, Lebedev V, Chumachenko T, Frolenkova O, Klymenko N. Methods for Measuring Grinding Temperatures. Paper presented at: 3rd Grabchenko's International Conference on Advanced Manufacturing Processes (InterPartner); 2022 Sep 07-10, 2021; Odessa, UKRAINE.
[55] Li L, Li B, Ehmann K F, et al. A thermo-mechanical model of dry orthogonal cutting and its experimental validation through embedded micro-scale thin film thermocouple arrays in PCBN tooling [J]. International journal of machine tools and manufacture, 2013, 70: 70-87.
[56] Kalvodova P, Zalud L. Accuracy Evaluation Method of Multispectral Data Fusion for Robotic Systems. Paper

presented at: 4th International Conference on Modelling and Simulation for Autonomous Systems (MESAS); 2018 Oct 24-26, 2017; Rome, ITALY.
[57] Kallmyer NE, Shin HJ, Brem EA, Israelsen WJ, Reuel NF. Nesting box imager: Contact-free, real-time measurement of activity, surface body temperature, and respiratory rate applied to hibernating mouse models. Plos Biology. 2019;17(7).
[58] Nguyen Phi L, Matsunaga Y, Hanari T, Yamada T, Muramatsu T. Experimental investigation of transient temperature characteristic in high power fiber laser cutting of a thick steel plate. Optics and Laser Technology. 2016;84:134-143.
[59] Jaeger J. C. Moving Sources of Heat and the Temperature at Sliding Contacts, Journal and Proceedings Royal Society of New South Wales, 1942, 76: 133-228.
[60] Miao ZY, Yuan SX. Analytical Modeling of Workpiece Surface Temperature Rise in Machining. Paper presented at: International Conference on Manufacturing Science and Engineering (ICMSE 2009); 2010 Dec 26-28, 2009; Zhuhai, PEOPLES R CHINA.
[61] Chen J, Xu M, Xie C, Du J, Dai H, Fang Q. A nonuniform moving heat source model for temperature simulation in ultrasonic-assisted cutting of titanium alloys. International Journal of Advanced Manufacturing Technology. 2018;97(5-8):3009-3021.
[62] Tong J, Xu Z-L, Li J-P, Zhang Y, Hou P-F. Green's function for a line heat source acting on the surface of a coated isotropic thermoelastic material. Journal of Thermal Stresses. 2019;42(2):279-293.
[63] Wright P. K., McCormick S. P., Miller T. R. Effect of rake face design on cutting tool temperature distribution. ASME Journal of Engineering for Industry, 102: 123-128.
[64] Venuvinod P. K., Lau W. S. Estimation of rake temperatures in free oblique cutting. International Journal of Machine Tool Design and Research, 1986, 26(1): 1-14.
[65] Stephenson D. A. Assessment of steady-state metal cutting temperature models based on simultaneous infrared and thermocouple Data," ASME Journal of Engineering for Industry, 1991,113: 121-128.
[66] Cakir E, Ozlu E, Bakkal M, Budak E. Investigation of temperature distribution in orthogonal cutting through dual-zone contact model on the rake face. International Journal of Advanced Manufacturing Technology. 2018;96(1-4):81-89.
[67] Islam C, Altintas Y. A Two-Dimensional Transient Thermal Model for Coated Cutting Tools. Journal of Manufacturing Science and Engineering-Transactions of the Asme. 2019;141(7).
[68] Lucic M, Nedic B, Marusic V, Baralic J, Mitrovic A. Numerical Analysis of the Temperature Field in the Cutting Zone in Continuous and Discontinuous Metal Cutting by Turning. Tehnicki Vjesnik-Technical Gazette. 2020;27(5):1486-1491.
[69] Umer U, Kishawy H, Abidi MH, Mian SH, Moiduddin K. Evaluation of Self-Propelled Rotary Tool in the Machining of Hardened Steel Using Finite Element Models. Materials. 2020;13(22).
[70] Li L, Li B, Ehmann KF, Li X. A thermo-mechanical model of dry orthogonal cutting and its experimental validation through embedded micro-scale thin film thermocouple arrays in PCBN tooling. International Journal of Machine Tools & Manufacture. 2013;70:70-87.
[71] Wu X, Li J, Jin Y, Zheng S. Temperature calculation of the tool and chip in slicing process with equal-rake angle arc-tooth slice tool. Mechanical Systems and Signal Processing. 2020;143.
[72] Nemetz AW, Daves W, Kluensner T, Praetzas C, Liu W, Teppernegg T, Czettl C, Haas F, Boelling C, Schaefer J. Experimentally validated calculation of the cutting edge temperature during dry milling of Ti6Al4V. Journal of Materials Processing Technology. 2020;278.
[73] Khavin G, Gasanov M, Permyakov A, Nevludova V. A Numerical-Analytical Model of the Temperature Field Distribution During Orthogonal Cutting of Composites. Paper presented at: 3rd International Conference on Design,

Simulation, Manufacturing - The Innovation Exchange (DSMIE); 2020 Jun 09-12, 2020; Kharkiv, UKRAINE.
[74] Zhao J, Liu Z, Wang B, Hu J, Wan Y. Tool coating effects on cutting temperature during metal cutting processes: Comprehensive review and future research directions. Mechanical Systems and Signal Processing. 2021;150.
[75] Chen Y, Li H, Wang J. Further Development of Oxley's Predictive Force Model for Orthogonal Cutting. Machining Science and Technology. 2015;19(1):86-111.
[76] Eldeeb AM, Shabana YM, Elsawaf A. Thermo-elastoplastic behavior of a rotating sandwich disc made of temperature-dependent functionally graded materials. Journal of Sandwich Structures & Materials. 2021;23(5):1761-1783.
[77] Yesilkaya KK, Yaman K. Heat Partition Effect on Cutting Tool Morphology in Orthogonal Metal Cutting Using Finite Element Method. Mechanika. 2019;25(4):326-334.
[78] Ying Z, Shu L, Sugita N. Experimental and Finite Element Analysis of Force and Temperature in Ultrasonic Vibration Assisted Bone Cutting. Annals of Biomedical Engineering. 2020;48(4):1281-1290.
[79] Gholamzadeh B, Soleimanimehr H. Finite element modeling of ultrasonic-assisted turning: cutting force and heat generation. Machining Science and Technology. 2019;23(6):869-885.
[80] Pop AB, Sandu AV, Sachelarie A, Titu AM. STUDYING THE BEHAVIOR OF THE C45 MATERIAL WHEN CHANGING THE TOOL GEOMETRY USING THE FINITE ELEMENT METHOD. Archives of Metallurgy and Materials. 2022;67(2):653-659.
[81] Sun Y, Li G, He Z, Kong X. The advance of research on constitutive model used in finite element simulation of metal cutting. Proceedings of the Institution of Mechanical Engineers Part C-Journal of Mechanical Engineering Science. 2022;236(9):4921-4945.
[82] Hamid A. A., Wifi A. S., Gallab M. A three dimensional finite element thermo-mechanical analysis of intermittent cutting process. Journal of Materials Processing Technology, 1996, 56: 643-654.
[83] Lazoglu I., Altintas Y. Prediction of tool and temperature in continuous and interrupted machining. International Journal of Machine Tools & Manufacture, 2002, 42: 1011-1022.
[84] Li Zhengjia, etc. Mathematical model of milling temperature and temperature field analysis for three-dimensional complex groove milling insert. Chinese Journal of Mechanical Engineering,2003, 16(4): 340-343
[85] Chen Ming, Yuan Renwei, Fan Xiaoyong, Yan Pingqi, Application of three-dimensional finite Element Analysis to temperature analysis of high-speed rail cutting, Journal of Mechanical Engineering, 2002, 38(7): 76-79.
[86] Hou Zhenbing, He Shaojie, Li Nuxian, Solid heat Transfer, Shanghai: Shanghai Science and Technology Press,1984
[87] Hahn RS. On the temperature developed at the shear plane in the metal cutting process: Proceedings of First U. S. National Congress of Applied Mechanics, 1951
[88] LIU Weixiang, DENG Zhaohui, Mathematical model of Surface Residual Stress in engineering Ceramics grinding [J]. Machinery Design & Manufacture,2004(05):49-51.
[89] TIAN Xinli, Xu Yanshen, Lin Bin, Theoretical Model of Residual Stress on Ceramic Grinding Surface [J]. China Mechanical Engineering,1999(07):12-14+3.
[90] Dongjin, W., Koji, T.,Advantages of Predict Multiple Variations and Sensitive Temperatures by Using the Novel Selective, International Journal of Automation Technology.
[91] C.S. Ding, M.L. Davison, Assessing Fit and Dimensionality in Least Squares Metric Multidimensional Scaling Using Akaike's Information Criterion, Educational and Psychological Measurement 70(2) (2010) 199-214.
[92] M.C. Shaw, Metal cutting principles, Oxford University Press, New York, 2005.
[93] N. Medina, P. Lambea, M.C. Manjabacas, V. Miguel, A. Martinez-Martinez,J. Coello, Evaluating temperature in faced milling operations by infrared ther-mography, Thermal Science 21 (6 Part B) (2017) 3051–3061.

[94] A. Simeone, E. Woolley, S. Rahimifard, Tool State Assessment for Reduction of Life Cycle Environmental Impacts of Aluminum Machining Processes via Infrared Temperature Monitoring, Procedia CIRP 29 (2015) 526–531. The 22nd CIRP Conference on Life Cycle Engineering
[95] G. Pittalà, M. Monno, A new approach to the prediction of temperature of the workpiece of face milling operations of TI-6Al-4V, Appl. Therm. Eng. 31 (2) (2011) 173–180.
[96] J. Kuczmaszewski, I. Zagórski, Methodological problems of temperature measurement in the cutting area during milling magnesium alloys, Management and Production Engineering Review Vol. 4, No. 3 (2013) 26–33.
[97] Gulenay Guner, Natasha Seetharaman, Sherif Elashri, Mirsad Mehaj, Ecevit Bilgili,Analysis of heat generation during the production of drug nanosuspensions in a wet stirred media mill,International Journal of Pharmaceutics,Volume 624,2022,122020.
[98] Elene De Cleyn, René Holm, Guy Van den Mooter,Exploration of the heat generation within the intensified vibratory mill,International Journal of Pharmaceutics,Volume 587,2020,119644.
[99] G. Chen, C. Ren, P. Zhang, K. Cui, Y. Li, Measurement and finite element simulation of micro-cutting temperatures of tool tip and workpiece, Int. J. Mach. Tools Manuf. 75 (2013) 16–26.
[100] N.A. Abukhshim, P.T. Mativenga and M.A. Sheikh. Int J Mach Tools Manuf, 46 (7–8) (2006), pp. 782-800
[101] Danil Yu. Pimenov, Munish Kumar Gupta, Leonardo R.R. da Silva, Maitri Kiran, Navneet Khanna, Grzegorz M. Krolczyk, Application of measurement systems in tool condition monitoring of Milling: A review of measurement science approach, Measurement, Volume 199, 2022, 111503, ISSN 0263-2241.
[102] Moreira M , Abro A M , Ferreira R , et al. Temperature monitoring of milling processes using a directional-spectral thermal radiation heat transfer formulation and thermography[J]. International Journal of Heat and Mass Transfer, 2021, 171(6 Part B):121051.
[103] R. Komanduri, Z. Hou, A review of the experimental techniques for the measurement of heat and temperatures generated in some manufacturing processes and tribology, Tribol. Int. 34 (10) (2001) 653–682.
[104] C. Lauro, L. Brandão, D. Baldo, R. Reis, J. Davim, Monitoring and processing signal applied in machining processes a review, Measurement 58 (2014) 73–86.
[105] S.O. Kasap, Electrical and Thermal Conduction in Solids 4th ed., McGraw-Hill,125–212.12 Akhtar W , Lazoglu I . A novel analytical algorithm for prediction of workpiece temperature in end milling [J]. CIRP Annals, 2022.
[106] Yy A , Ev B , Fm A , et al. Real-time monitoring of internal structural deformation and thermal events in lithium-ion cell via embedded distributed optical fibre.
[107] Lazoglu I, Altintas Y (2002) Prediction of tool and chip temperature in continuous and interrupted machining. Int J Mach Tools Manuf 42:1011–1022.
[108] Grzesik W, Bartoszuk M, Nieslony P. Finite difference analysis of the thermal behavior of coated tools in orthogonal cutting of steels [J]. International Journal of Machine Tools & Manufacture, 2004, 44(14):1451-1462.
[109] B. Lane, E. Whitenton, V. Madhavan, A. Donmez, Uncertainty of temperature measurements by infrared thermography for metal cutting applications,Metrologia 50 (6) (2013) 637–653.
[110] G. Yang, J. Hou, W. Zhou, L. Zhu, H. Duan, Non-contact temperature measurement by infrared pyrometer in high speed milling, Applied Mechanics and Materials 668–669 (2014) 969–972.
[111] Ryuji TANAKA. Koji TERAMOTO, Tohru ISHIDA, Yoshimi TAKEUCHI, Thermal State Visualization of Machining Workpiece by Means of a Sensor-Configured Heat Conduction Simulation, JSME International Journal Series C Mechanical Systems, Machine Elements and Manufacturing 49(2) (2006) 15.
[112] M. Davies, T. Ueda, R. M'Saoubi, B. Mullany and A. Cooke, On the measurement of temperature in material removal processes, CIRP Ann. 56 (2) (2007) 581–604.
[113] S. Makridakis, S. Wheelwright, R. Hyndman, Forecasting. Methods and Applications. New York, John Wiley

& Sons. (1998)
[114] S. Ganesh, Multivariate Linear Regression, Editor(s): Penelope Peterson, Eva Baker, Barry McGaw, International Encyclopedia of Education (Third Edition), Elsevier, 2010, Pages 324-331.
[115] Asma S , Sezer A , Ozdemir O . MLR and ANN models of significant wave height on the west coast of India [J]. Computers & Geosciences, 2012, 49:231-237.
[116] Cakmak G . The water temperature prediction of a double exposure solar cooker [J]. Environmental Progress & Sustainable Energy, 2014, 33(2):629-635.
[17] Akaike, H. A new look at the statistical model identification. IEEE Transactions on Automatic Control 19 (1974) 716-723.
[118] Stoica P , Selen Y . Model-order selection: a review of information criterion rules [J]. Signal Processing Magazine IEEE, 2004, 21(4):36-47.
[119] Overholser R , Xu R . Effective degrees of freedom and its application to conditional AIC for linear mixed-effects models with correlated error structures [J]. Journal of Multivariate Analysis, 2014, 132:160-170.
[120] Dongjin WU and Koji TERAMOTO, An evaluation criterion to select temperature measurement positions in end-milling, International Journal of Automation Technology, Vol.12, No.1, pp. 105-112, 2018
[121] Yuji SASAKI, et. al, Development of Real-Time Thermal Displacement Compensation System, Journal of the Japan Society for Precision Engineering, Vol.83, No.2, 2017, pp.121-124{in Japanese}.
[122] M. Yang, F. Zhang, and K. Teramoto, (2022). “Statistics-Based Measuring Point Selection for Monitoring the Thermal Deformation of a Workpiece in End-Milling”, Int. J. Automation Technology: IJAT2022, Vol.16 No.5, pp. 562-571.
[123] R. B. Dessau and C. B. Pipper, ““R”–project for statistical computing,” Ugeskrift for Laeger, Vol.170, No.5, pp. 328-330, 2008.
[124] S. Sahoo, M.K. Jha, On the statistical forecasting of groundwater levels in unconfined aquifer systems, Environmental Earth Sciences 73(7) (2015) 3119-3136.

Appendix

Figure index

Table index